ADDITIVE MANUFACTURING OF ELECTROMAGNETIC MULTIFUNCTIONAL COMPOSITES

by

Peter Pa

A dissertation submitted to the Faculty of the University of Delaware in partial fulfillment of the requirements for the degree of Doctor of Philosophy in Electrical and Computer Engineering

Fall 2015

ADDITIVE MANUFACTURING OF ELECTROMAGNETIC

MULTIFUNCTIONAL COMPOSITES

by

Peter Pa

Approved: ____

Kenneth E. Barner, Ph.D.
Chair of the Department of Electrical and Computer Engineering

Approved: ____

Babatunde A. Ogunnaike, Ph.D.
Dean of the College of Engineering

Approved: ____

Ann L. Ardis, Ph.D.
Interim Vice Provost for Graduate and Professional Education

I certify that I have read this dissertation and that in my opinion it meets the academic and professional standard required by the University as a dissertation for the degree of Doctor of Philosophy.

Signed: ____

Mark S. Mirotznik, Ph.D.
Professor in charge of dissertation

I certify that I have read this dissertation and that in my opinion it meets the academic and professional standard required by the University as a dissertation for the degree of Doctor of Philosophy.

Signed: ____

Shridhar Yarlagadda, Ph.D.
Member of dissertation committee

I certify that I have read this dissertation and that in my opinion it meets the academic and professional standard required by the University as a dissertation for the degree of Doctor of Philosophy.

Signed: ____

Amir Zaghloul, Ph.D.
Member of dissertation committee

I certify that I have read this dissertation and that in my opinion it meets the academic and professional standard required by the University as a dissertation for the degree of Doctor of Philosophy.

Signed: ____

Ian McMichael, Ph.D.
Member of dissertation committee

ACKNOWLEDGMENTS

I'd like to first and foremost thank my advisor Dr. Mark Mirotznik for all the help and guidance over the years. Additionally I'd like to thank my lab mates, Zach, Matt, Paul, Austin, who time and time again assisted me with a large part of this work. You all are truly great friends and colleagues. I'd also like to thank Ray McCauley for helping me with a lot of composite work and teaching me about composites.

I'd like to dedicate this dissertation to my family. To whom, I can certainly say that I wouldn't be who I am and where I am right now without you. And to Kimberly, my love, thank you for all the support and being there for me when I really needed you. Oh, the places "we'll" go.

TABLE OF CONTENTS

Appendix

LIST OF TABLES

LIST OF FIGURES

ABSTRACT

Electromagnetic multifunctional composites merge the excellent structural performance of structural composites with additional functionality such as sensing, communication, or electromagnetic interference protection. The multifunctionality aspect of these devices increases the functional capability of structures and can reduce weight, size, and cost. Often left addressed in the development of these structures, is the scalability and practicality of fabricating devices over large surface areas. In this dissertation, scalable methods of fabricating embedded electromagnetic devices are explored using highly scalable additive manufacturing techniques. Both screen printing and microdispensing of silver conductive inks are used to demonstrate common devices found in electromagnetic systems.

Specifically, transmission line feeds, frequency selective surfaces, high impedance surfaces, and antennas are demonstrated and fabricated within woven fabric structural composites. Through these devices, the electromechanical tradeoffs of embedded printed conductors were explored. It was found that silver conductive inks that were screen printed onto glass woven fabrics experienced a reduction of conductivity and an increase in electrical path length. Additionally, the mechanical shear strength and delamination resistance of a composite decreased compared to a baseline when printed with a continuous plane of conductive ink. At higher frequencies, screen printed, embedded frequency selective surfaces compared well against devices fabricated with copper clad polyimide. The high scalability of screen printing pairs well with the patterning of frequency selective surfaces over large structures. Microdispensing of silver conductive inks was also explored as a higher quality method of depositing silver inks onto woven fabrics. The high turnover of additive

manufacturing allowed for rapid processing of multiple antenna design iterations in a short time period. In addition, microdispensing allows for the deposition of higher conductivity, lower viscosity inks that were difficult to deposit onto woven fabrics via screen printing. The resulting antenna showed high conductivity, within an order of magnitude of copper, and excellent radiation performance. A final device was demonstrated using multimaterial additive manufacturing that combined an embedded antenna and high impedance surface fabricated within a single machine. A method for predicting the dielectric properties of geometrically controlled polycarbonate substrates was determined. This method was used to fabricate multiple substrates with varying dielectric properties using a single material. Additionally, the co-deposition of silver conductive ink and polycarbonate was used to additively manufacture both the embedded antenna and high impedance ground plane. The measured antenna showed improved performance when radiating above the high impedance surface relative to a continuous conducting surface at the same distance.

Chapter 1

INTRODUCTION

1.1 Composites in the Industry

Structural composite materials are replacing metal alloys as the principal structural reinforcement in many aircraft and naval vessels. Composites hold considerable advantages over metals including: higher tailorable strength, lighter weight, improved fatigue life, corrosion resistance, and reduction of assembly costs due to fewer fasteners. [1]. When considering composite materials in aircraft, the reduction in weight can translate to increased efficiency, increased payloads, and longer mission ranges. A large amount of electronics are necessary to maintain communications, gather data, and operate efficiently. A typical Boeing aircraft, pictured in Figure 1.1, can support a variety of different antennas all operating at separate frequency bands for purposes ranging from navigation (i.e. GPS) to ground and satellite communications.

When considering the design of such structures, common practice begins with the design of the load bearing structure first and foremost. Antenna systems and other electronics are designed secondary above or on the load bearing structure. Consequently, the secondary design of electronic structures results in a non-optimal structure and generally an associated weight penalty. In modern composites, the DDG-1000 Zumalt, pictured in Figure 1.2, fully composite deckhouse requires various apertures included in the structure to allow antenna communication and consequentially weakening the deckhouse structure. In addition, necessary external structures such as RADARs are structurally weak and need to be enclosed by radomes to protect from environmental exposure and loads. These radomes tend to be large in size and can increase radar cross sections (RCS) of structures.

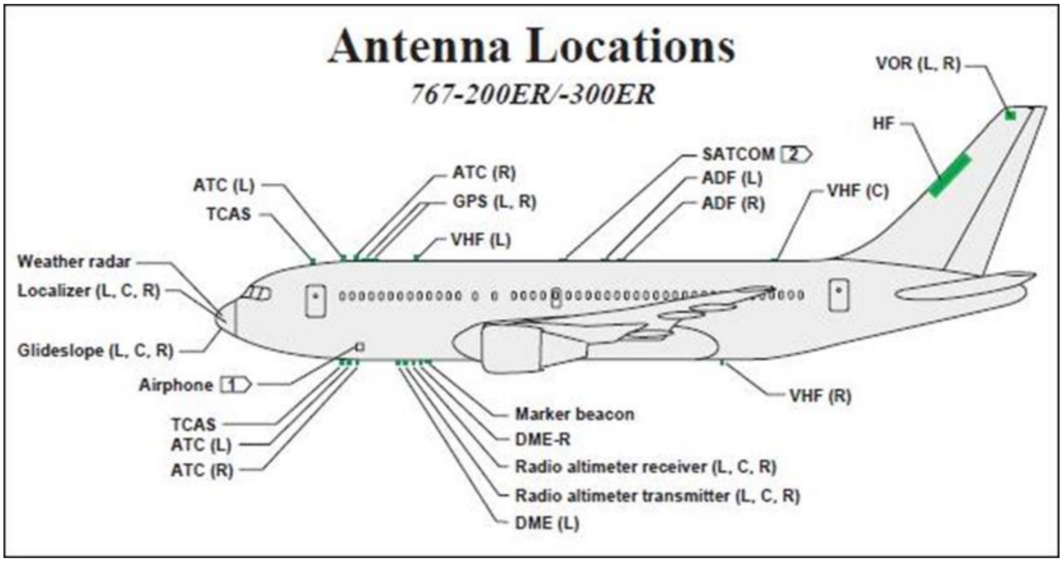

Figure 1.1. Antenna diagram of the Boeing 767

Structural sacrifices, i.e. increased RCS and reduced integrity, can be avoided or mitigated by considering and designing electronics as a part of the load bearing structure. The field of integrating non-structural elements as a part of the load bearing composite member is known as multifunctional composites. Structural functions encompass mechanical properties such as strength, stiffness, fracture toughness, and dampening [2]. Examples of common non-structural functions include electromagnetic interference shielding (EMI), sensing, actuation, self-healing capabilities, and communications. Structural electronics or smart structures incorporate the non-structural functions into the load bearing structure ultimately forming a multifunctional composite. By incorporating electronic systems such as communications antennas or electromagnetic interference (EMI) protection as part of the support, mechanical stresses and physical size can be reduced. In addition, incorporated electronic functions can be designed to be fully conformal thereby minimizing profile effects such as aerodynamic drag.

Figure 1.2 Composite deckhouse of the Zumwalt DDG-1000

1.2 Multifunctional Composites

Multifunctional composites have been investigated through various means in the literature, particularly electromagnetic multifunctional composites. One of the first instances of an embedded non-structural function embedded within a structural composite was the conformal load bearing antenna (CLAS) developed by A.J. Lockyer et. al under the "Smart-Skin Structure Technology Demonstration (S^3TD)" program [3,4]. In this work, a broadband multi-arm spiral antenna was embedded into a sandwich type composite structure intended as a model for upper or lower fuselage antennas operating at low frequencies below 2 GHz. The spiral antenna, detailed in Figure 1.3, was enclosed in a structural composite pan backed by an absorbing material to mitigate unwarranted reflections and to protect internal electronics.

Several other instances of integrating antennas and frequency selective surfaces within composite sandwich structures occurs in the literature [5-7]. In this method, copper clad films or printed circuit boards (PCB) are patterned using photolithographic methods then secondary bonded to composite sandwich laminate, as shown in Figure 1.4. Lastly, interweaving of conductive material has also been explored as a method of integrating conductors inside of structural composites. Yao et. al fabricated microstrip patch antennas and arrays by interweaving conductive filaments inside of the composite preforms [8,9]. Carbon fibers with glass fibers has also been investigated as a frequency selective surface within structural composites [10].

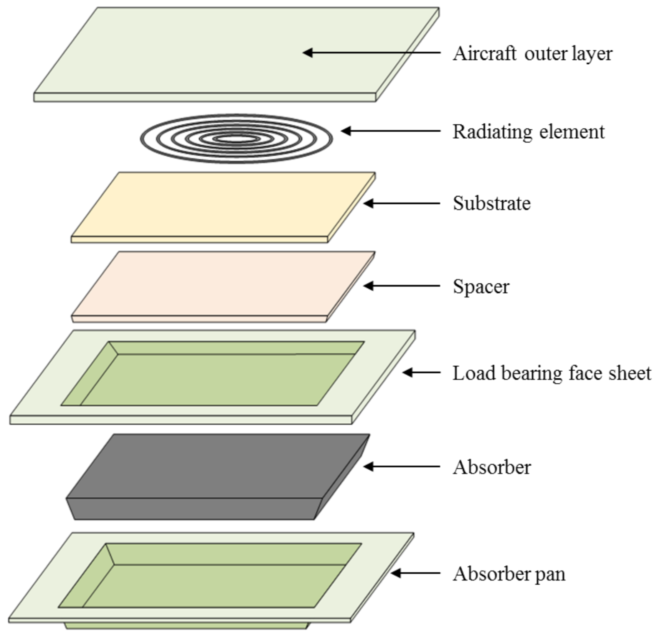

Figure 1.3 A conformal load bearing antenna structure (CLAS) as described in [3,4]

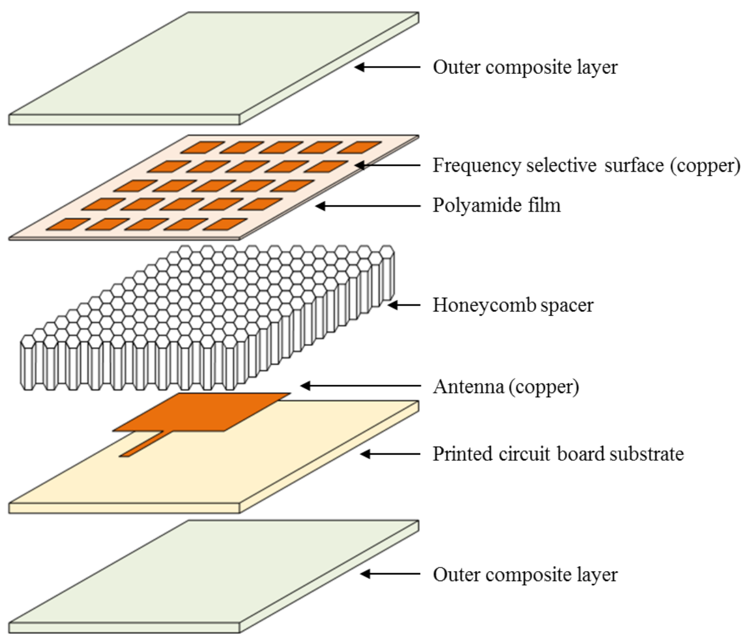

Figure 1.4 Example of integrated antennas and frequency selective surfaces in an alternative sandwich structure configuration as shown in [5-7]

A particular issue often left unaddressed in multifunctional structures is the scalability of the fabrication process for the complete EM and composite structure. Patterning of copper films over large surface areas can take significant time, is inherently wasteful, and requires the use of various chemical etchants. Weaving of carbon fibers can be incorporated quickly through fabric looms, however the conductivity of carbon fibers is several order of magnitudes below that of bulk copper. Alternatively, additive deposition of conductive inks offer many advantages over comparable subtractive methods. The use of conductive inks for EM applications holds significant promise for low cost, high volume production of embedded structural electronics. The use of additive deposition of conductors has been shown for the large scale patterning of transmission lines [11-15], frequency selective surfaces [16-19], and antennas [20-24] on thin films and textile substrates. The direct patterning of conductors on structural composite fabrics prior to composite processing is largely unexplored. *In this dissertation, the overall objective was to explore the use additive manufacturing to fabricate an embedded EM multifunctional composites in a cost effective and scalable fashion as shown in Figure 1.5.. Specifically, I individually demonstrated the use of silver conductive inks and screen printing for the fabrication of embedded transmission line feed structures and frequency selective surfaces within woven fabric composites and compared them to baseline devices. Additionally, another method of additive deposition of conductors, microdispensing, was explored as a higher quality fabrication method for embedded antennas within a structural composite. These methods are individually characterized at low frequencies, then compared at higher frequencies (above 20 GHz). Finally, multi-material additive manufacturing was demonstrated as a method of fabricating complex 3-D networks of conductors.*

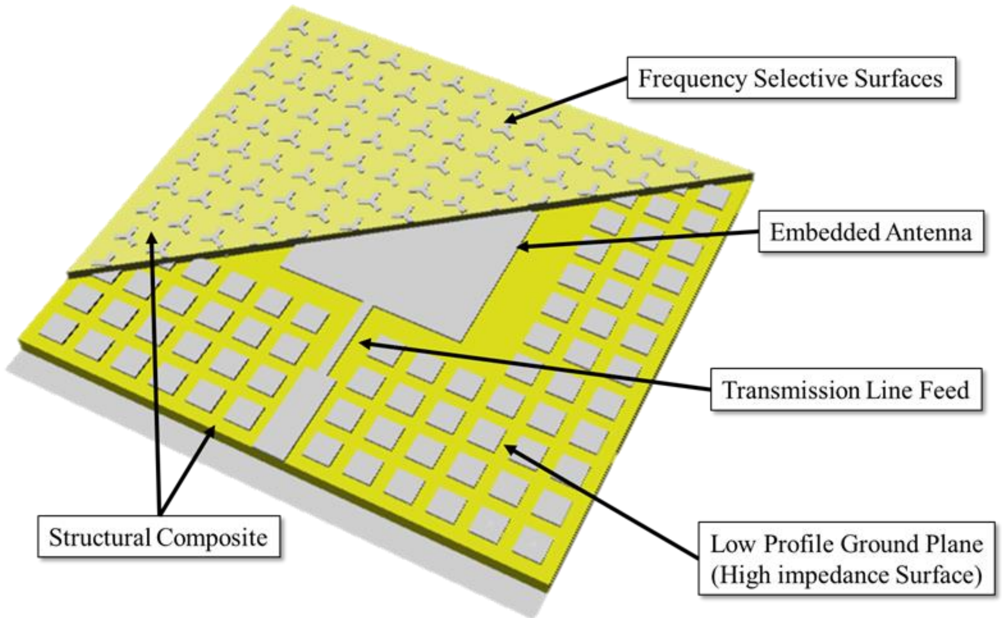

Figure 1.5 Multiple embedded functions embedded within a single composite laminate

1.3 Significant Contributions of this Work

There were a number of significant contributions to the field of multifunctional composites that resulted from this dissertation. Specifically,

- First instance of additively manufactured transmission lines embedded within a structural composite.
- An increase in the electrical path length of screen printed conductors embedded within structural composites was determined.
- Mechanical characterization of structural composites with embedded silver conductive ink was performed and compared to a baseline.

- First instance of additively manufactured antenna embedded within a structural composite.
- A conductivity characterization of microdispensed conductive ink embedded within structural composite was performed.
- Microdispensing and screen printing of conductive inks embedded within structural composite were characterized above 20 GHz by comparison of frequency selective surface performance
- Multimaterial additive manufacturing was explored as a method of fabricating three dimensional conductive networks. To illustrate this fabrication method, an embedded dipole antenna with a high impedance surface was modeled, fabricated, and measured.
- Control of the volume fraction of additively manufactured substrates was used to design permittivity

These new findings resulted in the following publications:

1. P. Pa, S. Yarlagadda, R. McCauley and M.S. Mirotznik, ' Integrating Metamaterials within a Structural Composite using Additive Manufacturing Methods', IEEE International Symposium on Antennas and Propagation , Chicago IL, 2012

2. P.Pa, R. McCauley, S. Yarlagadda, M.S. Mirotznik, ‘Scaled Manufacturing Techniques for High Impedance Surfaces Integrated within Structural Composites’, IEEE International Symposium on Antennas and Propagation, Orlando FL, 2013

3. P.Pa, A. Good, Z. Larimore, M. Mills, S. Yarlagadda, M.S. Mirotznik, ‘Functional Additive Manufacture of Low Profile Antennas Embedded Within a Structural Composite’, RAPID May 2015

4. P.Pa, R.McCauley, Z.Larimore, M.Mills, S.Yarlaggada, M.S.Mirotznik, ‘High Frequency Characterization of Conductive Inks Embedded within

a Structural Composite', IOP Smart Materials and Structures, Vol 24, No. 6, June 2015

5. P.Pa, M.S. Mirotznik, 'High Frequency Characterization of Conductive Inks Embedded within a Structural Composite', IEEE International Symposium on Antennas and Propagation, Vancouver, CN, July 2015

6. P.Pa, Z. Larimore, P.Parsons, M.S. Mirotznik, Multi-material additive manufacturing of embedded low profile antennas'. Electronic Letters. Vol. 51. No.20. pp. 1561-1562. October 2015

7. P.Pa, M.Mills, A. Good, N. Hudak, B. Garrett, S. Yarlaggada, M.S.Mirotznik, 'Screen Printed Structurally Embedded Frequency Selective Surfaces',IOP Smart Materials and Structures (Under Review)

8. P.Pa, Z.Larimore, M.Mills, J. Liu, S. Yarlaggada, M.S.Mirotznik, 'Additive Manufacture of GPS Antenna Embedded within a Structural Composite, IEEE Antennas and Propagation (Submitted)

Other publications and conference proceedings:

1. D.R Roper, B. L. Good, R. McCauley, S. Yarlagadda, J. Smith, A. Good, P.Pa, M.S. Mirotznik, 'Additive Manufacturing of Graded Dielectrics', IOP Smart Materials and Structures, Vol. 23, No. 4, 2014

2. M.S. Mirotznik, S. Yarlagadda, R. McCauley and P. Pa, 'Broadband Electromagnetic Modeling of Woven Fabric Composites', IEEE Microwave Theory and Techniques, Vol. 60, No. 1, January 2012, pp. 158-169.

3. R. McCauley, P.Pa, S. Yarlagadda, M. Keefe, M.S. Mirotznik, 'Mechanical Behavior of Composite Laminates with High Impedance Surfaces' Society for the Advancement of Material and Process Engineering, Baltimore MD, 2012.

4. E. Lee, E. Barry, K. Duncan, P. Pa and M.S. Mirotznik, 'Modeling, Simulation and Fabrication of a Transparent Meshed Microstrip Patch Antenna', IEEE International Symposium on Antennas and Propagation, Chicago IL, 2012

5. Z. Larimore, P. Pa, M. Mills, E. Schaffling, S. Yarlagadda, M.S. Mirotznik, 'Scalable Process for creating Structually Embedded Low Profile Ground Planes Via Interlaminar Needling', SAMPE, Seattle WA, 2014

6. P.Pa, M. Mills, Z. Larimore, S. Yarlagadda, M.S. Mirotznik, 'Graded Surface Wave Absorbers using Resistive Screen Printing', IEEE International Symposium on Antennas and Propagation, Memphis TN, 2014

1.4 Dissertation Outline

The dissertation is organized as follows. Chapter 2 is a background section intended to inform the reader of structural composites and the fabrication methods used to build all the multifunctional composite structures shown in this dissertation. Chapter 3 is a study of microstrip transmission lines embedded within a structural composite. The microstrip attenuation is used as a method of determining the composite influences on the printed conductive inks. In addition, a mechanical study was performed to see the influence of embedded conductive ink on the mechanical properties of the composite. Chapter 4 discussed and investigates the microdispensing of conductive inks onto woven glass composites as a higher conductivity and higher resolution deposition method of embedded antennas. A composite embedded GPS antenna was modeled, fabricated, and measured. The measured antenna results were compared to an optimized model to determine the conductivity of the microdispensed inks. Chapter 5 compares the two methods of additive manufacturing discussed in this dissertation, screen printing and microdispensing. A frequency selective surface was modeled and fabricated using both additive methods. The measured data is compared and used as a method to observe the behavior of the printed conductors at high frequencies (above 20 GHz). Chapter 6 discusses the use of multimaterial additive manufacturing of polycarbonate and silver conductive ink to fabricate more structural embedded electronics. An embedded dipole antenna and a high impedance surface as a low profile ground were fabricated in a polycarbonate substrate. In addition, a method of controlling the spatial fill fraction of additively deposited material was used to control the dielectric properties for each device substrate. This fabrication method was used an initial model for integrating multiple electromagnetic functions within a structural composite. Chapter 7 concludes the dissertation and discusses future work.

Chapter 2

BACKGROUND

The concept of electromagnetic multifunctional composites is multidisciplinary in nature. Hence, a significant amount of background information is necessary to cover the scope of structural composites, electromagnetic applications, and the field of additive manufacturing. The following sections will discuss on a high level the concepts of the aforementioned topics.

2.1 Composite Overview and Fabrication

Structure and reinforcement in high performance aircraft, vehicles, and ships are transitioning from metal alloys to structural composites. Advanced composites hold many advantages over traditional metal alloys including: lighter weight, tailorability for optimum strength and stiffness, improved fatigue life, corrosion resistance, and possible reduced assembly costs from fewer detail parts and fasteners. [1,25]. Reductions in weight can translate to improved performance, greater payloads, longer mission ranges, and fuel savings. The following sections are intended to inform the reader on basic materials and processing used to fabricate structural composites and their use in electromagnetic media and applications. Special focus will be applied to the materials and processing methods used in the process of fabricating the multifunctional electromagnetic structures discussed in this dissertation.

2.1.1 Composite Reinforcement

Structural composites are mainly comprised of two constituent materials, reinforcement and matrix. Reinforcements provide the high strength and stiffness of composites. Common materials used include carbon, aramid (Kevlar), and glass typically in the form of high aspect ratio continuous fibers. There are other configurations for structural composites including particulate and chopped fiber composites that can decrease cost in conjunction with a decrease in structural properties and will not be discussed in the scope of this dissertation. Structural fabrics can also come in woven and non-woven varieties. The two most common weave types are the plain weave and satin weave, pictured in Figure 2.1. Plain weaves are considered the simplest weave where every warp and fill yarn wraps over and then under each successive warp and fill yarn. The plain weave has the most interlaces per unit area making it the tightest type of weave. This makes the fabric resistant to distortion when handling. However, due to the tight weave it is more difficult to form over complex contours and the increased amount of fiber crimp or fiber waviness reduces the strength and stiffness of the composite. Satin weaves minimize interlacing of yarns and thus are more susceptible to distortion. Satin weaves are generally used for curved parts due to the minimal interlacing of yarns. The satin weave can come in multiple harnesses. The five harness satin weave skips over four fill yarns and then under one fill yarn. Due to less fiber crimp, satin weaves are stronger than the plain weaves and also provide a smooth surface finish.

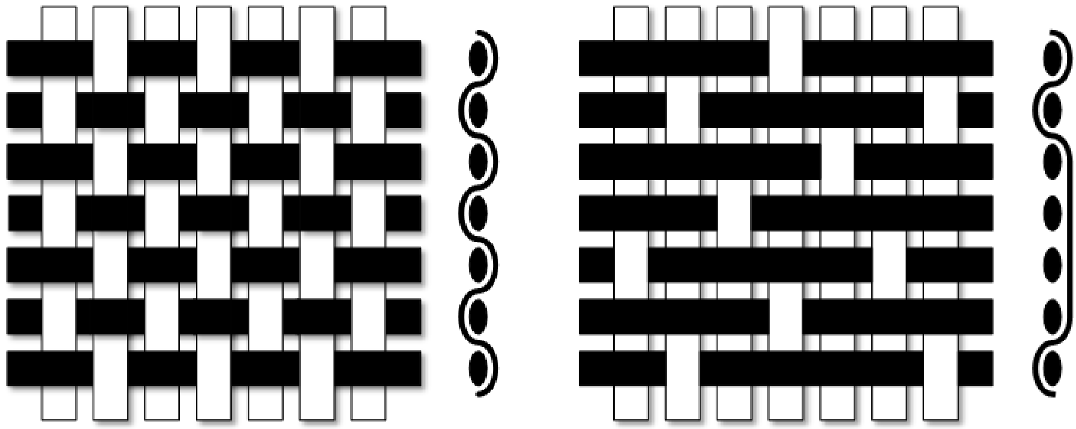

Figure 2.1 Plain weave fabric (pictured left) and 5 harness satin weave (pictured right)

Fully formed composite laminates are made from stacking two or more highly anisotropic fabric sheets. Continuous fiber composite materials typically consist of multiple individual layers or plies and are oriented in directions that will enhance the strength in that particular load direction [1]. Due to the anisotropic nature of the fabric, fiber direction directly impacts the directional mechanical properties of the composite. Thus, various orientations for the fabrics are possible and are designed based on the load conditions of the particular composite. Two common ply orientations are shown in Figure 2.2. Uni-directional layups are extremely strong and stiff in the direction of most fibers (0 degree orientation). However, they are very weak in other load directions due to the load being mainly distributed to the weaker matrix material. In addition, the weave of the fabric dictate the dielectric properties of the composite which will be discussed in a later section. The ply orientation used in this work was uni-directional with in a [0;0_F] where the fabric was flipped about the midplane to balance weave stresses. [25].

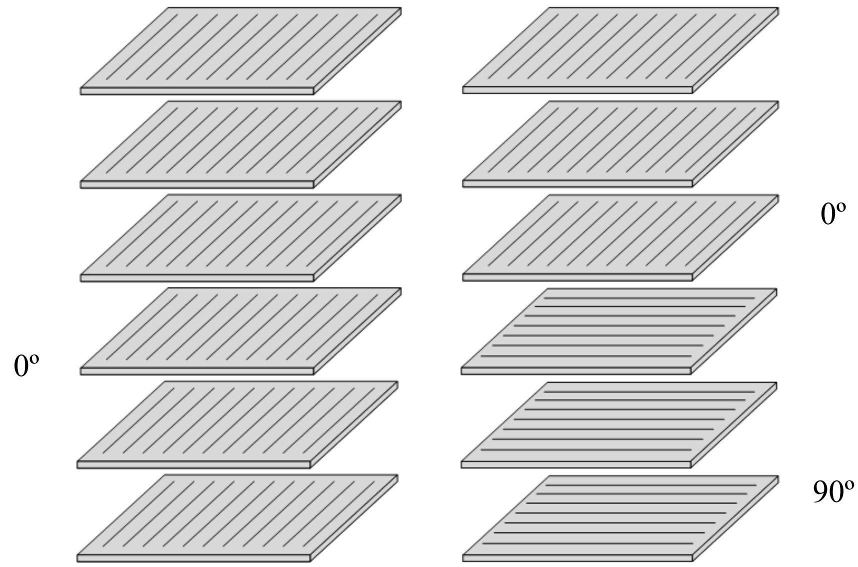

Figure 2.2 Different orientations of the composite fabric plies: 0º Unidirectional layup (pictured left) and 0º,90º midplane orthogonal layup (picture right)

2.1.2 Composite Matrix

Structural reinforcement in composites are held together via the matrix. The matrix acts as a mechanism to maintain the fiber's orientation, spacing, and protection from abrasion and environmental damage [1]. In addition, the matrix is critical in transmitting loads from the matrix to the fibers through shear loading at the interface. The matrix can consist of several materials including polymers, metals, and ceramics. In the interest of scope, the only matrix material that will be considered is the polymer matrix.

Two types of polymer matrix materials exist: thermoplastic and thermosetting. Thermoplastic matrix is a high viscosity resin that is processed by heating the material above the melting temperature. The low melting temperature of the resin is subject to slumping over time and not generally used in high performance aircraft and ships. In contrast, thermoset resins are low molecular weight low viscosity resins that are processed by initiating a non-reversible chemical reaction that cross-links and chemically binds the polymer surrounding the fiber reinforcement. Common thermosetting polymers are vinyl esters, epoxies, and cyanate esters.

Thermoset resins must be initiated typically by mixing a part A resin with a part B resin with a catalyst. Pre-preg or “preimpregnated” composite fabrics are fibers or woven cloths impregnated with a controlled amount of the thermoset resin. Figure 2.3 shows a woven glass fabric with and without the preimpregnated resin.

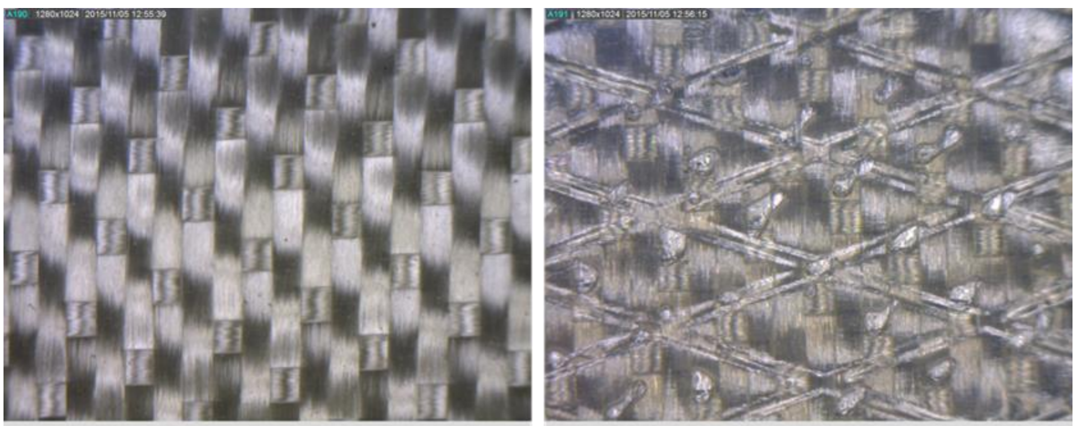

a) b)

Figure 2.3 a)50x magnification of 5 harness woven S-Glass fabric b) 50x magnification of the 6781 S-Glass woven fabric with the BTCy-1 preimpregnated resin

The resin is B-staged such that it becomes tacky and semisolid. This allows the layers to be stacked to form a laminate to be fully cured later. Prior to processing, it is important to maintain the prepreg at low temperatures (below 0 C) and humidity to slow the advancement and prevent the full curing and cross-linking of the thermoset resin. Once the laminate is prepared for manufacture, the prepreg is raised to a controlled temperature, which allows the resin to reflow throughout the fiber reinforcement stack and then fully cure and form a solid composite laminate.

2.1.3 Composite Manufacturing

A variety of methods exist to process and ultimately manufacture a structural composite with associated advantages and disadvantages [1]. With the prepreg composite material used in this study, a vacuum bag layup was performed inside of an autoclave. Autoclave curing is the most prevalent method of fabricating high quality composite laminates in the aerospace industry and electronic industry for radomes. A layup of the composite plies, pictured in Figure 2.4, is placed in a vacuum bag that applies vacuum pressure to the laminate during the curing process. Within the vacuum bag, a layer of release film is applied between the laminate and the tool and caul plate to ensure separation after the cure. The tool is the geometry which the composite material is to be manufacture to and control the finished shape and form of the laminate. The caul plate applies a smooth surface finish to the other surface of the laminate. A layer of breathing material, made of a cellulose cloth, is draped on the laminate to smooth out sharp edges and prevent the laminate puncturing the vacuum bag. Finally, a bagging film is sealed around the laminate with a high temperature double sided tape.

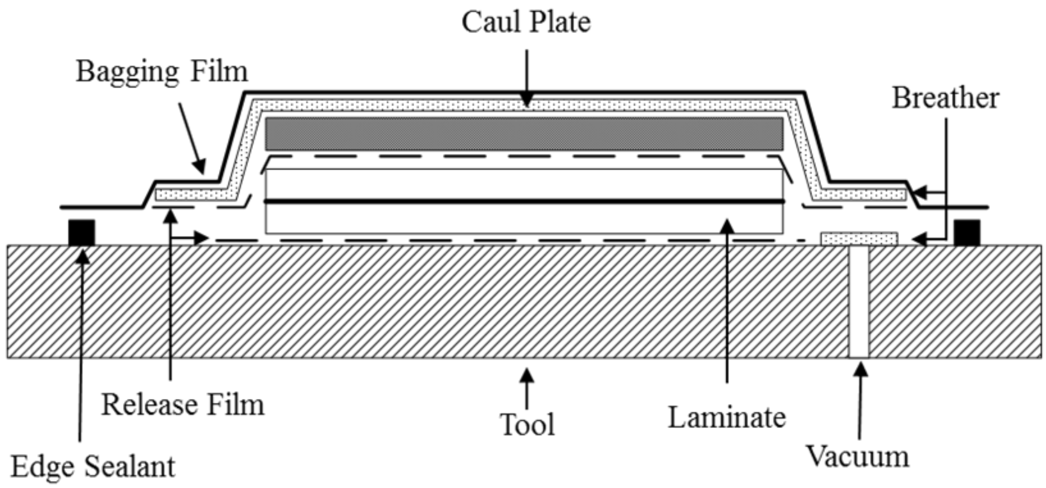

Figure 2.4 Diagram showing a typical autoclave layup

The autoclave applies hydrostatic pressure to the composite laminate during the curing cycle. Pressure is supplied by pumping heated inert gas, in this instance nitrogen, inside of the sealed chamber. Gas is circulated by a large fan which also acts as a mechanism to transfer heat to the laminate during the cure cycle. Figure 2.5 depicts the autoclave used in this work at the University of Delaware's Center for Composite Materials.

Figure 2.5 The autoclave (pictured with a preform layup)

The processing parameters within the autoclave are dictated by material properties of the resin. A Tencate BTCy-1 6781 S-glass/ Cyanate Ester prepreg was selected for this work. This material is an industry standard for high performance aerospace applications and good dielectric properties for radomes. The processing parameters are detailed in the Table 2.1. A graph depicting the temperature, pressure, and vacuum over time within the autoclave is shown in Figure 2.6.

Table 2.1 Recipe used for forming the BTCy-1 6781 composite in autoclave

Material	Vacuum	Pressure	Segment 1 Temp.	Segment 1 Time	Segment 2 Temp	Segment 2 Time
BTCy-1 6781	30 InMg	50 psi	350 F	100 min	120 F	30 min

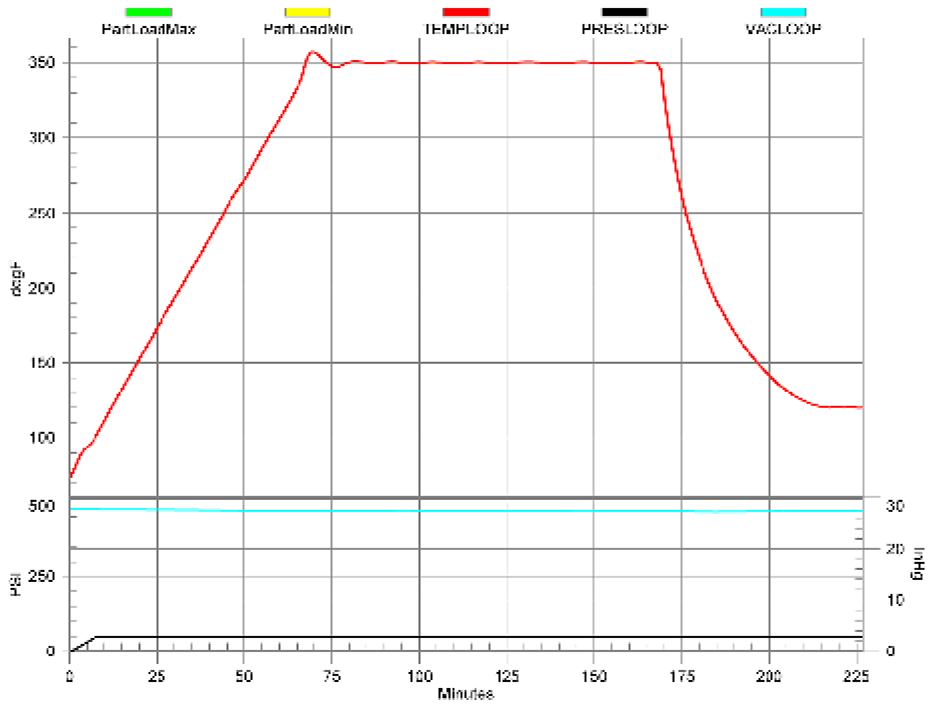

Figure 2.6 Processing chart of the temperature (red), vacuum (blue), and pressure (black) over time within the autoclave for BTCy-1 6781.

2.2 Dielectric Properties of Structural Composites

One of the first models of the dielectric properties of composites was developed through effective media theory [26-29]. This method provides a closed form approximation of a composite material's effective dielectric constant as a function of the dielectric properties of the fibers and resin and the relative volume fraction of one the constituent materials. Satin weave fabrics, as is used in this study, exhibit isotropic dielectric properties due to the symmetric number of glass weaves relative to the 0 and 90 orientation as described in [30]. Hence, the composite can then be modeled as an isotropic medium and effective medium theory.

The structural composite material chosen for this study is a high strength low EM loss glass composite prepreg, Tencate BTCy-1 6781 S-glass Cyanate Ester. This material is an industry standard for high performance aerospace applications and good dielectric properties for radomes. Most composite systems do not fit this requirement for EM application. The dielectric properties of the composite were determined using the method referenced above and are shown in Table 2.2. The volume fractions of a high quality structural composite are expected to fall between 40-60% fiber to resin matrix which can result in a range of dielectric constants between 3.8 and 4.3.

Table 2.2 Tencate BTCy-1 6781 Dielectric Properties [31]

Material	Dielectric Constant, ε_r	Loss Tangent, tan δ
BTCy-1 Cyanate Ester (Datasheet @ 10 GHz)	2.7	0.001
6781 S-Glass (Datasheet @ 10 GHz)	5.21	0.006
BTCy-1 6781 Glass Cyanate Ester Composite (Volume fraction 40-60%)	3.8-4.3	0.003-0.004

2.3 Additive Manufacture of Conductors

Additive manufacture patterning of conductors, also known as direct write, selectively deposits conductive material, typically silver or carbon inks, on a desired material. The advantage of additive deposition versus subtractive patterning methods, such as photolithography or milling, is a greater range of possible material substrates, ability to print conformal to surfaces, minimal material waste, and in some instances scalability. Various methods of additive deposition exist including: inkjet printing, screen printing, aerosol jet, and microdispensing extrusion each with respective advantages and disadvantages well described in [32-34].

Common to all of the methods described above is the deposition of a non-bulk metallic conductor in a liquid or paste form. The Methode 6130S and DuPont CB 028 commercially available silver conductive inks were selected for this study. These conductive inks are made from an aggregate of silver flakes suspended in a carrier compound giving it a paste like viscosity that is ideal for screen printing. The ink is comprised of silver conductive flakes dispersed in a viscous compound suitable for screen printing. To maximize the conductivity of the silver inks, the compound must be heated to decompose the volatile organic compounds in the ink and establish a conductive path through deposited silver flakes. The processing parameters and conductivities of the silver conductive inks used in this study are listed in Table 2.4.

Table 2.3 Conductors used in this study (Bulk and conductive ink)

Conductor	Conductive Filler	Viscosity	Cure Temperature	Cure Time	Sheet Resistivity	Conductivity (*values determined from data sheet)
Copper (Bulk)	Copper	N/a	N/a	N/a	0.5 mΩ/□	5.8×10^7 S/m
Methode 6130S	Silver	80000 cP	95 C	45 min	60 mΩ/□	1.3×10^6 S/m*
Dupont CB028	Silver	30000 cP	160 C	60 min	7-10 mΩ/□	1×10^7 S/m*

Two methods for the additive deposition of conductors were selected for this work: screen printing and microdispensing. The following sections will discuss the deposition methods in detail.

2.3.1 Screen Printing

Screen printing has been adapted from the commercial textile industry for the high resolution deposition of circuits for printed circuit boards (PCB) [34]. The screen printing of conductive inks offer the advantage of high throughput using roll to roll methods that can process several yards per minute. Deposition is performed by passing a squeegee over a patterned mesh reinforced stencil with a bead of the material to be printed, a common process in the screen printing industry.

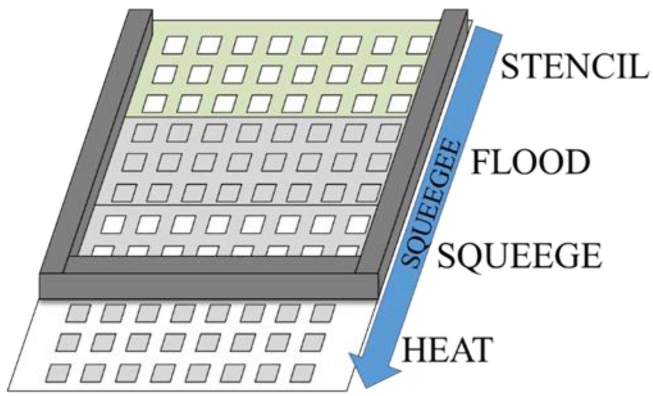

Figure 2.7 Process flow of screen printing conductive ink: 1) Mesh reinforced stencil is patterned with a photosensitive emulsion similar to photolithography. 2) Conductive ink is flooded over the stencil allowing the ink to fill the open areas. 3) Stencil is placed over the substrate and a squeegee passes over the stencil to push the ink through the stencil onto the substrate. 4) Ink is treated in an oven at 95 C to maximize conductivity.

Screen printing of conductive inks has been used for various applications including large scale printing of microwave electronics, printed electronic circuits, and e-textiles [11-17,34]. The process flow of the screen printing is described Figure 2.7. A mesh reinforced stencil is covered with a thin film (1 mil) of photosensitive emulsion.

The emulsion is covered with an opaque image and exposed with a UV light source. The non-exposed areas are then removed by a developing fluid. The conductive ink is then flooded over the patterned stencil by dragging a bead of conductive ink over the screen at a low pressure sufficient to spread a thin film of the ink on the surface of the stencil. The ink is deposited onto a substrate by passing the squeegee over the stencil a second time at a higher pressure which presses the ink onto the substrate. Conductivity of the ink is maximized by heating the printed ink to decompose the volatile organic compounds.

2.3.2 Microdispensing

Microdispensing is a form of extrusion based deposition. Positive pressure is used to extrude fluid materials through a small orifice. The system is controlled through pneumatic pressure that can be varied and regulated to exercise precise deposition. The machine used in in this work is the nScrypt 3Dn-300. This system, depicted in Figure 2.8, integrates dual deposition heads allowing for simultaneous dispensing of two different materials.

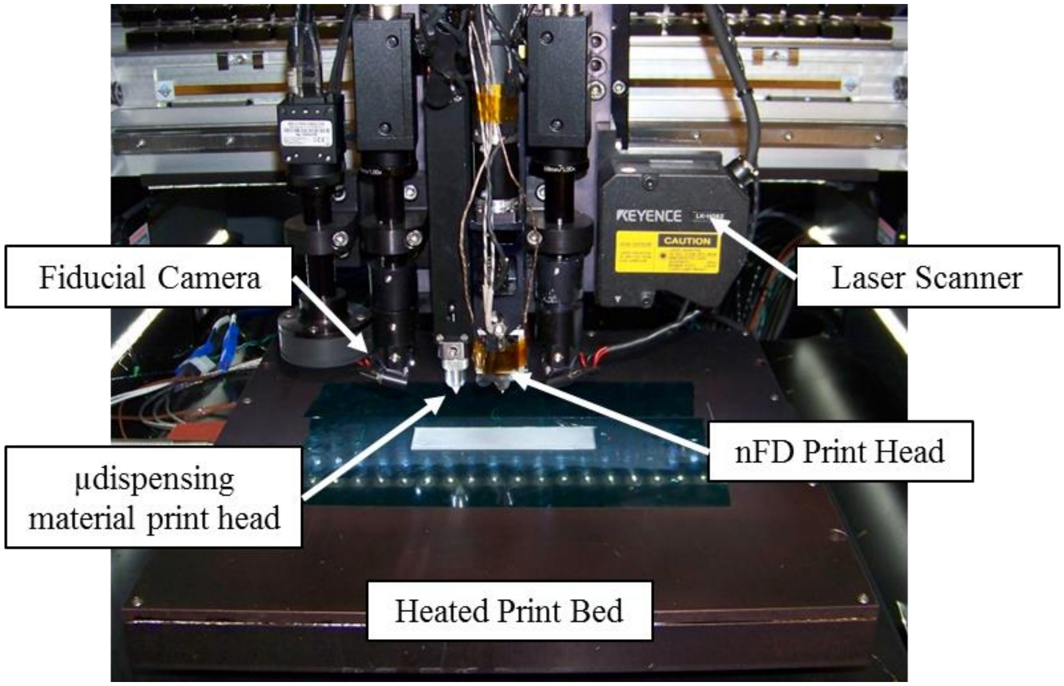

Figure 2.8 Close up view of the nScrypt 3Dn-300 microdispensing printer

Specifically, one print head dispenses a thermoplastic stock using a fused deposition extrusion process. A second head integrates nScrypt's patented micro-dispensing technology. This impressive technology is capable of printing any liquid or paste material with viscosities ranging from 0-1000000 cps with feature sizes as small as 20 µm all at a maximum write speed of 300 mm/s. The maximum build volume of the machine is 300mm x 300mm x 150mm. In addition, the machine is equipped with two fiducial cameras to observe the printing process and a laser scanner that can scan a surface prior to printing and adjust the printing parameters to print directly onto curved or complex contours. Microdispensing of conductive inks has been shown in development of many 3D printed conformal electronics [32,33,35]. The work presented in this dissertation, to the author’s knowledge is one of the first instances of microdispensed embedded electronics within structural composites.

Chapter 3

SCREEN PRINTING OF MICROSTRIP TRANSMISSION LINES

Microstrip transmission lines are commonly used for microwave feed structures due to their simple design and ease of manufacture. In this chapter, a 50 ohm microstrip transmission line is screen printed using a silver conductive ink and embedded within a low loss structural composite material. The attenuation of the composite embedded microstrip line is compared to microstrip baselines fabricated using a standard printed circuit board material. It is shown that microstrip transmission lines printed directly onto structural fabrics experience an increase in electrical path length due to silver conductive ink conforming to the undulation of the woven fabric. Additionally, there is increased attenuation of the silver conductive ink when screen printed onto the woven fabric compared to when screen printed onto a planar, non-porous material. However, it was found that the attenuation of the structural fabric printed microstrips decreased with additional printed passes of the silver conductive ink.

3.1 Introduction

Transmission lines are essential as feed networks for antennas. Planar transmission lines, as pictured in Figure 3.1, are a low profile solution for guiding electromagnetic waves in embedded structures.

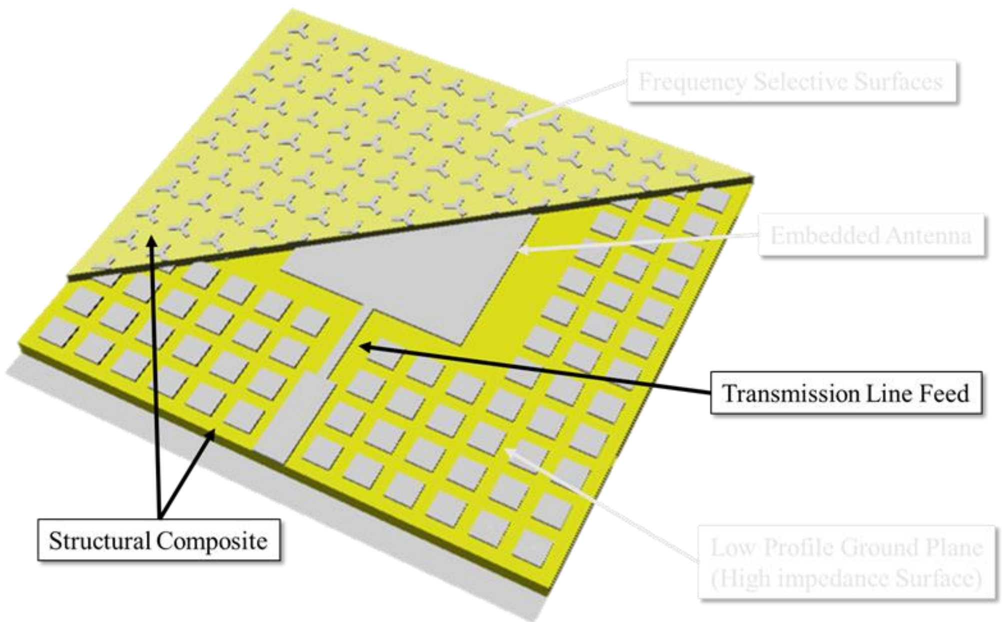

Figure 3.1 Example of feed network for multifunctional composite with embedded antenna and transmission line feed

The microstrip transmission line consists of a metallic strip situated above a dielectric called the substrate backed by a continuous metallic ground shown in Figure 3.2. It is fundamental for the transmission line to consist of two separate conductors to support a transverse electromagnetic (TEM) mode, although the microstrip transmission line supports a quasi-TEM mode due to some of the propagated fields travel in the material above the strip. The microstrip transmission line is ideal for low profile guidance of EM energy within a multifunctional structural composite combined with the additive deposition of conductors. Screen printed microstrip transmission lines has already been studied on printed circuit boards [11,12,34] and on textile fabrics[14,15]. It is observed that the reduced conductivity of the silver conductive ink increases the attenuation of the energy that transmitted over the microstrip line versus bulk conductors. It is unknown how composite processing of the silver printed composite fabrics will influence the transmission characteristics of the microstrip lines. In this chapter, we study the electromechanical tradeoffs of screen printed silver conductive microstrip lines as compared to a baseline made of subtractive manufacturing of copper clad composites.

3.2 Microstrip Design

The microstrip transmission line, as shown in Figure 3.2, is a planar adaptation of the coaxial transmission line [36]. Design equations for the impedance and the effective dielectric constant are empirically derived based on the substrate material, height of the substrate, and the width of the strip line.

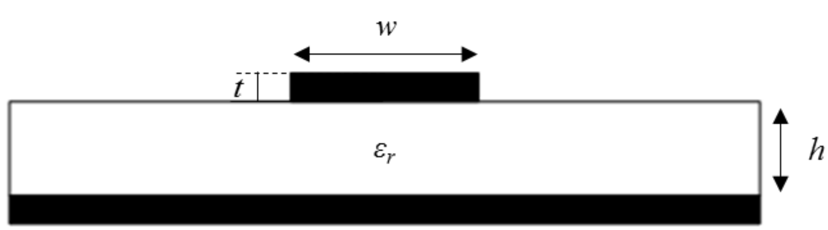

Figure 3.2 Cross section of microstrip transmission line

The design and equations necessary to determine the impedance and effective dielectric constant the microstrip transmission line are well known and discussed in [36]. A 50 Ω microstrip transmission line was designed, then modeled using a commercial finite element analysis software, Ansys High Frequency Structure Simulator (HFSS). In the model, pictured in Figure 3.3, a 200mm microstrip line was designed with solderless SMA end launch connectors (Southwest Microwave Inc.) that were selected to avoid variably induced capacitances from solder or conductive epoxy. Additionally, a small taper was included at both ends of the transmission line near the connectors to balance the transmission lines by cancelling out the small induced capacitance that was generated at the contact location between the signal probe of the connector and the microstrip line.

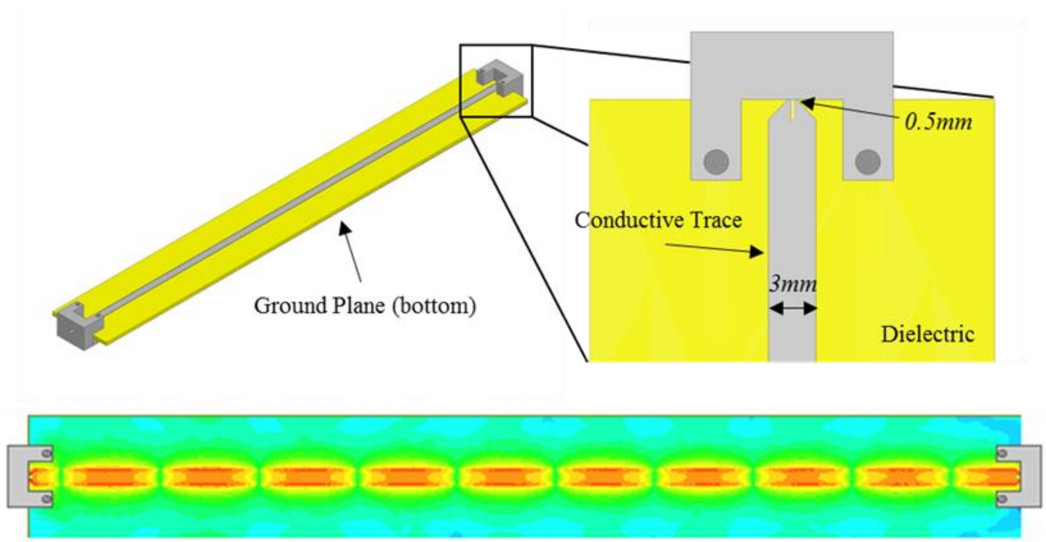

Figure 3.3 HFSS model of the microstrip transmission line with parametrically determined taper (top). Mode profile at 4 GHz of simulated microstrip transmission line (bottom).

Table 3.1 Overview of microstrip test samples

	Substrate Material	Substrate ε_r, $\tan(\delta)$	Conductive Material	Fabrication Process
Sample Type #1 (baseline)	Rogers 4350b	3.66, 0.004	Copper	Lithographic Etching
Sample Type #2	Rogers 4350b	3.66, 0.004	Methode 6130S	Screen Printing (single pass)
Sample Type #3	BTCy-1 6781 Woven Glass Composite Prepreg	4.2, 0.004	Copper	Lithographic Etching
Sample Type #4a	BTCy-1 6781 Woven Glass Composite Prepreg	4.2, 0.004	Methode 6130S	Screen Printing (single pass)
Sample Type #4b	BTCy-1 6781 Woven Glass Composite Prepreg	4.2, 0.004	Methode 6130S	Screen Printing (multiple pass)

3.3 Sample Fabrication

To evaluate the microwave properties of screen printed conductive inks within a FRP, we fabricated five sample configurations (listed in Table 3.1). All configurations used the same width for the conductive trace.

3.3.1 PCB Copper Conductor Baseline (Sample type #1 (baseline sample))

We first fabricated a baseline sample consisting of copper traces and a Rogers^{TM} 4350b substrate. This sample provides a good reference point for comparison with the printed samples. Its microstrip was fabricated using standard practice lithographic and wet etching methods. The board was masked using a matte black spray paint. The transmission line design was then ablated using a computer numeric controlled (CNC) laser from Full Spectrum Laser. Laser ablation left exposed copper that was removed using a ferric chloride copper etchant. The resulting transmission line width and height were measured using standard and confocal microscopy (Figure 3.4). We obtained a line width of 2.83mm and a height of 35µm with an average surface roughness of 2.04µm.

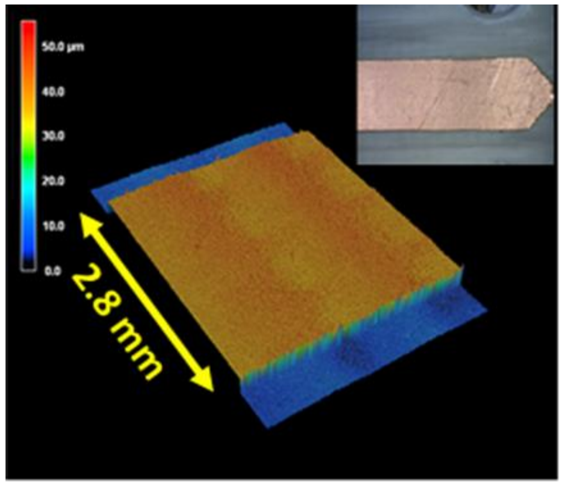

Figure 3.4 Confocal and standard microscopy of copper conductor microstrip transmission line on RogersTM 4350b (Sample #1)

3.3.2 Silver Conductive Ink Screen Printed on Rodgers 4350b (Sample type #2)

In our second configuration, we fabricated a transmission line using a semi-automatic Nano-print screen printer to print silver ink on the same Rodgers 4350b substrate as the baseline sample. A mask with 325 thread/inch mesh, 0.011 inch wire diameter at 28.5 degrees, and 1 mil emulsion thickness was professionally patterned by Utz, LLC. The microstrip trace was printed using Methode 6130S silver conductive ink on a single side of the Rodgers board, and was then cured (at manufacturer specifications) by baking in a 95 °C oven for 45 minutes. The board was then flipped, patterned with the ground plane and cured as before. The silver printed transmission lines were measured as above and had a line width of 3.02 mm, a height of 20µm, and an average surface roughness of 2µm (Figure 3.5).

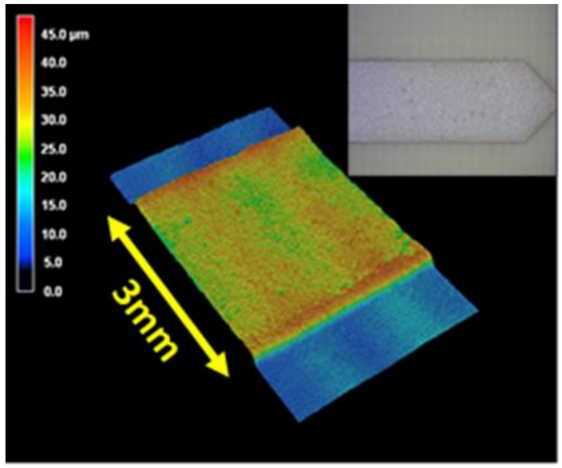

Figure 3.5 Confocal and standard microscopy of silver conductive ink transmission line on RogersTM 4350b (Sample #2)

3.3.3 Woven Fabric Composite Substrate with Copper Conductors (Sample type #3 (baseline sample))

In the third sample configuration, we integrated copper traces and ground planes within a woven fabric composite. The solid composite substrate was first fabricated using a stack built of 4 layers of S-2 Glass/ BTCy-1 Cyanate Ester prepreg sandwiched between two layers of dry S-glass fabric and 2 layers of co-cured 1oz copper foil on the bottom and top surfaces. The dry fabric layers were included to mimic the stacking procedure that was used for the silver printed samples described in the next section. The preform was vacuum bagged, placed within an autoclave and cured at 344.74 kPa peak pressure and 176.6 °C temperature for 90 minutes (according to manufacturer specifications). After curing, the copper microstrip trace and ground plane were fabricated from the co-cured 1oz copper foil. The resulting transmission line had a width of 2.8 mm and a height of 75 µm with an average surface roughness of 3.2 µm.

3.3.4 Woven Fabric Composite Substrate with Screen Printed Conductive Ink (Sample types #4a and 4b)

Our last two samples were constructed by screen printing silver ink onto a woven fabric composite. The microstrip trace and ground plane layers were first screen printed onto dry 8 oz. S-glass woven fabrics. During this step we varied the number of screen print passes from a single pass (Sample #4a) to multiple (up to four) passes (Sample #4b). During each pass additional ink was deposited creating a thicker and more homogeneous print. For the multi-pass samples the ink deposited on each pass was allowed to partially dry before the next pass. The final printed fabrics were heated using the same processing parameters as the silver printed PCB microstrips as in sample type #2. To integrate the printed layers with the composite substrate, the transmission lines and ground plane were separated and placed respectively above and below four layers of S-glass/ BTCy-1 Cyanate Ester prepreg in a mid-plane symmetric stack. The entire stack was vacuum bagged and cured in an autoclave as described in the previous section. Transmission line width was measured at 3 mm, surface height variation was measured by confocal microscopy shown in Figure 3.6 and is discussed in the next section. Printed ink thickness was not measured due to resin flow surrounding the conductive ink. To investigate the homogeneity, approximate height, and surface roughness of single and multi-pass prints, we performed X-ray computed tomography (CT) on the samples using a Skyscan 1174 micro-CT scanner. Single pass samples (Figure 3.7) show minor penetration of the silver conductive ink around the fiberglass fabric. Due to undulation of the satin weave, ink settling on the woven fabric can be seen on the underside of the printed area (Figure 5b). The thickness of the printed ink varied between 25µm and 95µm. This likely has a measureable influence on the conductivity and electrical length of the sample.

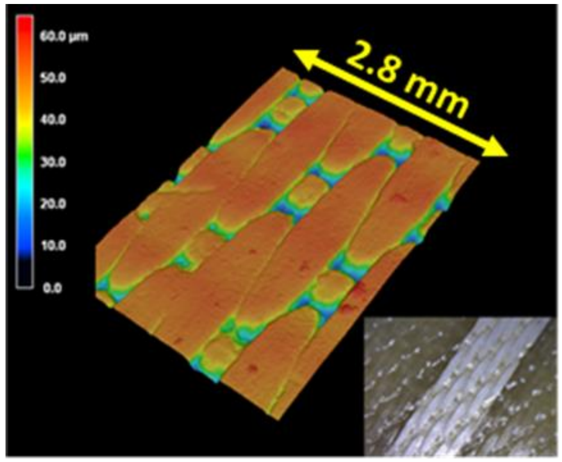

Figure 3.6 Confocal and standard microscopy of silver conductive ink on woven fabric composites after autoclave (Sample #4b)

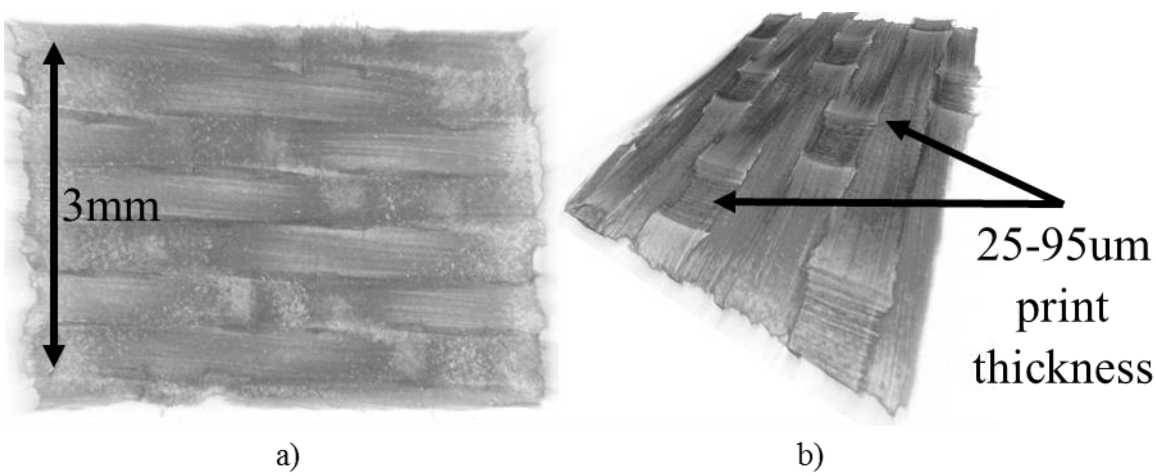

Figure 3.7 a) Top view of CT image scan of the autoclaved conductive ink on fiberglass fabric. b) CT image of composite sample reveals the underside of the printed ink with hills and valleys that range from 25um to 95um printed ink thickness.

3.4 Extraction of Conductivity using a Rigorous EM Model

To determine the conductivity of the silver conductive inks, we performed a direct comparison to a rigorous electromagnetic model. We measured transmission line

S-parameters using an Agilent E8364B portable network analyzer (PNA) that was calibrated using the economy 3.5mm calibration kit 85052D. Transmission lines were connected and time gated to remove any reflections. We compared these measurements to an electromagnetic model generated by Ansys HFSS where the conductivity of a modeled microstrip conductor was parametrically varied. By comparing the measured attenuation over the frequency band with simulated values, we extracted the transmission line conductivity.

3.4.1 General HFSS Model

We used commercial finite element analysis software, High Frequency Structure Simulator (HFSS) sold by Ansys Inc, to model the fabricated microstrip transmission lines (Figure 3.2). To achieve a realistic model that was as close to the fabricated sample as possible, we included the excitation connector in the model. The connectors were solderless SMA end launch connectors (Southwest Microwave, Inc.) that were selected to avoid variably induced capacitances produced by solder or conductive epoxy. We added a small taper at both ends of the transmission line near the connectors to balance the transmission lines by cancelling out the small induced capacitance that was generated at the contact location between the signal probe of the connector and the microstrip line.

3.4.2 Planar Conductivity Extraction (Samples #1, #2)

We adjusted the general model to include the Rogers™ 4350b substrate and the width of the copper microstrip measured by confocal microscopy (see above). We fine tuned the model to match transmission phase by de-embedding the model excitation. This adjustment is necessary to balance variance due to connector artifacts between measurements. We set the optimal de-embed distance of the port to 4.2 mm, and kept this factor consistent for all simulations to mimic the phase incurred from the connectors. Figure 3.8 plots the modeled and measured data from the copper and silver printed transmission lines on Rogers[TM] 4350b. We verified the reported DC conductivity (σ_i = 1.3 x 10^6 S/m) of the Methode 6130S silver conductive ink through simulation. We found the relative conductivity of the Methode 6130S to bulk copper (σ_o = 5.96x 10^7 S/m) to be approximately 0.022 σ_o.

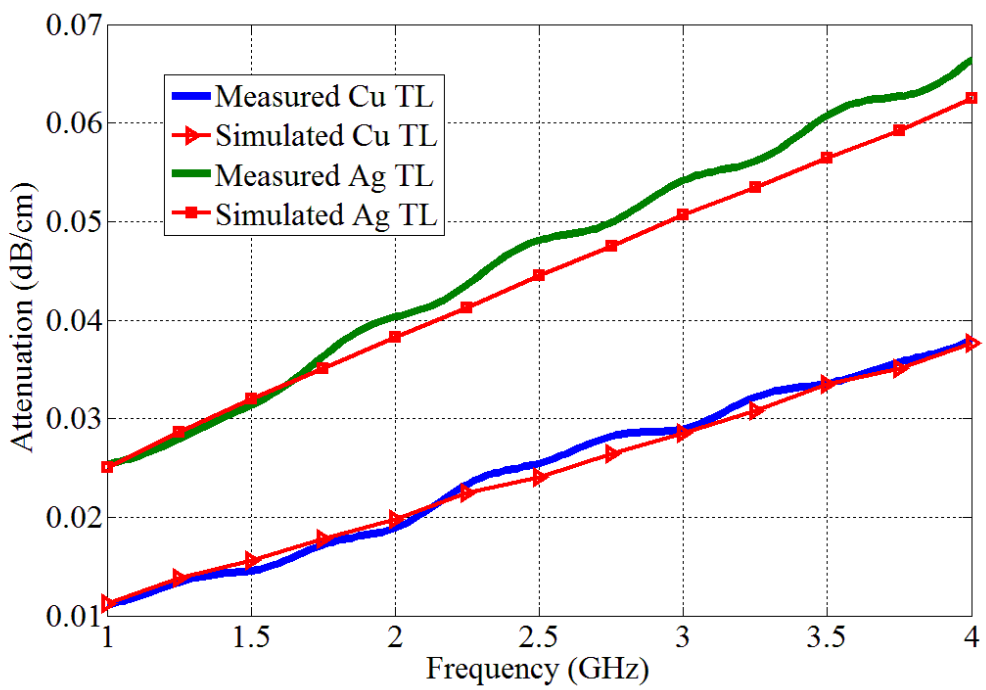

Figure 3.8 Comparison of transmission between silver printed conductive microstrip line and copper microstrip line on Rogers 4350b shows that silver ink conductivity is 2.2% of bulk copper conductivity

3.4.3 Woven Fabric Composite Transmission Line Model and Single Pass Conductivity Extraction (Samples #3, #4)

The copper transmission line fabricated on the BTCy-1 6781 (Sample #3) was used to verify the in-plane dielectric constant of the structural composite. The measured transmission phase of the copper microstrip (i.e., ∠S21) agreed well with the modeled transmission phase using a dielectric constant of $\varepsilon_r = 4.2$ for the substrate. However, the measured phase of the silver printed transmission lines showed a slight discrepancy from the modeled results when using the same dielectric constant (i.e., $\varepsilon_r = 4.2$). We determined through detailed surface metrology that this discrepancy resulted from undulations in the 7-harness satin weave. The undulations cause a slightly longer effective electrical length for the silver printed transmission lines (Figure 3.9). To correct this, we increased the physical transmission line length in the HFSS model to the true electrical length of the silver printed ink on a woven fabric. Using confocal microscopy shown in Figure 3.7, we found this electrical length to be approximately 1.75% longer (203.5 mm) than the physical length (200 mm) as demonstrated in Figure 3.9. After making this adjustment, the modeled and measured transmission phases were in excellent agreement (Figure 3.10).

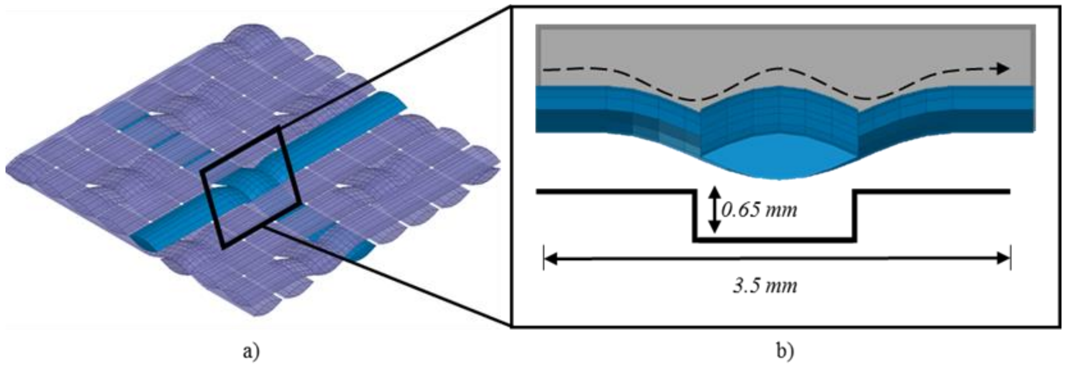

Figure 3.9 a) 3D CAD model of 7 harness fabric weave. b) Cross section of the weave reveals undulation of printed conductor resulting in a 1.75% path length increase of the transmission line

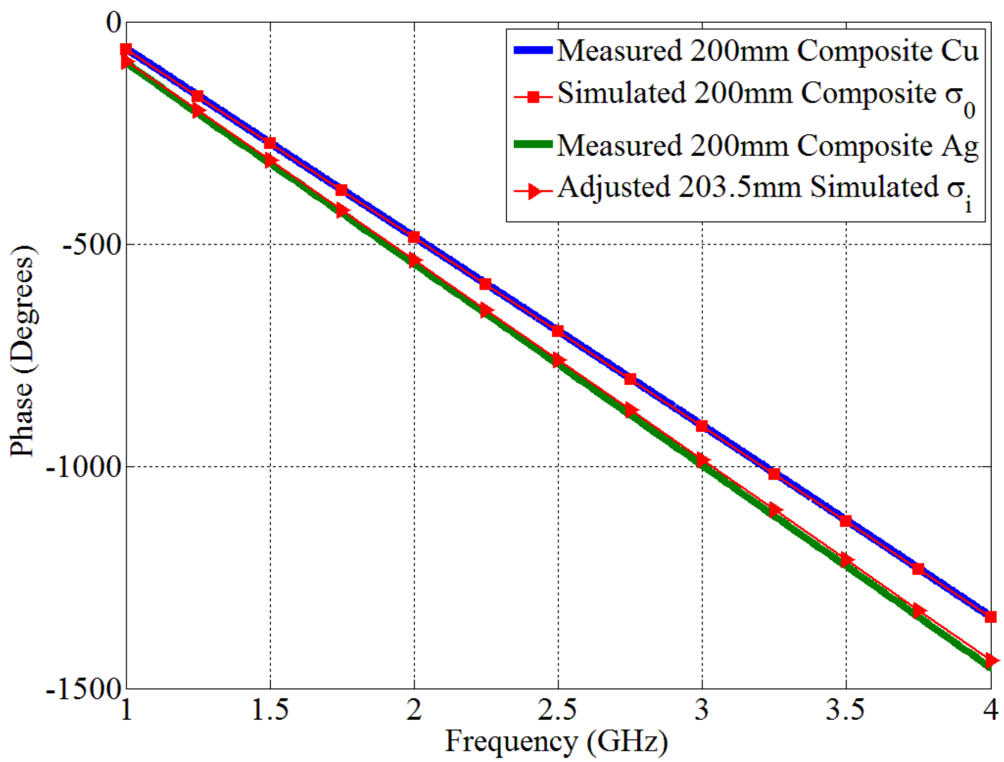

Figure 3.10 Measured and predicted transmission of phase of the 200mm composite microstrip transmission lines.

We used this corrected HFSS model to extract the conductivity values of the silver ink from the measured frequency dependent attenuation plots shown in Figure 3.12. The extracted conductivity values for all samples are given in Table 3.2. They indicate that silver ink printed on the structural fabric has a lower effective conductivity than silver printed on PCB. The conductivity of a single pass printing of silver on fabric (σ_1 = 3.3 x 10^5 S/m) is only 25% that of silver printed on a planar PCB substrate (σ_i = 1.3 x 10^6 S/m; Sample #2). However, each subsequent print pass steadily increases the conductivity until, after four print passes, the conductivity is 80% higher (6 x 10^5 S/m) than the single print pass or 46% that of the silver printed on PCB, σ_i . This is not surprising since the effective electrical conductivity is sensitive to both the total amount of printed silver as well as the print uniformity. Multiple print passes increase the total amount of ink while simultaneously filling in gaps missed during previous print passes. This reasoning is supported by CT imagery of the silver ink printed on fiber glass fabric that shows pockets and voids in the printed ink layer as well as repeated sections of thick and thin printed areas (Figure 3.11). All these printing artifacts significantly affect the overall conductivity. While we did not go beyond four print passes on the fiberglass substrate, we expect more passes to increase the conductivity until it approaches 1.3 x 10^6 S/m, the measured conductivity of silver ink printed on the planar Rogers™ substrate (Sample #2).

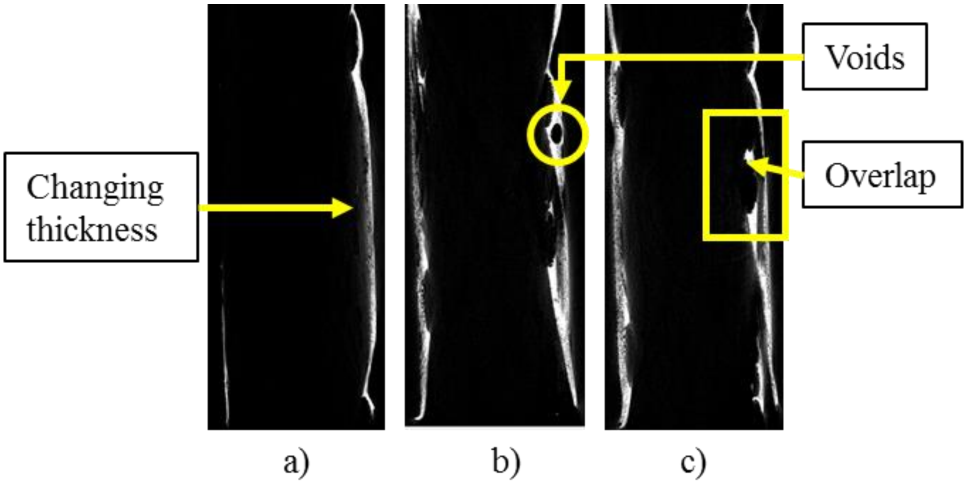

Figure 3.11 Cross sectional CT imagery of 4 pass (Sample #4b) silver embedded ink shows a) undulation of ink on fabric weave with thin and thick areas of ink; b) an air pocket, or void, forming within the conductive ink; and c) an overlap area where ink flows underneath the fiber bundles.

3.4.4 Conductivity Summary

The conductivity data summarized in Table 3.2 provides a few observations. First, when the silver based ink is screen printed on a nearly planar substrate, such as the Rogers™ 4350b material, the high frequency conductivity approaches the DC conductivity of the inks reported by the vendor (1.3 x 10^6 S/m). This result is consistent with values on planar substrates acquired using other conductive characterization methods [10-14]. Second, all samples fabricated using conductive inks have conductivity values over an order of magnitude lower than our baseline samples that were fabricated using solid copper transmission lines. Third, when our silver based ink is screen printed onto a woven structural fabric, the conductivity values are significantly lower (i.e., 5x) than those of planar surface prints. We found through confocal and micro-CT imaging that this decrease results from the undulations inherent in the woven fabric that create a complicated non-uniform print surface. Multiple print passes improve the uniformity and thus increase the effective conductivity of the transmission line. Reported conductivities are on a suitable order for use in EM systems.

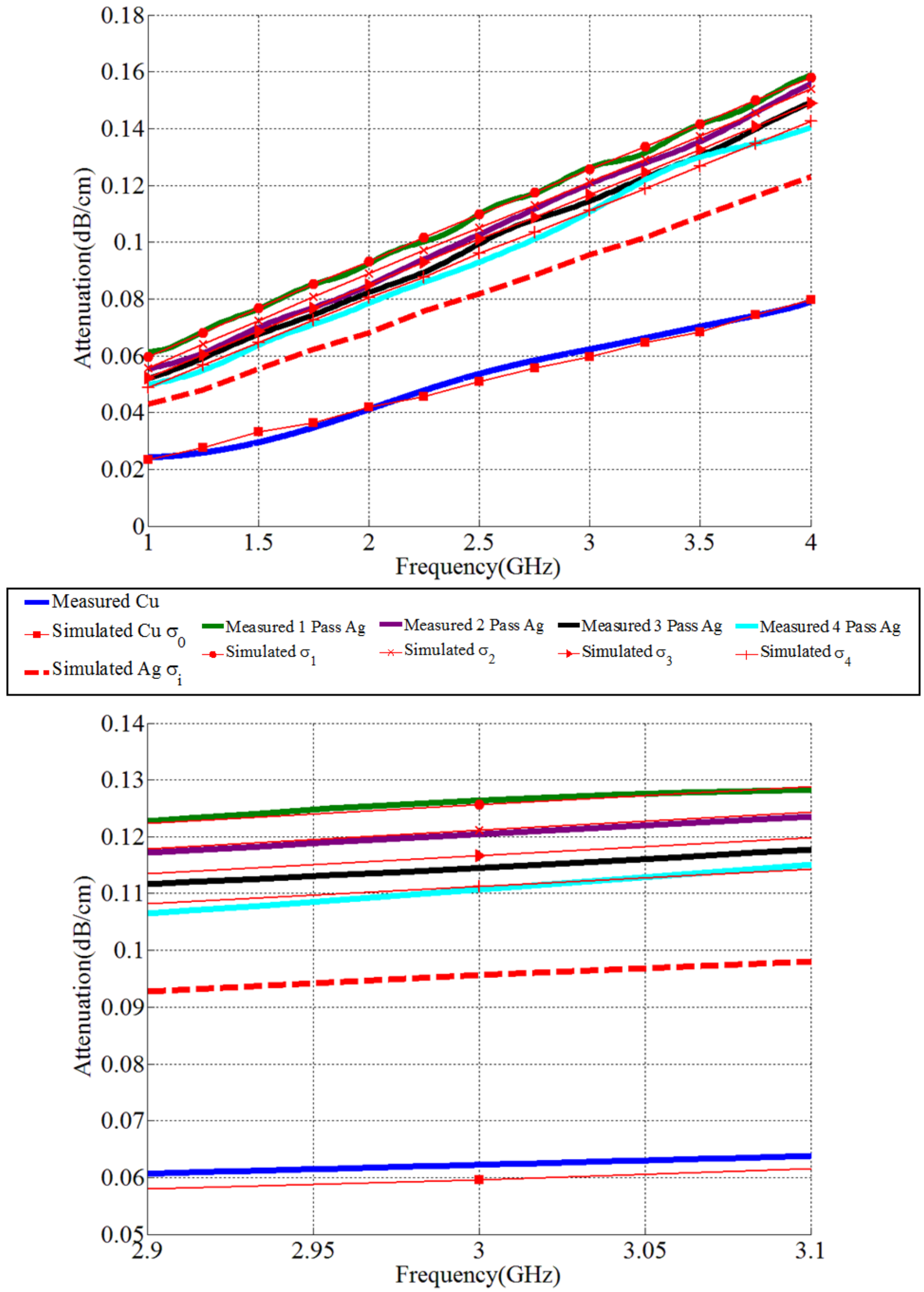

Figure 3.12 top) Measured and simulated data of composite microstrip transmission line. bottom) Expansion of 3 GHz data for silver printed composite transmission line. Red dashed line shows simulated theoretical maximum for conductivity of silver ink.

Table 3.2 Summary of Conductivities

Sample	Conductor	Conductivity
Sample #1 (Baseline)	Copper (Baseline), σ_o	5.96×10^7 S/m
Sample #2	Methode 6130S (Planar DC Conductivity) and Extracted σ_i	1.3×10^6 S/m
Sample #3 (Baseline)	Copper (Baseline), σ_o	5.96×10^7 S/m
Sample#4a	Methode 6130S (1 Pass on Structural Fabric), Extracted σ_1	3.3×10^5 S/m
Sample#4b	Methode 6130S (2 Pass on Structural Fabric), Extracted σ_2	4×10^5 S/m
Sample#4b	Methode 6130S (3 Pass on Structural Fabric), Extracted σ_3	5.8×10^5 S/m
Sample#4b	Methode 6130S (4 Pass on Structural Fabric), Extracted σ_4	6×10^5 S/m

3.5 Mechanical Testing

To determine the mechanical impact of the embedded conductive inks, we performed tests to assess adhesion of printed layers to the composite. We selected the 3 point short beam shear test and the floating roller peel test to investigate the shear strength and peel strength, respectively, of the embedded conductive inks within composite laminates.

3.5.1 Short Beam Shear

The short beam shear test was performed to the ASTM D2344 standard. The baseline consisted of 24 layers of BTCy-1 6781 8oz. S-glass assembled in a mid-plane symmetric layup, yielding a 6.35mm thick composite. Due to the thickness of the sample, every 8 layers of prepreg were debulked under vacuum prior to consolidation. The experimental sample, also debulked as described, contained 23 layers of the prepreg and a midplane oriented single layer of dry s-glass printed with a continuous plane of

Methode 6130S silver conductive ink cured at manufacturer specifications. The layups were processed in the autoclave at a peak temperature of 344.74 kPa peak pressure and 176.6 °C temperature for 90 minutes. The samples were then cut to approximately 12.7mm x 38.1mm x 6.86mm coupons.

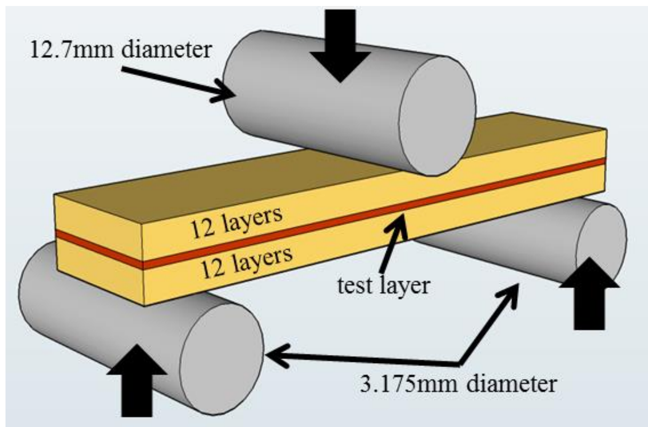

Figure 3.13 Diagram of short beam shear test fixture

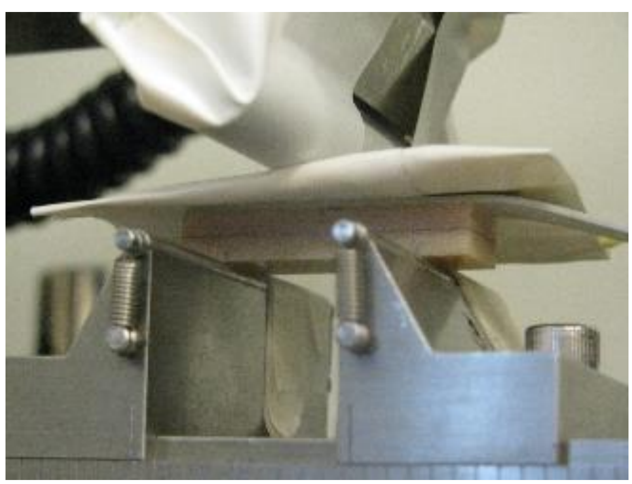

Figure 3.14 Short beam shear test fixture on Instron 5567

These coupons were loaded in the warp direction by an Instron 5567 with a 30kN load cell at a rate of 12.7mm/min. Rubber pads were placed on the top load to prevent premature failure due to crushing. The test fixture is shown in Figure 3.13 with details illustrated in Figure 3.14. Figure 3.15 plots the results. Baseline samples experienced bond failure, Figure 3.16, with a maximum load of 8717.02 N indicating an average short beam shear strength of 1762.4 +/- 29.64 psi. Silver conductive ink embedded samples experienced bond failure with a maximum load of 6867.26 N and an average short beam shear strength of 1543.9 psi with a standard deviation of 124.78.

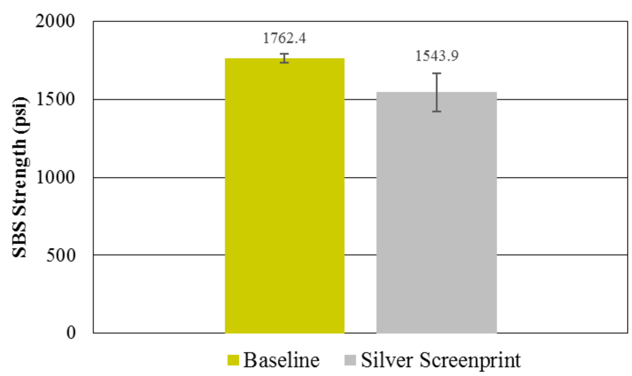

Figure 3.15 Short beam shear (SBS) results for baseline and silver conductive ink samples.

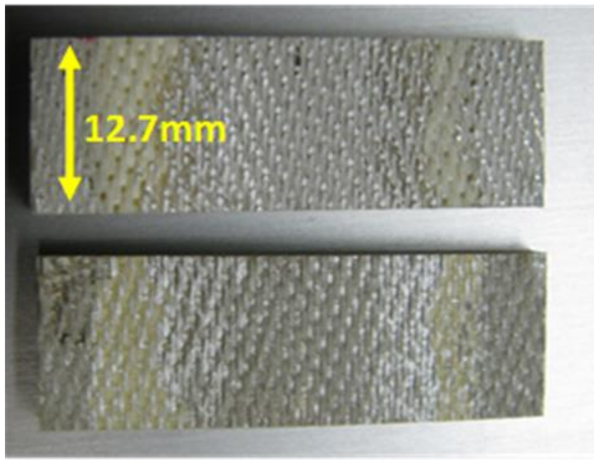

Figure 3.16 Silver conductive ink samples showing failure results of short beam shear. Failure mode indicates bond failure between silver conductive ink and resin

3.5.2 Floating Roller Peel

The floating roller peel test was performed to the ASTM D3167 standard. The control baseline contained 8 layers of BTCy-1 6781 8oz. S-glass producing a thickness of approximately 12.7mm after autoclaving processing as described above. Via a burn off procedure, we determined a fiber volume fraction of the baseline of 44.2%. A layer of release film was set 1 layer below the surface to allow for the test fixture (Figure 3.17). As per the ASTM standard, the control was cut to 6 samples of 12.7mm x 254mm. The experimental sample was fabricated using the same method as the baseline, with the modification that the sublayer below the release film was replaced with a dry sheet of s-glass printed with a continuous plane of silver conductive ink. The samples were loaded at a rate of 6 in/min with an Instron 5565 500N load cell. Figure 16 plots the results. The baseline sample reported an average peel strength of 20.714 +/- 1.059 N/cm. Inspection of the samples revealed a cohesive failure within the resin (Figure 3.18). The silver screen printed sample reported an average peel strength of 19.501 N/cm with a standard deviation of 1.14N/cm. Sample inspection showed adhesive failure between the silver conductive ink and the resin/fibers (Figure 3.19).

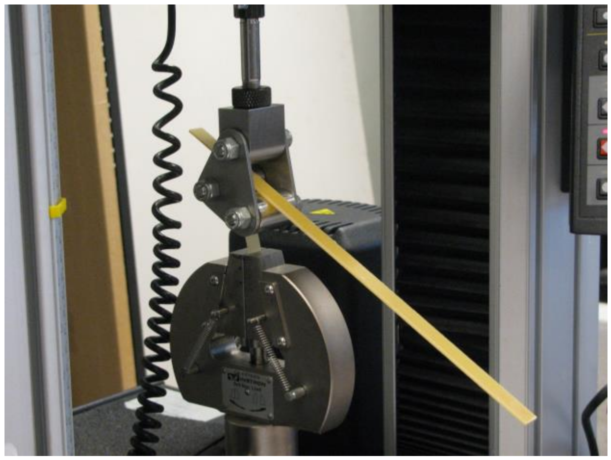

Figure 3.17 Floating roller peel test fixture loaded on an Instron 5565

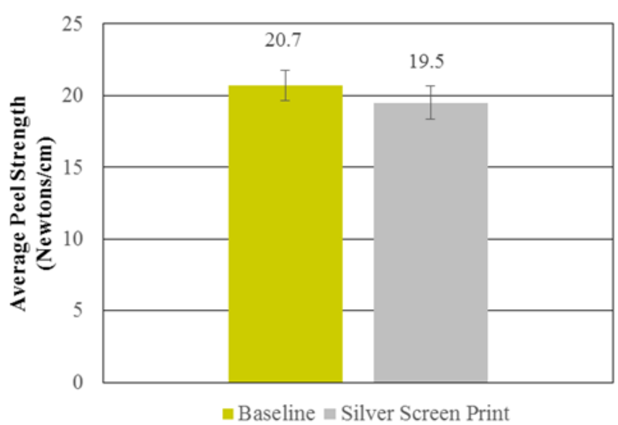

Figure 3.18 Floating roller peel results for baseline and silver conductive ink samples

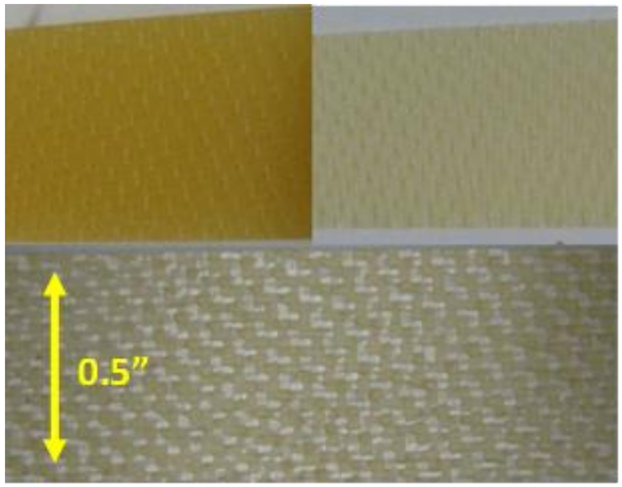

Figure 3.19 Failure mode results. Top: bottom (left) and top (right) layers of baseline sample show cohesive bond failure within the resin. Bottom: silver conductive ink samples show cohesive failure between the silver conductive particles and the resin.

3.5.3 Mechanical Summary

A fiber reinforced low EM loss composite with embedded silver conducting ground plane was evaluated for short beam shear strength and peel strength then compared against a baseline. The short beam shear strength of the silver printed sample was an average of 13% below the evaluated baseline. The printed sample also showed a much larger standard deviation against the baseline. The peel strength along the silver printed boundary showed promising results with only a marginal average decrease in peel strength of %6. This initial mechanical study certainly calls for a more in depth characterization of the mechanical impact of silver inclusions, however the initial results are promising towards integrated EM feeds and structures.

3.6 Conclusions

In this chapter, we investigated the high frequency conductivity of silver conductive inks embedded within a structural composite substrate. For the substrate, we used a low loss structural composite system S-glass/ BTCy-1 Cyanate Ester as it proved to be an adequate substrate for electromagnetic functionality integration. We compared transmission line simulated and measured values and confirmed the reported conductivity of the Methode 6130S silver ink on planar substrates. We also determined that this ink's conductivity on a fabric weave composite is 25% its conductivity on planar substrates at a single print pass. This lower conductivity is due to an inadequate amount of continuous silver printed on the composite fabric. Thus multiple print passes are necessary for increasing the conductivity so it approaches the values for planar prints. Our initial mechanical study of the silver printed composite samples provided promising results. Compared to continuous printed silver planes, our silver printed composites show an average decrease in shear strength of ~21% and in bond strength of ~6%. This study demonstrated the electrical and mechanical viability of embedding silver, printed electromagnetic systems within a truly structural composite.

Chapter 4

MICRODISPENSING OF STRUCTURALLY EMBEDDED ANTENNAS

In the previous two chapters, two different EM devices were fabricated within a structural composite by means of screen printing silver conductive ink onto a woven glass fabric. It was found on both occasions that the EM performance of these devices were reduced when screen printed onto the woven fabric composite as compared to both bulk conductors and the silver ink printed onto a planar and nonporous material. Reduced conductivity of screen printed inks may be outweighed by the high scalability of screen printing. For example, when engineering the RCS of structures by patterning an entire composite hull or deckhouse with an FSS. However, concerning feed structures and antennas, a reduction in conductivity has larger implications which directly increases attenuation and reduces range and gain. Microdispensing of conductive inks offers consistent deposition and smaller minimum feature sizes over screen printing at the cost of scalability. In this chapter, microdispensing is explored as a higher quality method of fabricating embedded antennas within a structural composite as shown in Figure 5.1

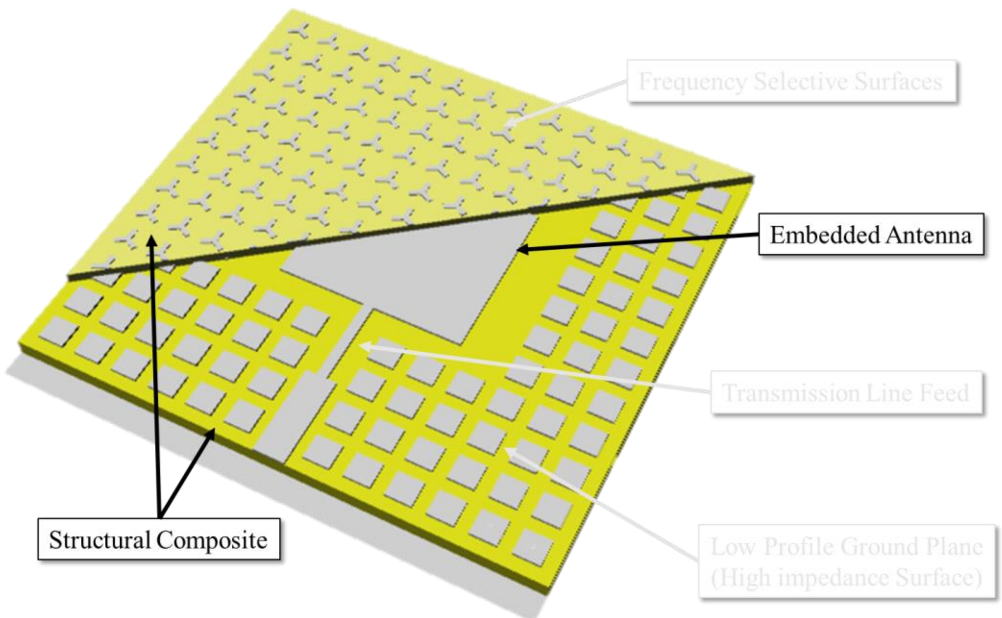

Figure 4.1 Example of a multifunctional composite with an embedded microstrip antenna and feed

4.1 Introduction

Microdispensing is a direct write process that deposits conductive inks onto a substrate without the need of a pre-patterned stencil [32, 33]. CT imagery of the previously discussed screen printed microstrip transmission lines, as shown in Figure 3.11, revealed that pressure from squeezing the conductive ink through the stencil onto the woven fabric forced conductive ink between fiber bundles and also left voids in the printed traces which ultimately reduced the effective conductivity of the printed conductors. In contrast, microdispensing is a gentler process of depositing ink that places no pressure on the substrate. The implications of this gentler deposition process allows the user to use lower viscosity and higher conductivity inks and will promote reduced voids and ink penetration into the woven fabric. The resulting conductive traces on woven fabrics can have a higher conductivity than those printed with screen printing technology. In this chapter, as the final portion for an EM multifunctional composite, a conformal load bearing antenna was fabricated and embedded within a structural composite. Microdispensing of conductive inks was used in place of screen printing as a conductor patterning method to enable the use of higher conductivity inks and faster relative throughput of prototype antennas.

4.2 Conformal Load Bearing Antenna Design

Conformal load bearing antennas are a specific class of antenna that are low profile and do not contribute to a structure's aerodynamic drag. Size, weight, and radar cross section (RCS) can all be reduced relative to standard protruding antennas in addition to performing as a load bearing member of a structure [3-9]. Several load bearing antenna structures in the literature have required the use of a secondary bonding to a composite enclosure or sandwich structure. In place of secondary bonded platforms, antennas that are printed directly onto fabric do not require the breaking of load bearing fibers or specific sandwich constructions. In addition, printed composite antennas are self-protected from environmental exposure and maximize the functional area of structures while performing as a load bearing member.

A microstrip patch antenna geometry was selected for this study. The patch antenna is a low weight and low profile antenna ideal for aerospace applications. The design and radiation characteristics of the antenna are well known. A reference for the design equations are included in [40]. The antenna consists of a square conductive patch and ground plane separated by a dielectric. The edge of the antenna is fed by a microstrip transmission line. A model for the antenna was designed in a commercial finite element analysis software (Ansys HFSS). Because the input impedance of square patch antennas are generally very high, it is difficult to match the feed with the antenna simply by feeding the edge of the patch. The input impedance decreases as the feed location approaches the center of the patch. To match the edge feed, an inset of patch was included to match impedance of the feed location to be 50 ohms. Circular polarization, as is used in GPS data transmission, was generated by truncating the corners of the antenna and offsetting the feed location relative to the center of the patch antenna. An optimization of the antenna geometry was performed in HFSS, the resulting antenna dimensions are shown in Figure 5.2 and detailed in Table 5.1. BTCy-1 6781 was selected as the antenna substrate material to be consistent with the previous sections. The material was modeled as isotropic dielectric with relative dielectric constant, ε_r, of 4 and loss tangent, $\tan(\delta)$, of 0.004.

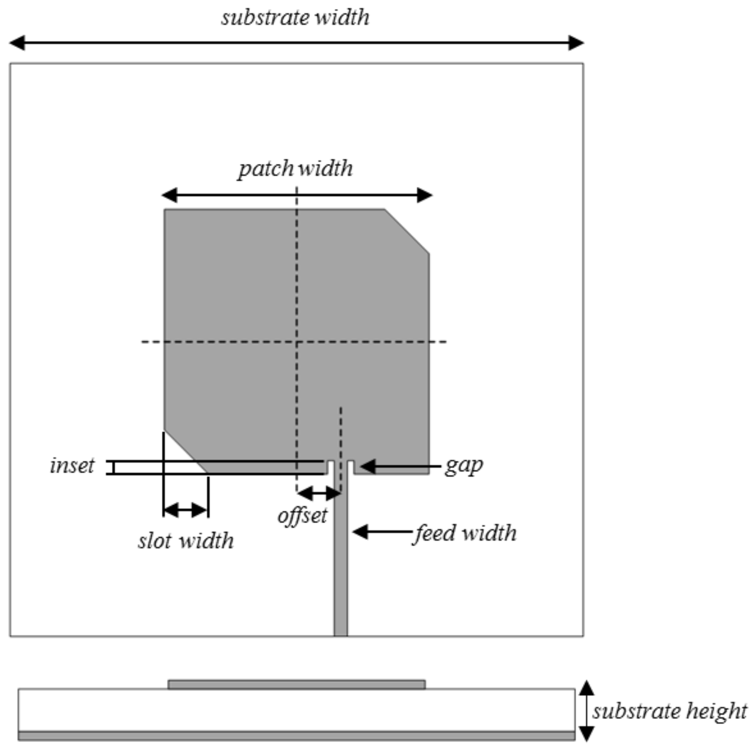

Figure 4.2 Microstrip antenna design with truncated corners to induce a circular polarization

Table 4.1 Optimized truncated patch antenna dimensions

substrate width	substrate height	patch width	slot width	offset	feed width	gap	inset
120mm	1.35mm	46.3mm	5.34mm	3.89mm	2.5mm	1mm	2.07mm

The modeled antenna shows a good impedance match at 1.575 GHz with a return loss of approximately -15dB as shown in Figure 5.3. The simulated axial ratio is shown in Figure 5.4. Satisfactory axial ratio performance is considered below 3dB. The 3dB bandwidth of the antenna is 50 MHz with a minimum of approximately 2.6 dB at 1.575 GHz.

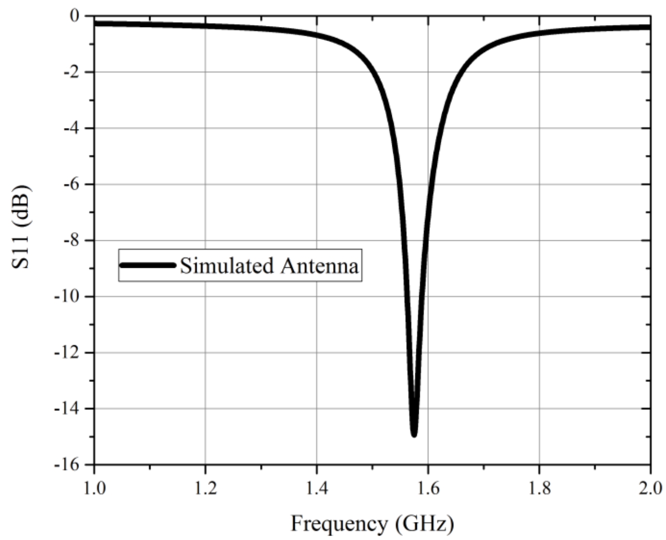

Figure 4.3 The modeled antenna shows a good impedance match at 1.575 GHz with a return loss of approximately -15dB

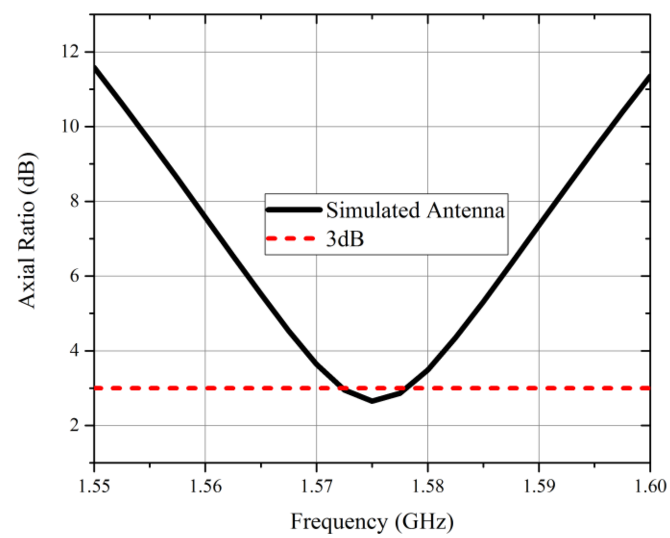

Figure 4.4 Simulated axial ratio of the GPS antenna at 1.575 GHz. 3dB band width is 0.05 GHz.

The radiation pattern of the antenna is simulated in Figure 5.5. Radiation into the half space is consistent with microstrip patch antenna geometries.

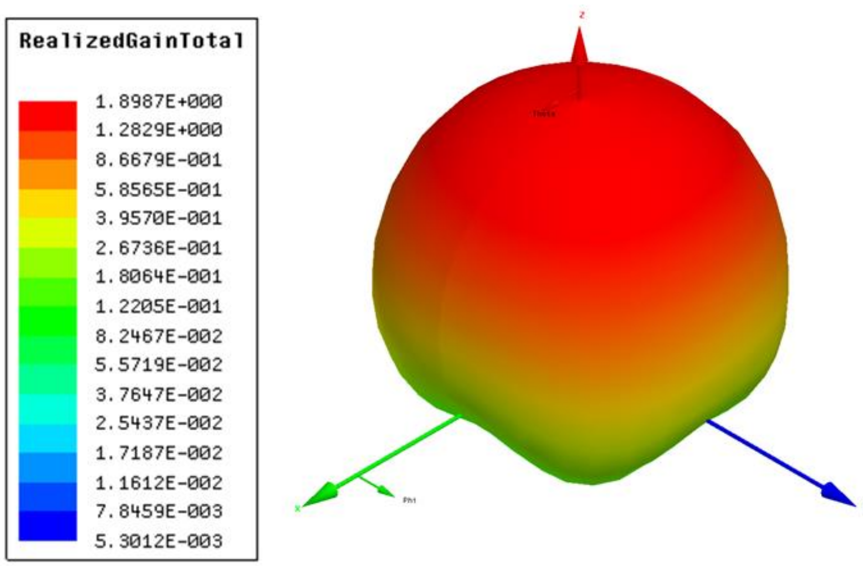

Figure 4.5 Radiation pattern of the microstrip patch antenna at 1.575 GHz

Figure 5.6 details the realized gain of the truncated microstrip patch antenna. A relatively low broadside gain of 3dB is observed but is consistent with circularly polarized microstrip antennas.

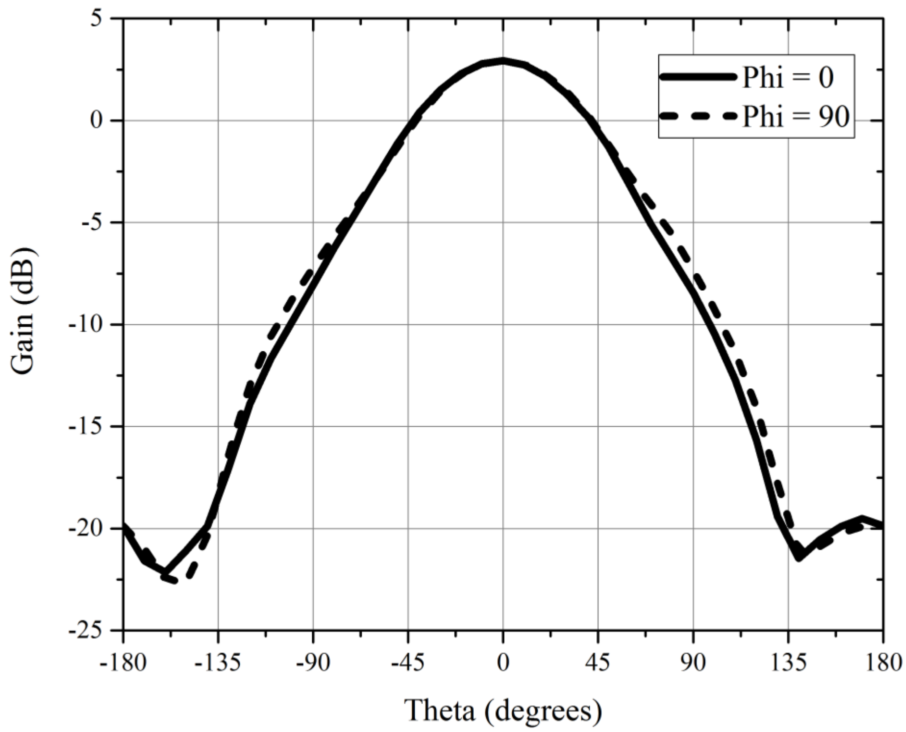

Figure 4.6 Simulated gain of the truncated patch antenna at 1.575 GHz. The maximum gain occurs at broadside radiation at approximately 3dB

4.3 Fabrication

An nScrypt 3Dn-300 microdispensing printed was used to fabricate the microstrip antenna. DuPont CB028 silver conductive paste was selected for its higher reported conductivity as compared to the Methode 6130S detailed in Table 2.3. The material was loaded in a 5mL syringe and deposited onto the 8oz 7 harness satin weave S-2 glass fabric picture in Figure 5.7.

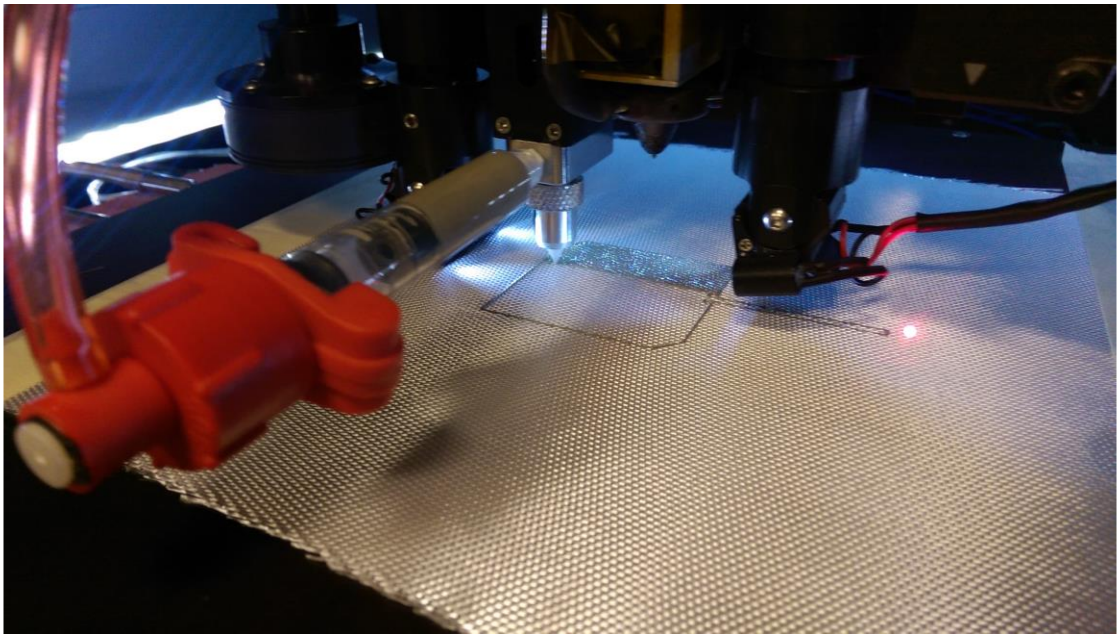

Figure 4.7 A close up view of the nScrypt microdispensing printer depositing DuPont CB028 silver conductive ink onto a woven glass fabric

The printed antenna and ground plane were heated in an oven at temperature of 160 C for one hour as per manufacturer specification to decompose volatile compounds and maximize conductivity. To achieve an approximate thickness of 1.35mm, four layers of the BTCy-1 6781 prepreg composite material was stacked in a midplane symmetric layup. The printed antenna and ground plane were placed on the top and bottom of the layup respectively. A small strip of non-bonding tape was placed on the edges of the microstrip feed and ground to ensure an exposed conductive area for connectors after composite processing. The completed layup is detailed in Figure 5.8.

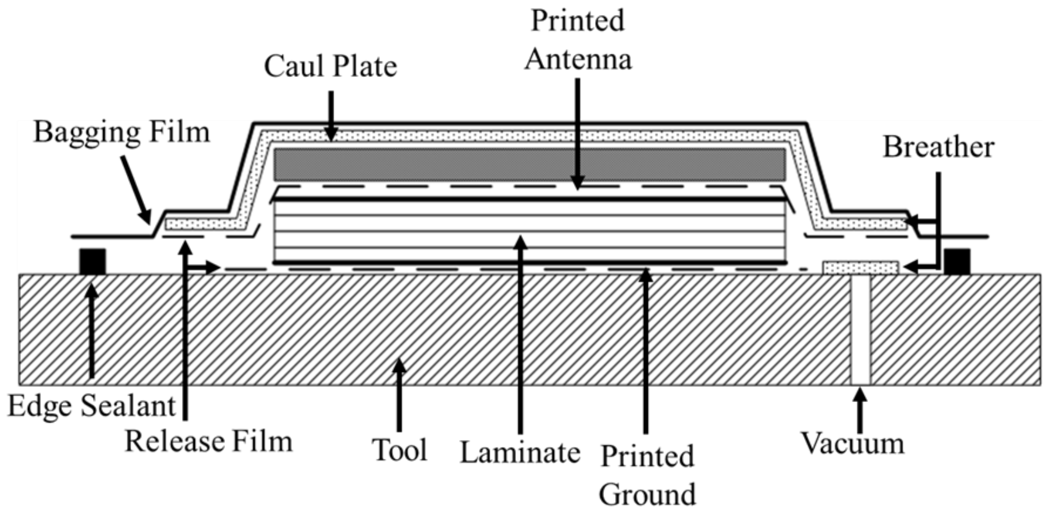

Figure 4.8 Autoclave Layup of GPS Antenna

The layup was processed in an autoclave in the same manner as described in previous chapters. Once cooled to room temperature, the finished composite laminate was removed from the autoclave and cut to shape by a diamond bladed table saw. Solderless Southwest end launch connectors were attached to composite antenna, as pictured in Figure 5.9. Good resin wetting was observed around the conductive printed areas as shown by a smooth surface finish. Small surface voids were observed on the non-printed composited areas indicative of insufficient resin content for the additional non-impregnated woven glass areas.

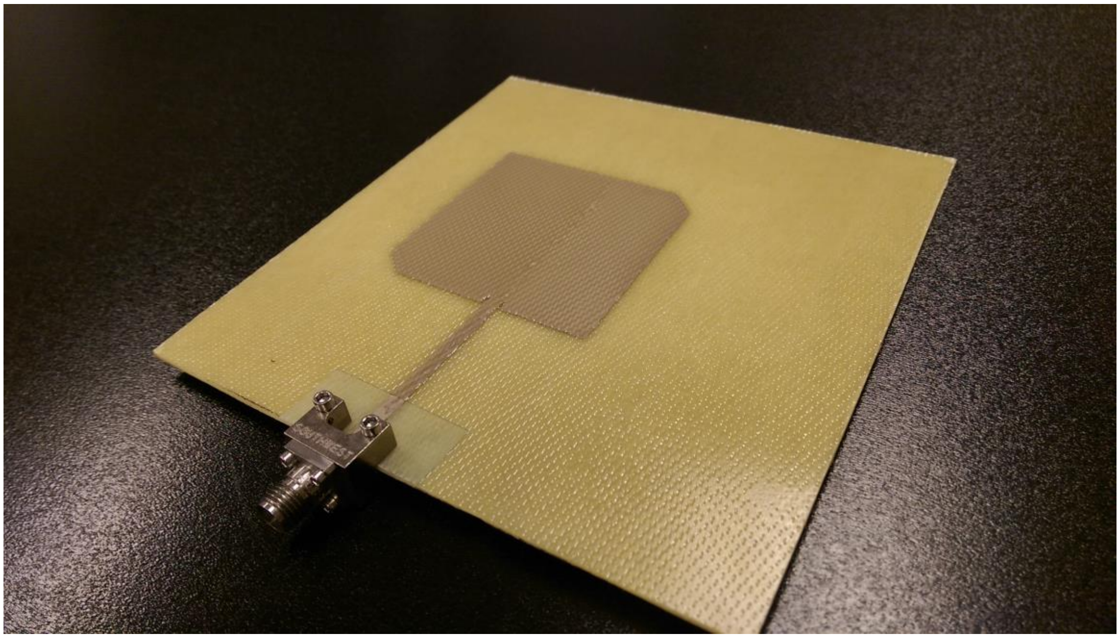

Figure 4.9 Image of finished composite embedded GPS antenna with attached connector

4.4 Measurement and Results

The antenna was connected to an Agilent E8364B portable network analyzer. A one port SOLT calibration was performed using an Agilent 85052D 3.5mm economy calibration kit. The antenna was measured between 1-2 GHz. The measured S_{11} results are plotted with the simulated antenna data in Figure 5.10.

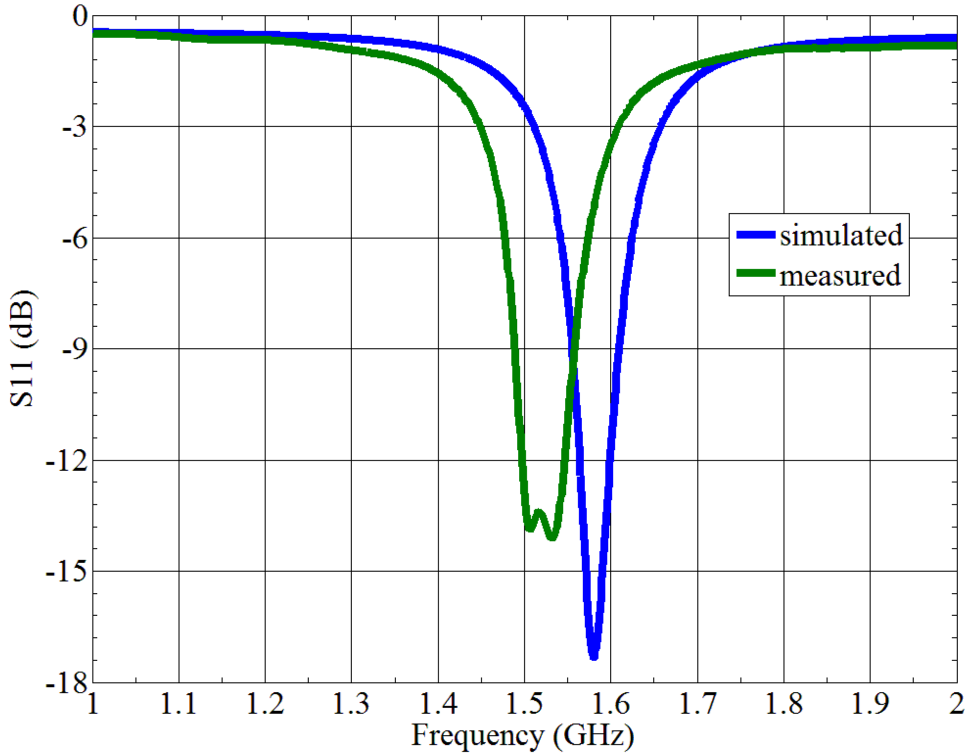

Figure 4.10 Comparison of the measured and simulated S_{11} of the composite embedded patch antenna

A 500 MHz shift downward in was observed in the measured antenna relative to the modeled antenna. In addition, a small impedance mismatch at the can be seen by the standing wave noticed on the measured S_{11} peak due to a wider feed width being fabricated than simulated. While the GPS L1 band is narrow at 1.575 GHz, the fabricated antenna would not operate well as a GPS receiver. A baseline composite was using the same layup of the embedded antenna was fabricated and found to have a dielectric constant higher than originally modeled. The corrected ε_r of the material was measured to be 4.25. Antenna geometry was re-optimized and is listed in Table 5.2.

Table 4.2 Re-optimized truncated patch antenna dimensions

substrate width	substrate height	patch width	slot width	offset	feed width	gap	inset
120mm	1.45mm	45.9mm	5.09mm	3.89mm	2.5mm	1mm	2.07mm

With the nScrypt microdispensing system, it was simple to modify the design and deposit the conductive ink with little lead time. Another antenna was fabricated using the same methods listed previously. The measured antenna and re-optimized simulation are shown in Figure 5.11.

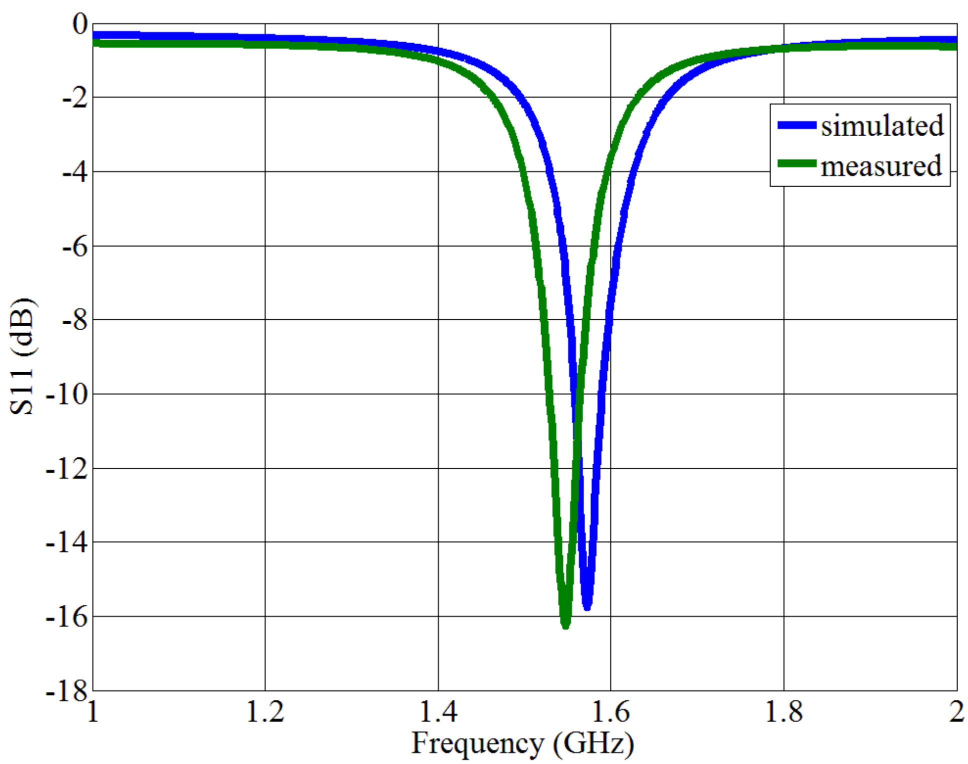

Figure 4.11 Comparison of the measured and simulated S_{11} of the second fabricated antenna

The second antenna similarly experienced a spreading of conductive ink, which increased the size of the geometry and the spread the inset feed. Unlike the first fabricated antenna, there are no standing wave influences on the measured S_{11}. Using this measured data, it is possible to determine an approximation of the printed ink conductivity. First, metrology was performed on the fabricated antennas to determine the actual physical dimensions of the microdispensed conductors. The measured dimensions are shown Table 5.3 for both antennas.

Table 4.3 Measured and simulated antenna geometries (dimensions in mm)

antenna	subst. width	subst. height	patch width	slot width	offset	feed width	gap	inset
Model 1	120	1.35	46.3	5.34	3.89	2.5	1	2.07
Fab. 1	120	1.45	47.36	5.64	3.89	2.82	0.75	1.82
Model 2	120	1.45	45.9	5.09	3.89	2.5	1	2.07
Fab. 2	120	1.45	46.4	5.64	3.89	3.33	0	0

The physical parameters measured in the second antenna were included in modeled antenna. Due to spreading of the ink, the matching gap and inset were removed from the model. Two parameters of the antenna were not possible to measure directly: effective dielectric properties of the composite and conductivity of the silver conductive ink when microdispensed onto structural woven fabric. These values were considered unknowns. A study was performed in HFSS to determine the effects of the substrate permittivity, Figure 5.12, and patch antenna conductivity, Figure 5.13, on the S11 of the embedded antenna.

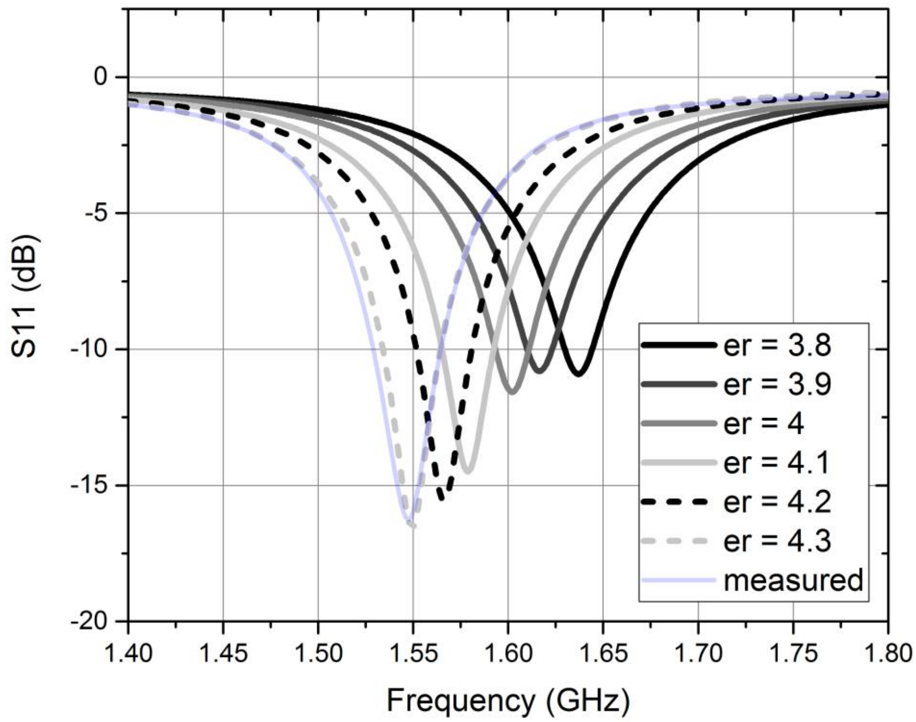

Figure 4.12 Dielectric study of the modeled composite substrate. It can be seen as the dielectric constant is increased the impedance match of the antenna predictably improves.

The dielectric study of the composite substrate permittivity shows as the permittivity increases, the resonance is shifted downwards in frequency, increased impedance match as the resonance depth increases, and a narrower bandwidth occurs. It is also observed that the simulated S_{11} converge very quickly at higher and lower frequencies relative to the resonance point for all simulated antennas. The influence of modeled silver conductive ink was more profound. A logarithmic study of the ink conductivity was modeled in HFSS. As conductivity decreases, bandwidth increases and attenuating influences can be seen at frequencies higher and lower relative to the resonance point. At two orders of magnitude below reported conductivity, the bandwidth is significantly larger and the -3dB S11 at frequencies outside of the resonance bandwidth indicates increased attenuation and reduced antenna efficiency.

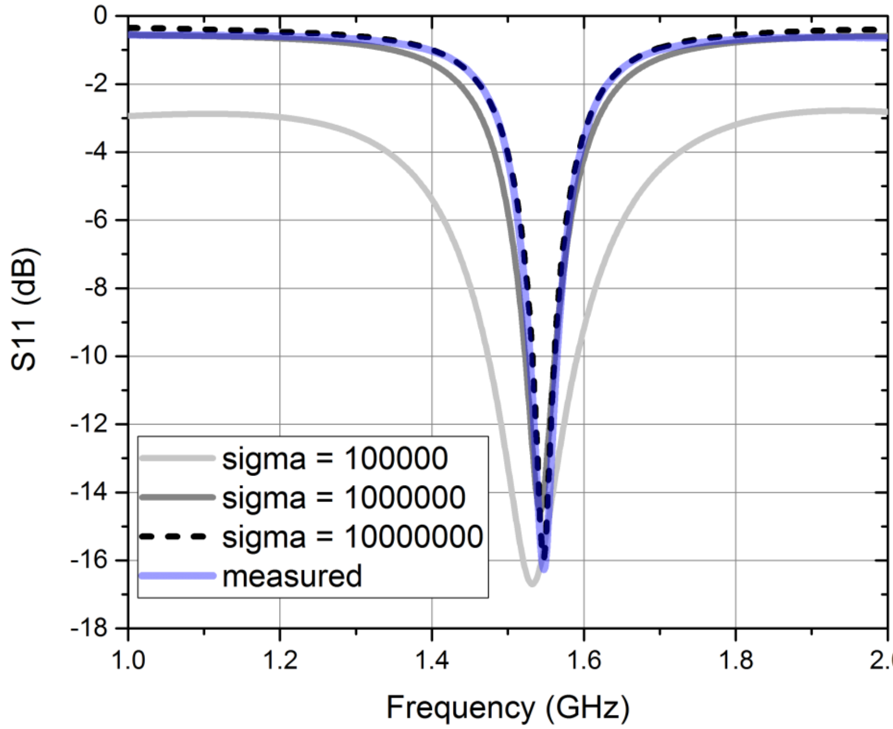

Figure 4.13 Conductive study of the modeled silver conductive ink.

Following the study, the unknown substrate permittivity and conductivity were optimized within HFSS. The known measured dimensions of the second antenna were kept constant. Resulting simulated and measured data compared in Figure 5.14.

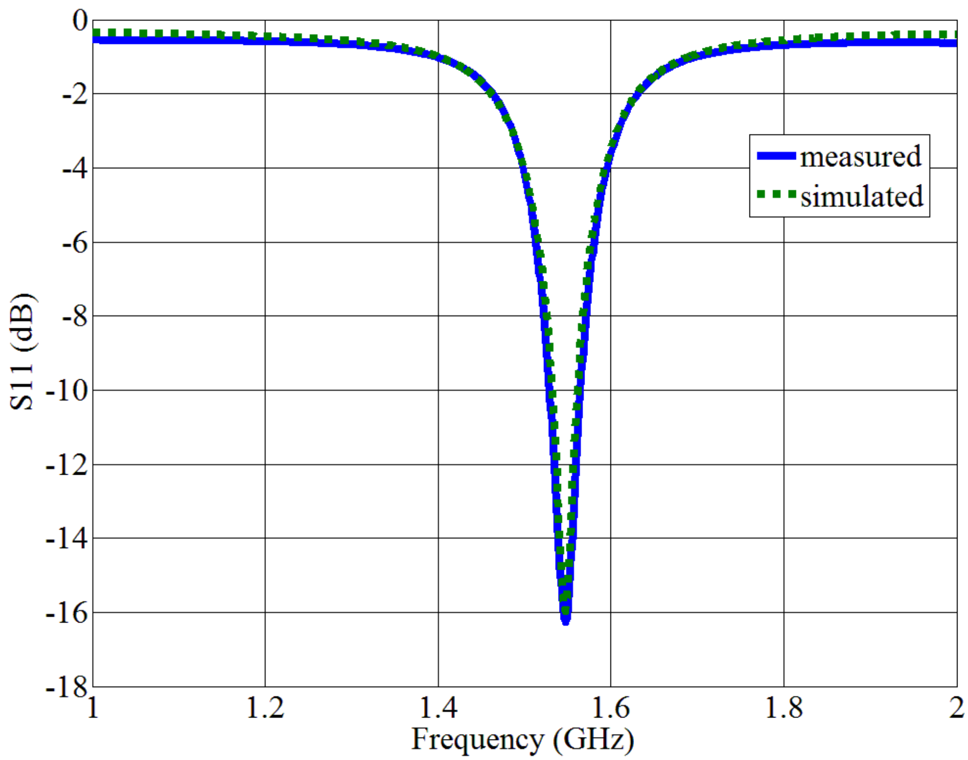

Figure 4.14 Corrected simulation of the antenna with conductivity values close to $1x10^7$ S/m and substrate permittivity of 4.25

The shift in frequency was represented by a substrate permittivity determined to be 4.25. The impedance match of the antenna resulted in a satisfactory return loss of -16.2 dB. S_{11} bandwidth is directly correlated with the conductivity of the antenna geometry. The measured data showed a slightly higher bandwidth than the simulated antenna with a conductivity set to the reported data sheet conductivity of the DuPont CB028, 1 x 10^7 S/m. This relatively high conductivity result is encouraging towards the development of embedded silver printed conductors. This results is also indicates that microdispensing can pattern conductors one order of magnitude higher than the conductivity measured via screen printing of silver conductive ink shown in Chapter 3.

4.5 Conclusions

In this chapter, a low profile microstrip patch antenna was designed, fabricated, and embedded within a woven fabric composite laminate via microdispensing of silver conductive ink. The antenna was measured and found to have a 500 MHz discrepancy and non-modeled standing wave when compared to the modeled antenna. Using the relatively little set up time and high throughput of microdispensing, another antenna design was quickly fabricated and measured. Although the second fabricated antenna was measured to have an operational frequency lower than modeled, good antenna impedance matching was observed. Metrology was performed on the antenna to determine the physical dimensions. A final model was used to match the modeled conductivity of the silver conductive ink when microdispensed on the woven glass fabric and found little impact to the data sheet reported conductivity.

Chapter 5

ADDITIVE MANUFACTURE OF STRUCTURAL FREQUENCY SELECTIVE SURFACES

In this chapter we investigated the use of additive manufacturing for embedding frequency selective surfaces (FSS) within a woven fabric structural composite. Specifically, we explored the use of both conductive screen printing and microdispensing as a low cost and scalable manufacturing process for realizing multifunctional structural composites that possess both good mechanical and electromagnetic (EM) properties. In addition, this is the first instance of a additively manufactured FSS within a structural composite. The FSS performance was also used as method of characterizing the effect of composite manufacturing process on the conductive properties of embedded conductive inks at high frequencies, i.e above 20 GHz. The FSS layers were fabricated by direct deposition of silver conductive ink onto a woven structural glass fabric. To evaluate this manufacturing process both capacitive and inductive FSS were designed within the Ka-Band (i.e. 26-42 GHz). The fabricated FSSs were then embedded within a woven fabric composite and experimentally characterized.

5.1 Introduction

Frequency selective surfaces (FSS) act as spatial filters that can be engineered to transmit or reflect incident EM radiation [37]. The integration of FSSs within a structural composite has been investigated in the literature using a variety of methods. A common fabrication methodology is adhering patterned copper foils within or on the surface of a composite laminate or composite sandwich structure [6]. Others have investigated using more textile approaches in which they interweave carbon fibers with glass fibers to create a frequency selective surface within a structural composite [9]. One concern with these approaches is the scalability of the manufacturing process to a large composite structure. For instance, patterning of copper films over large surface areas can be labor intensive and requires the use of various chemical etchants. Weaving of carbon fibers can be scaled to large surfaces using standard fabric looms, however, the electrical conductivity of the carbon fiber is orders of magnitudes below that of bulk copper. This results in a large degradation in EM performance. Moreover, the ability to create complicated geometrical features, such as those used in most FSS designs, is not easily accomplished using weaving techniques. Alternatively, additive deposition of conductive inks offers many advantages over comparable subtractive methods. The use of conductive inks for EM applications holds significant promise as a low cost, high volume manufacturing method for embedded structural electronics and EM components. The EM and mechanical compatibility of silver conductive inks embedded within woven fiber reinforced polymeric (FRP) composites was studied up to 4 GHz in the previous chapter and to 20 GHz in [16]. Higher frequency behavior (above 20 GHz) of silver conductive inks embedded within structural composites has not yet been reported.

In this chapter, we characterize the high frequency performance (> 20 GHz) of an embedded structural frequency selective surfaces fabricated via both conductive screen printing and microdispensing as shown in Figure 5.1. Specifically, we designed two FSS patterns, a band pass and band reject filter, and fabricated those designs via conductive additive manufacturing onto woven glass fabric substrates. The printed layers were then embedded and formed within a structural composite laminate and compared for EM performance.

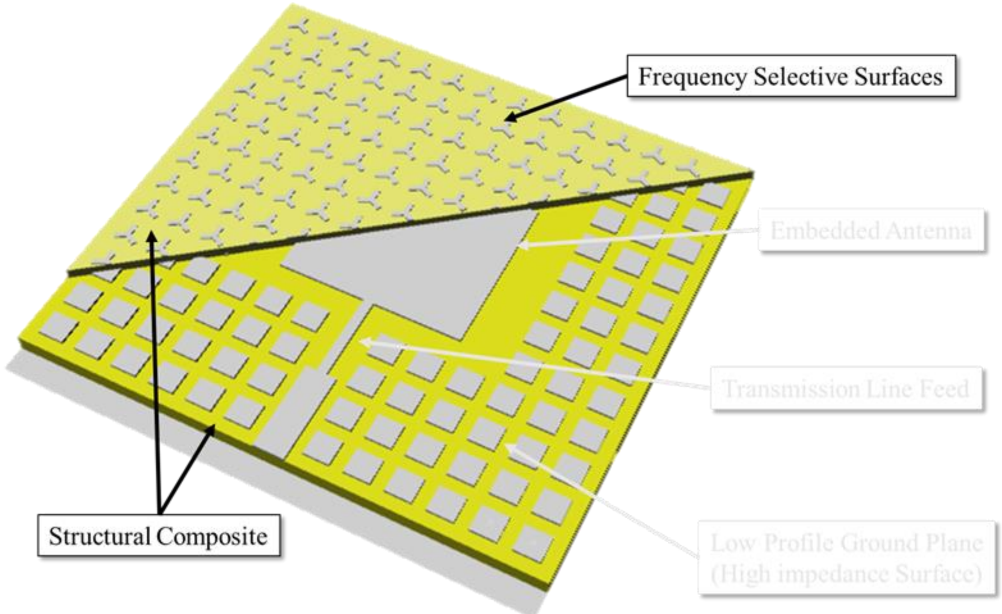

Figure 5.1 Multifunctional composite with embedded antenna and frequency selective surface

5.2 Design

The proper design of a FSS embedded multifunctional composite involves the simultaneous design of many critical parameters including: structural composite reinforcement and matrix, conductor fabrication, and frequency selective surface design. To study the high frequency properties of the silver screen printed ink embedded within the structural composite a series of frequency selective surface test samples were fabricated.

FSSs are a common means of reducing the radar cross section (RCS) of aircraft and an effective method of electromagnetic interference (EMI) mitigation [37]. Their ability to selectively transmit or reject incident electromagnetic (EM) radiation is used to only allow frequency bands of interest through to a receiver. There are a wide variety of possible element designs for specific filter responses such as band reject, band pass, dual resonance, etc. Categorically these are all variants on two basic designs shown in Figure 5.2, solid and slot type geometries also known as capacitive and inductive elements respectively.

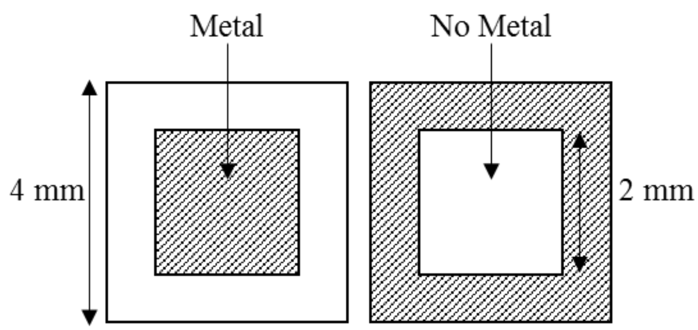

Figure 5.2 Frequency selective surface geometries can be categorized as capacitive (left) and inductive (right) with reciprocal filter responses. The hashed areas represent metallic material.

The most common of the surfaces are the passive type element that depend on incident radiation to excite currents on the array of metal elements, which selectively reflects or transmits the incident radiation. The frequency response is governed by element geometry and size. Capacitive type elements, pictured in Figure 2 left, are solid metallic shapes and behave as band-stop filters. Inductive type elements are the reciprocal of the capacitive type shape and in turn behave as band-pass filters. It is generally considered that resonance occurs when element size is approximately $\lambda/2$, where λ is the wavelength of the incident radiation. Both solid and slot type FSSs are presently investigated to cover the gamut of possible FSS designs that could be found in a practical structure. A square patch and slot FSS element were designed using a commercial finite element analysis software, Ansys HFSS. A design with a 2 mm square and slot at a 4mm period was selected for a resonance frequency at the center of the Ka-Band (35.5 GHz). A dielectric constant of 4.2 was assumed for the composite material substrate. The conductor used in simulation was based on the conductivity of copper. The simulated data is plotted in Figure 5.3.

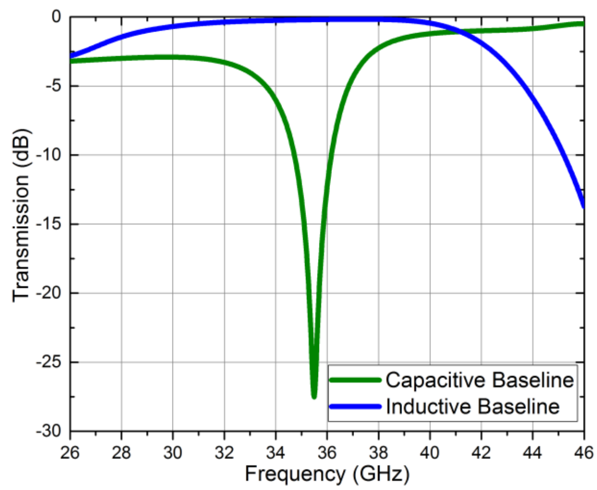

Figure 5.3 Simulated frequency response of the capacitive type FSS (green line) and the inductive type FSS (blue line). The capacitive type FSS behaves as a band stop filter centered at 35.5 GHz. The inductive type FSS shows band pass filter behavior with a peak approximately at 36.5 GHz.

5.3 Fabrication and Microscopy

The FSS geometries were directly printed onto a dry layer of the S-2 glass fabric. Composite processing of the structural FSS was consistent with the methods previously described. In the composite layup, to achieve a thickness of 2mm, the layup was consistent of 7 layers of BTCy-1 6781 prepreg in a unidirectional layup with the printed FSS fabric set in the midplane of the layup for a total of 8 plies of woven glass. The following sections cover the microscopy of the printed FSS elements.

5.3.1 Silver Screen Printed S-Glass

The Methode 6130S silver conductive ink was used as the screen printed conductive material. The higher viscosity of the conductive ink relative to the DuPont conductor was more suited to the screen printing process such that minimized ink spreading and permeating into the woven glass fabric. Microscopy of the screen printed FSS elements are shown in Figure 5.4. Spreading and slight rounding of corners of the capacitive elements can be seen from the 50x magnified image. The inductive FSS showed improved element accuracy with slight under printing of the element along the length of the glass fiber. Undulation of the conductive ink on the woven fabric can be seen on Figure 5.4. This was previously found in the previous chapter to ultimately reduce the conductivity of the silver ink and an effective increase of length.

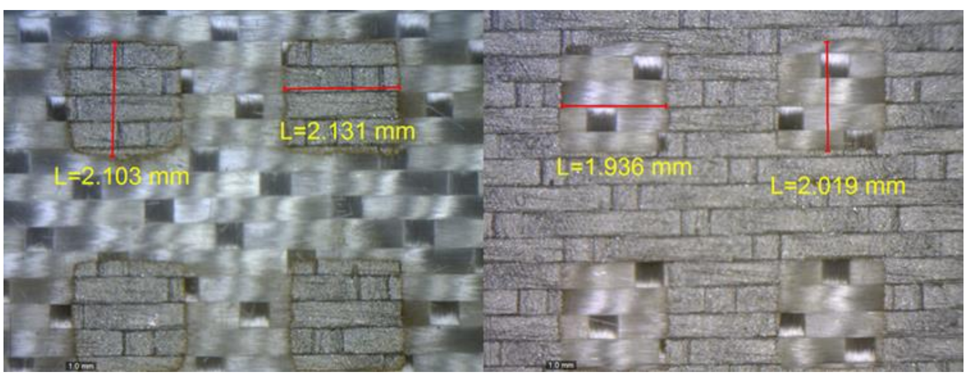

Figure 5.4 50x Magnification of 7 harness S-2 Glass after Methode 6130S silver conductive ink screen printed FSS after 45 min at 90 C. Undulation of the conductive ink appears as the ink conforms to the woven fabric.

The cross section microscopy of the finished composite, shown in Figure 5.5, demonstrates the undulation of the silver conductor to the weave of the fabric. It is apparent from the cross section images that the thin deposition of conductive ink conforms to the weave of the fabric. The approximate print thickness was measured to be 43 µm.

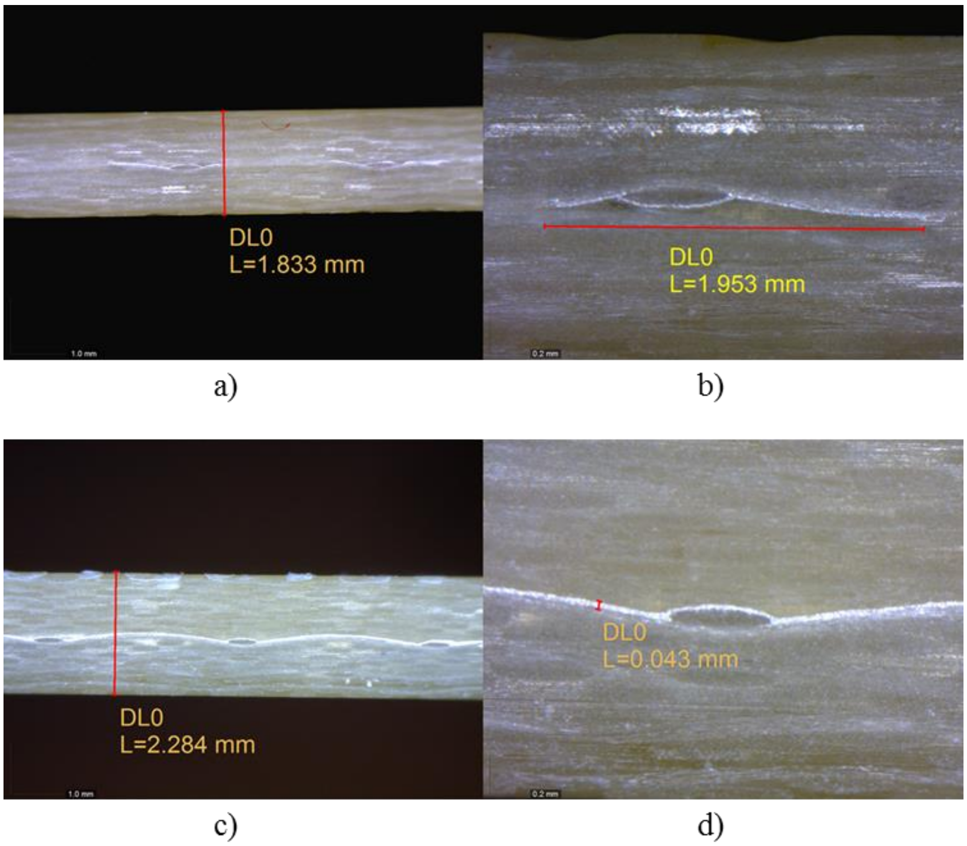

Figure 5.5 Cross section microscopy of the screen printed composite FSS. a) 50x magnification of the capacitive FSS. b) 200x magnification of a capacitive patch element shows thin deposition and conforming to fiber bundles. c) 50x magnification of inductive type FSS with a semi-continuous deposition. d) 200x magnification of inductive FSS with a silver ink thickness of approximately 43 µm.

5.3.2 Microdispensed FSS on S-Glass Fabric

The microdispensing of the FSS geometries was performed using the DuPont CB028 silver conductive ink. It was previously determined that the lower viscosity ink demonstrated conductivities higher than the comparable Methode 6130S when printed onto fabric at low frequencies. Additionally, the microdispensing deposition method does not apply pressure onto the woven fabric substrate. This prevents the lower viscosity conductor from permeating into the woven fabric and improved conductivity. Microscopy of the microdispensed FSSs are shown in Figure 5.5.

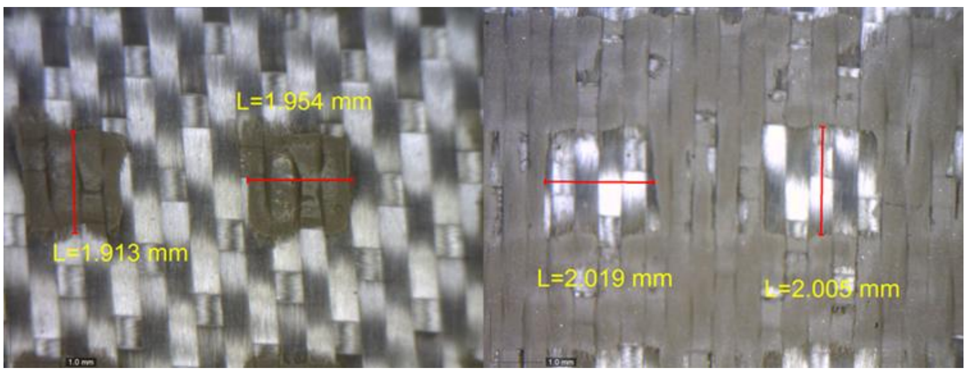

Figure 5.6 50x Magnification of Methode 6130S silver conductive ink screen printed onto Kapton polyimide. Spreading of the conductive ink on the Kapton was observed.

The microdispensed geometries showed large inconsistencies when printing small elements over large surface areas. The capacitive elements showed high rounding of the corners and inconsistent deposition around the edges. Inductive printed geometries showed improved slot resolution, but inconsistent printing with many breaks and gaps in the printed FSS. The cross section microscopy of the finished composite samples are shown in Figure 5.6.

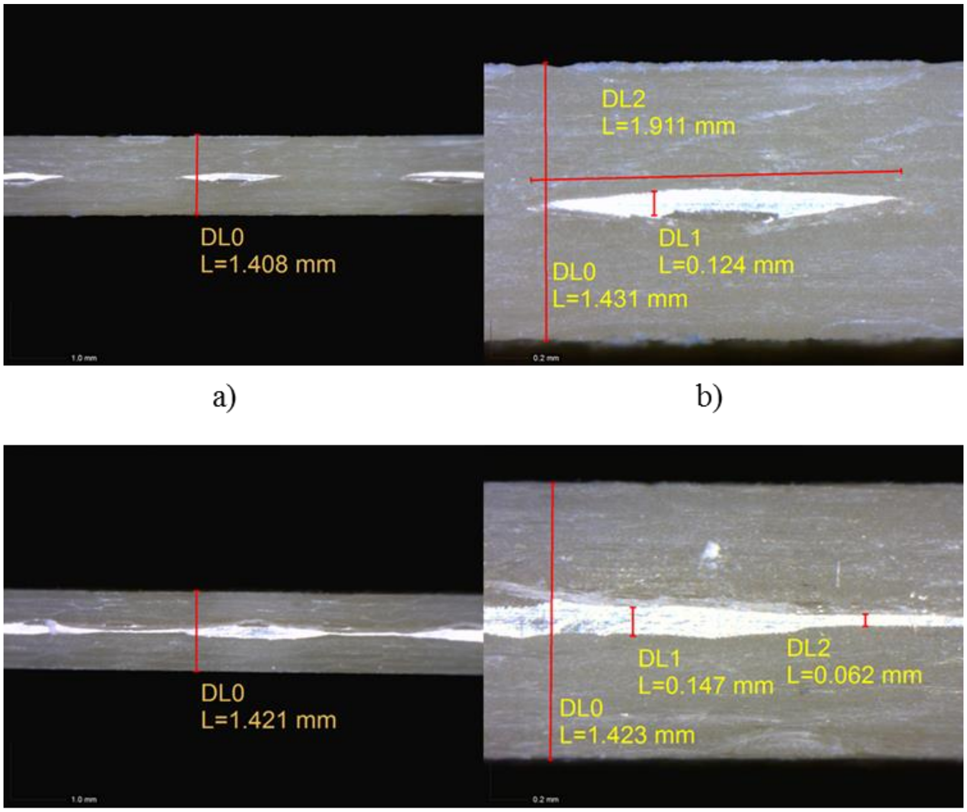

a) b) c) d)

Figure 5.7 Cross section microscopy of the microdispensed composite FSSs. a) 50x magnification of the capacitive microdispensed square element. The composite thickness was notably thinner than the screen printed samples. b) 200x magnification of the capacitive element shows significantly thicker deposition of conductive ink at 124 µm and pinching at the edges. c) 50x magnification of the inductive wire elements. Thick and thin areas are representative of double printed overlap areas. d) 200x magnification of the inductive wires.

The microdispensed conductors were significantly thicker, between 60-147 µm, than the screen printed counter parts. A clear boundary between the conductive ink and the woven fabric is demonstrated by the sharp lines of the printed elements. Pinching of the capacitive elements is also shown at the edges. Overlapping of the printed inductive surfaces resulted in a thick and thin depositions. Although the microscopy of the dry microdispensed elements showed inconsistencies in the printed elements, it is apparent from the cross sections that there is still a significant volume of deposited conductors.

5.4 Results

5.4.1 Measurement Setup

The material under test (MUT) was placed in a sample holder within an anechoic chamber, pictured in Figure 5.9, lined with radar absorbing material to minimize scattering. Dual focused beam antennas were mounted on linear translational stages and spaced at a 30 inch focal distance from the MUT. The antennas were connected to an Agilent E8364B portable network analyzer and were calibrated using a THRU open air transmission.

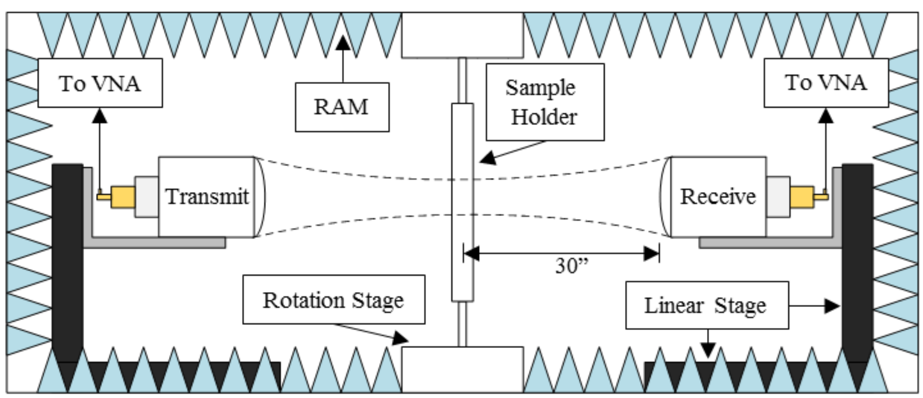

Figure 5.8 Focused beam antenna measurement system inside of a radar absorbing anechoic chamber. The samples are placed in a sample holder connected to a rotational stage at the 30” focal distance of the antennas. Antennas are connected to a portable network analyzer and are swept from 26-42 GHz.

5.4.2 Results: Screen printed FSS

The FSSs were measured at two different polarizations, 0º and 90º, relative to the weave of the printed fabric shown in Figure 5.8. The influence of the woven fabric produces an anisotropy in the conductivity and filter response of the capacitive FSS. When the electric field was aligned with the long weave of the satin fabric, 90º orientation, the transmission response of the FSS improved 4dB over the 0º orientation.

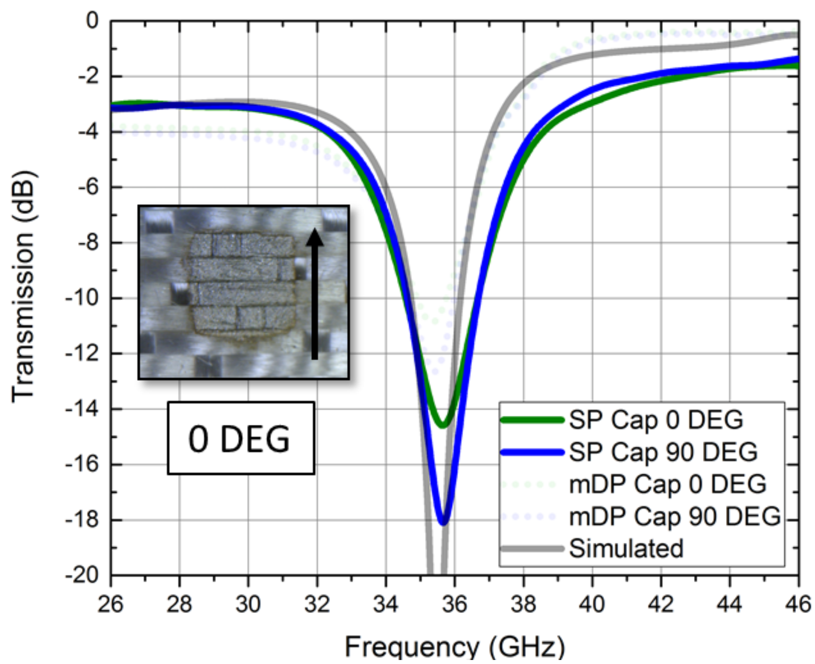

Figure 5.9 Measured transmission response of the screen printed (SP) capacitive FSS.

The screen printed inductive type FSS was also measured at two different polarizations, Figure 5.9. Interestingly, there is no apparent polarization dependence of the FSS and shows good performance relative to the simulated FSS using a copper conductor.

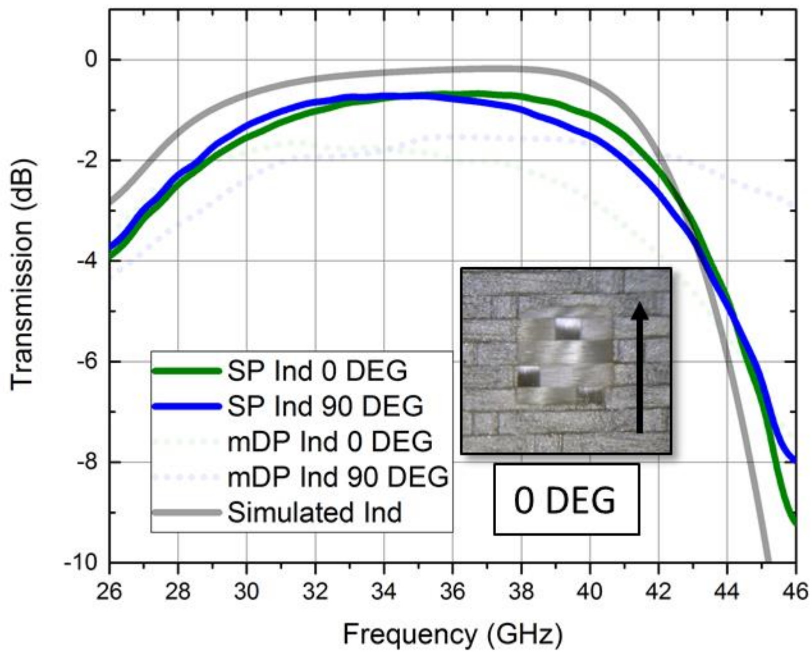

Figure 5.10 Measured transmission response of the screen printed (SP) inductive FSS.

5.4.3 Results: Microdispensed FSS

The capacitive type microdispensed FSS showed a similar polarization dependence with a polarization difference of approximately 2dB, shown in Figure 5.10. This polarization dependence was consistent with electric field alignment at the 90º polarization as was seen with the screen printed FSS. The filter response was measured to be lower than the screen printed capacitive FSS with a 6dB discrepancy at the 90º polarization. There was a large inconsistency in the amount of conductive ink that was microdispensed between square elements. This would have significant impact on the filter response and depth that was measured.

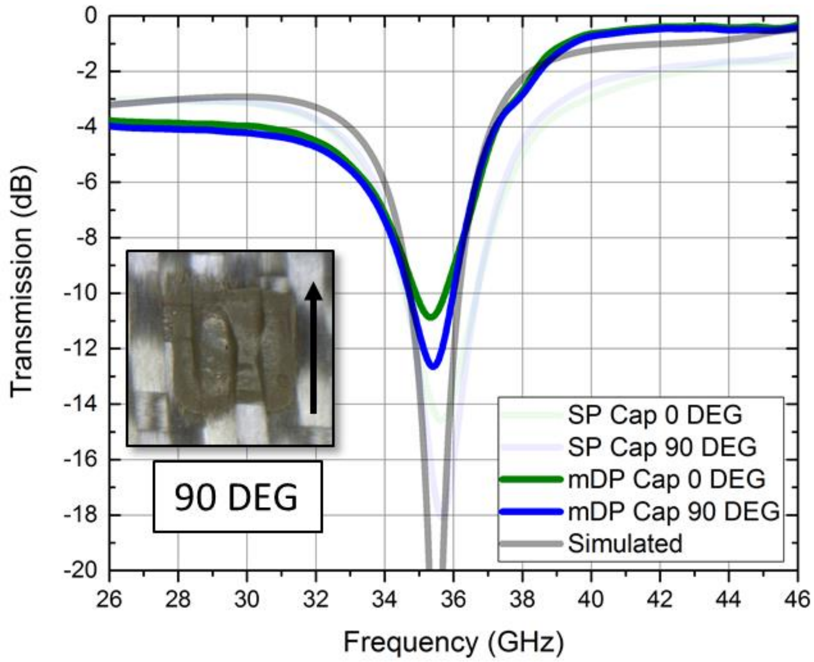

Figure 5.11 Measured transmission response of the microdispensed (mDP) capacitive FSS

The inductive type microdispensed FSS was measured to have a significant polarization dependence as seen in Figure 5.11. A large shift in the maximum of the band pass filter was measured between polarizations and an apparent increase in bandwidth occurred in the 90º polarization relative to the 0º. The microdispensed inductive FSS also was measured to have a maximum band pass response 1dB below the screen printed inductive FSS. The reduced performance of the microdispensed FSS is also conclusive of the inconsistent deposition of conductive ink influencing the filter response.

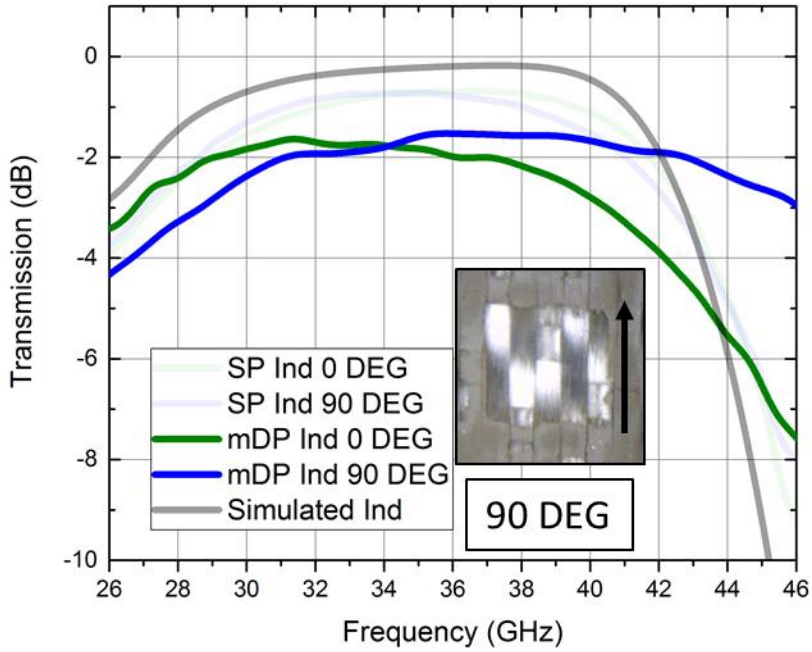

Figure 5.12 The inductive type microdispensed (mDP) FSS was measured to have a significant polarization dependence

5.4.4 Results: Comparison of the Additively Manufactured FSS

A comparison of all the measured data of the capacitive and inductive type FSS are shown in Figure 5.12 and Figure 5.13. The polarization dependence of the all the FSSs is clear in all measured samples with the best resonance depth of the 90º orientation. It is apparent that when the electric field is aligned with the length of the satin weave, there is an increase in conductivity seen by incident radiation. The consistent printing of the screen printing clearly performed better than the inconsistent ink deposited by microdispensing.

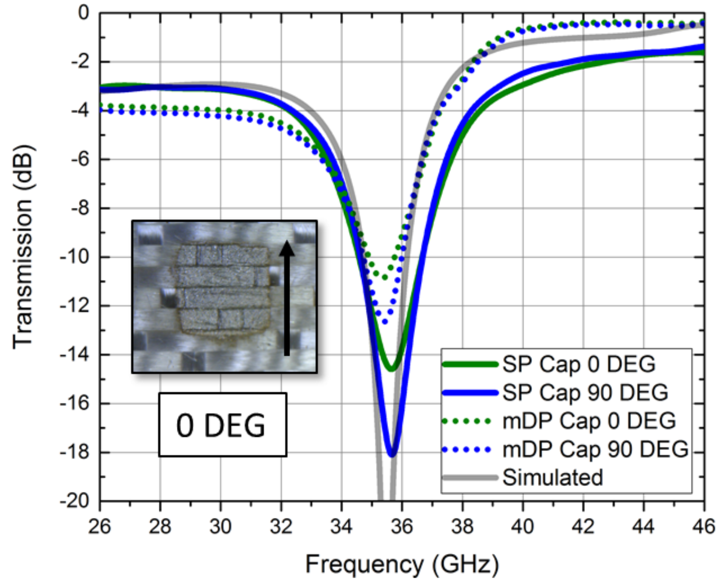

Figure 5.13 Comparison measured screen printed (SP) and microdispensed (mDP) capacitive FSS

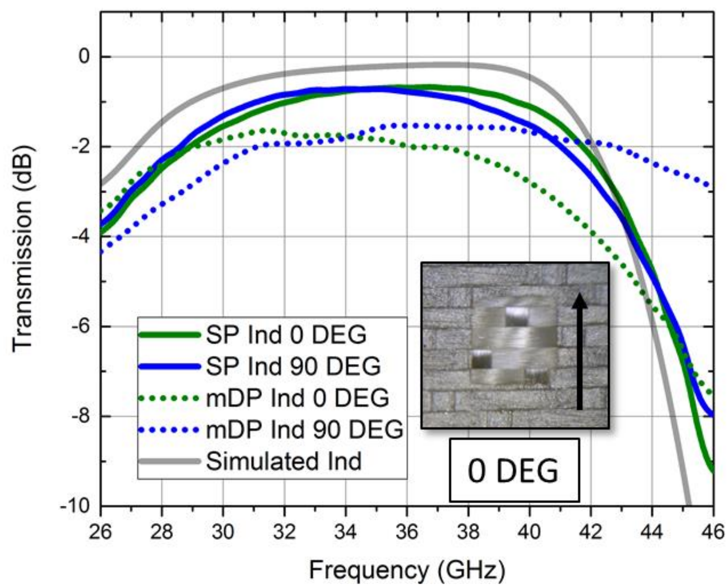

Figure 5.14 Comparison measured screen printed (SP) and microdispensed (mDP) inductive FSS

5.5 Conclusions

In this chapter, an electromagnetic multifunctional composite was fabricated by embedding two additively manufactured frequency selective surfaces within structural composites. The two additive manufacturing methods, screen printing and microdispensing, were compared against each other and the filter response of the fabricated frequency selective surfaces were used as a metric to determine the influence of the conductive ink at high frequencies, above 20 GHz. Screen printing of the lower conductivity ink, although had a lower bulk conductivity, produced more consistent geometries resulting in improved filter responses of both the capacitive and inductive type frequency selective surfaces. The microdispensing, although used higher conductivity inks, showed poor performance relative to the simulation and screen printed surfaces. We can expect that the filter response of the microdispensed surfaces can be improved by increasing the resolution of microdispensed geometries. In both surfaces, an anisotropic behavior was observed in the filter response of the capacitive type frequency selective surfaces. This can be considered and modeled as an anisotropic conductivity that is dependent on the weave of the printed fabric. In future work, improved microdispensing of the frequency selective surfaces and a model of the anisotropy of the printed conductive inks on woven fabrics will be explored.

Chapter 6

ADDITIVE MANUFACTURE OF EMBEDDED ANTENNA AND LOW PROFILE GROUND PLANE

It was shown in [41] that the optimal stand-off distance of an antenna above a conducting ground plane can be reduced by patterning the surface with a special texture, also known as a high impedance surface (HIS). The design of this surface requires a three dimensional network of conductors that is difficult to fabricate using traditional subtractive methods. In place of milling and photolithography, additive manufacturing (AM) fabricate structures layer by layer. Using multiple material AM, it is possible to build a three dimensional network of conductors embedded within a solid structure without sacrificing structural integrity.

In this chapter I present a low profile antenna, including an integrated high impedance surface (HIS) ground plane, fully fabricated using multi-material additive manufacturing (AM). It is shown that by combining standard fused deposition modelling (FDM) with conductive micro-dispensing printing it is possible to realize mechanically robust antenna systems that contain spatially variable dielectric properties and intricate 3D conducting networks. To illustrate this capability a low profile antenna, consisting of a standard 2.6 GHz half wavelength printed dipole, balun and AMC ground plane, was designed, fabricated and experimentally validated. The various dielectric constants implicit in these structures are usually multiple substrate layers with different dielectric properties. This is replaced with a single thermoplastic material where the dielectric constant is varied spatially by geometrically controlling the local fill volume. The input impedance and radiation pattern of the fabricated antenna were measured and compared to predicted results.

6.1 Low Profile Ground Plane and Dipole Antenna Design

The gain of most antennas can be enhanced by placing a reflecting backplane, also known as a ground plane, some distance, *h*, behind the antenna. The optimal position for antenna above a conducting ground plane is λ/4, such that the reflected energy from the ground plane undergoes a full 2π phase cycle [36]. At low frequencies, the optimal λ/4 distance becomes very large and unpractical for low profile structures. Sievenpiper et. al. [41] showed that by replacing the conductive ground plane with a HIS it is possible to create a much thinner antenna. The HIS reduces the minimum stand-off distance of an antenna above a ground by having a frequency dependent reflection phase that switches polarity and crosses a 0 phase point as shown in Figure 6.1

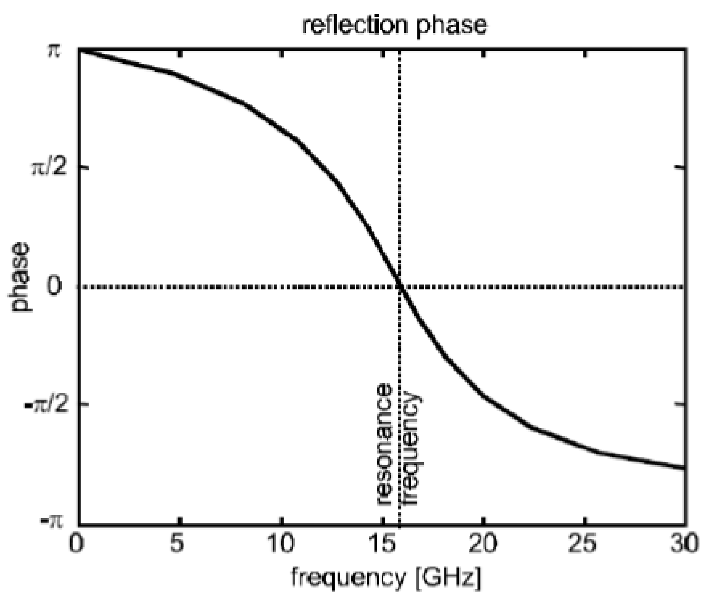

Figure 6.1 Frequency dependent reflection phase of a high impedance surface. The 0 degree crossing point is considered the operational frequency.

At the resonance frequency, the 0 crossing point, the HIS reflects incident radiation consistent with a perfect magnetic conductor (PMC). This is also the reason why the HIS is also known as an artificial magnetic conductor (AMC). It was recently found in [42] that the optimal reflection phase is not necessarily at the 0 degree phase point and is in fact dependent on the geometry of the antenna. Moreover, by including conducting vias it is possible to block surface waves within a designed bandgap.

Following the approach described in [41] and [42] an edge fed parallel strip $\lambda/2$ dipole and HIS were designed using Ansys HFSS. The dipole antenna was designed on a dielectric material of 2.9 to represent a bulk polycarbonate material. The signal arm was designed on the top surface of the substrate. The balun and ground arm of the antenna are on the bottom of the dielectric. The total arm length of the dipole antenna was designed to be 45mm. The antenna was also fed by a 50 ohm microstrip. The ground plane of the microstrip was linearly tapered to act as a balun. The S_{11} and the radiation pattern are shown on figures 6.2 and 6.3 respectively.

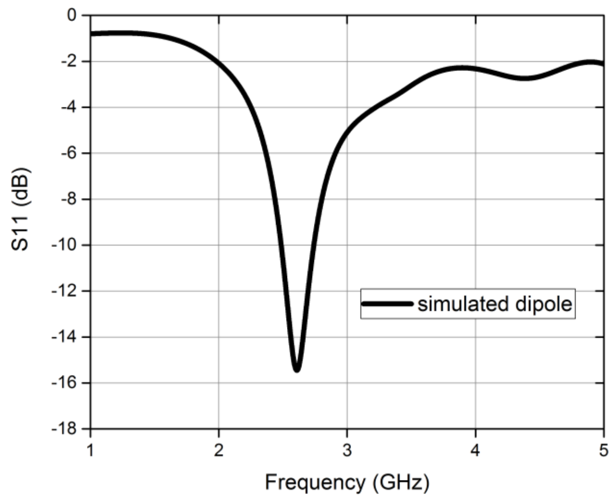

Figure 6.2 Simulated S11 of the freestanding dipole antenna with balun

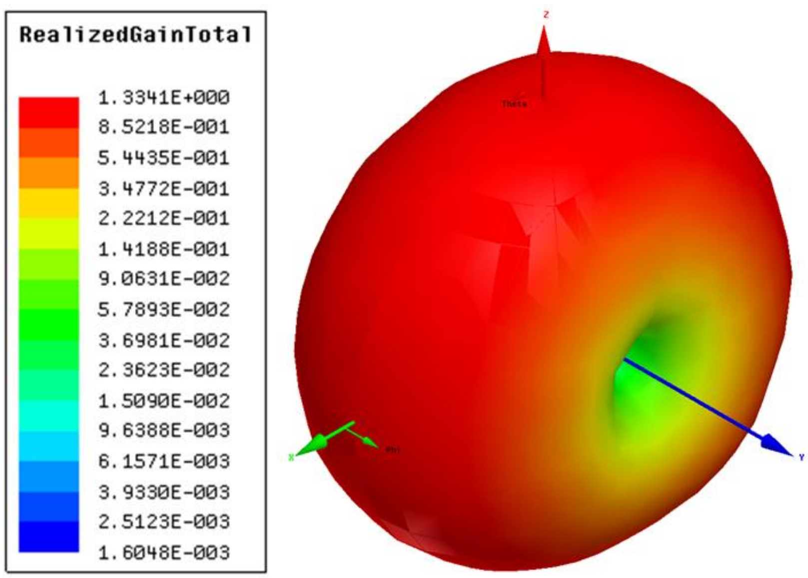

Figure 6.3 Simulated radiation pattern of the freestanding dipole antenna and balun

Since its inception, numerous designs that behave as a HIS have been proposed on a variety of materials including PCBs and textiles [41-46]. The design chosen for this study was the original mushroom type structure proposed in [41]. The design consists of an array of conducting squares connected to a continuous ground plane as shown in Figure 6.4. The dimensions of the HIS were optimized to have a 90° reflection phase at the operational frequency of 2.6 GHz shown in figure 6.5.

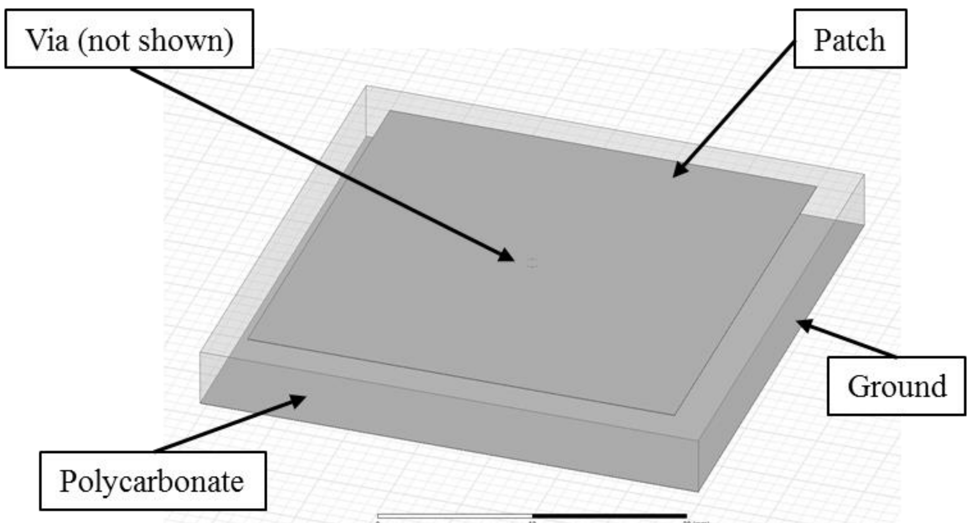

Figure 6.4 HFSS model of a unit cell of the HIS. Centered in the patch is a grounding via connecting the patch and ground

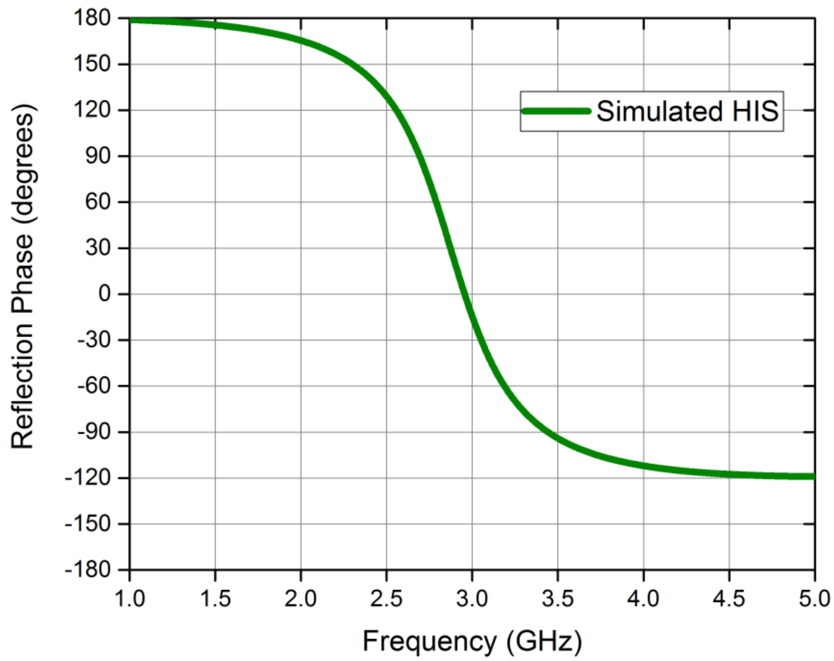

Figure 6.5 Simulated data of the frequency dependent reflection phase of the HIS. The HIS was designed to have a 90 degree reflection phase point at 2.6 GHz as is consistent with the results in [37]

The final antenna design and material properties are presented in Figure 6.6 and Figure 6.7. A 5mm spacer was designed between the antenna and HIS to minimize coupling the antenna and HIS. Because the material is fabricated additively, the effective dielectric properties of the substrates can be controlled. The dielectric constants of the HIS substrate, spacer layer and antenna layer were optimized and found to be ε_{HIS}=1.75, ε_{spacer}=1.5 and $\varepsilon_{antenna}$=2.9 respectively. As described in more detail later, to realize these dielectric constants the FDM process was used to control the local fill volume of a low loss thermoplastic (polycarbonate) material.

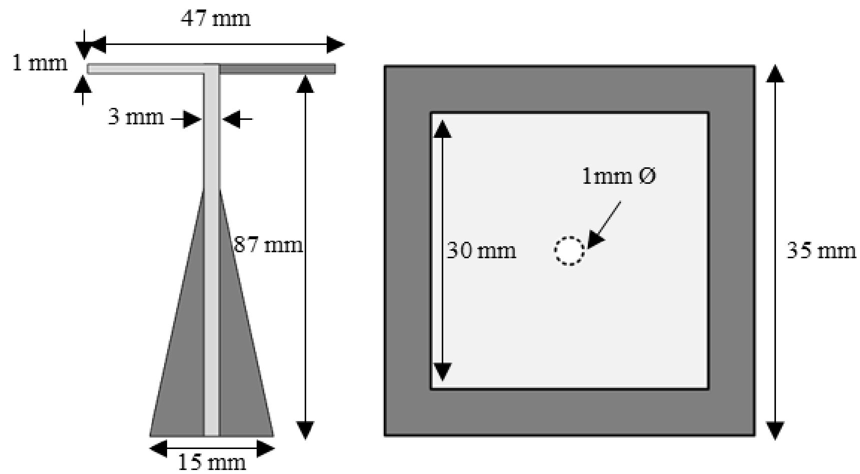

5

Figure 6.6 Detailed view of the dipole with balun and the HIS.

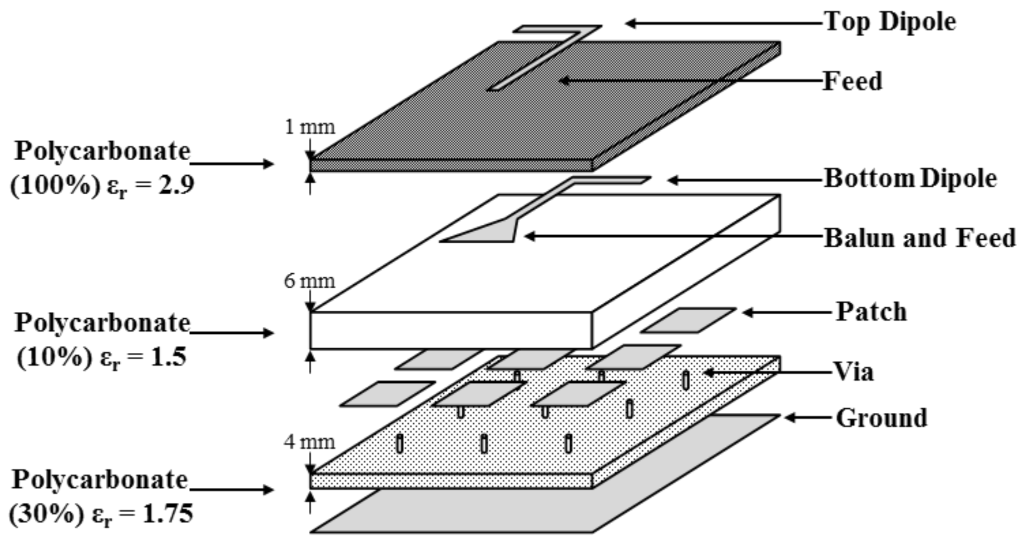

Figure 6.7 Exploded view of the antenna and high impedance surface configuration. The antenna was printed on fully filled polycarbonate substrate. The antenna and HIS were separated by a sparsely filled spacer with a 10% fill for a low dielectric constant. The HIS was fabricated with a controlled dielectric constant to tune the operational frequency of the HIS.

The full HFSS model is pictured in Figure 6.8. In the model, the antenna was excited by a lumped port between the microstrip feed and the tapered ground. The simulation was performed for the antenna in freestanding (no ground), 6mm above a PEC, and 6mm above the HIS. The results are shown in figure 6.9. It is apparent from the simulation results, that antenna S_{11} is seriously degraded when 5mm above a PEC. S_{11} of the antenna when operating above the HIS experiences a shift and broadening in frequency.

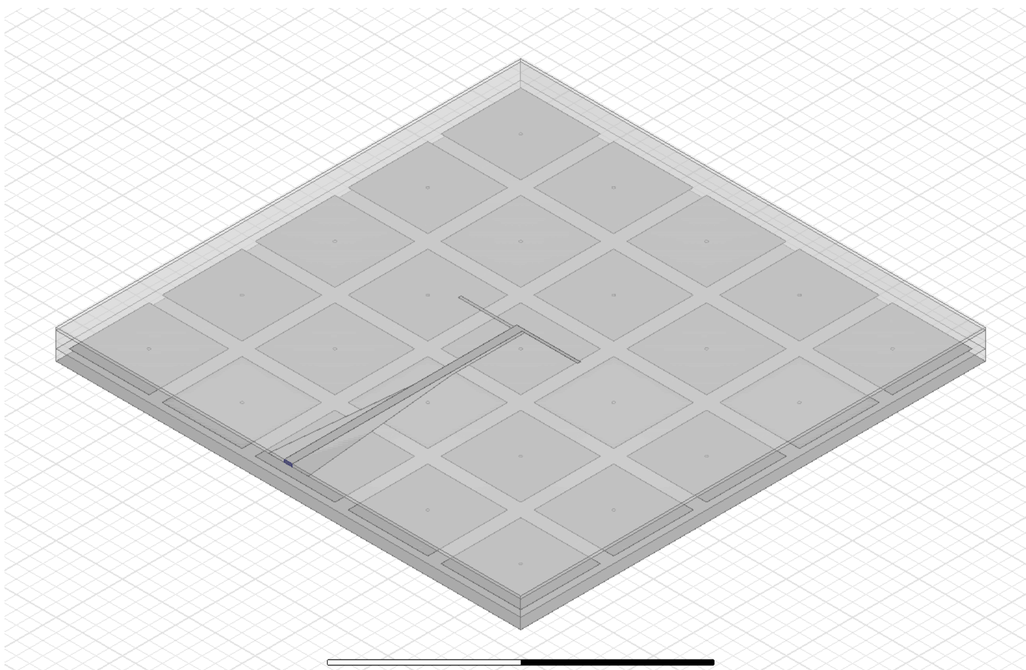

Figure 6.8 HFSS model of the dipole antenna on the HIS

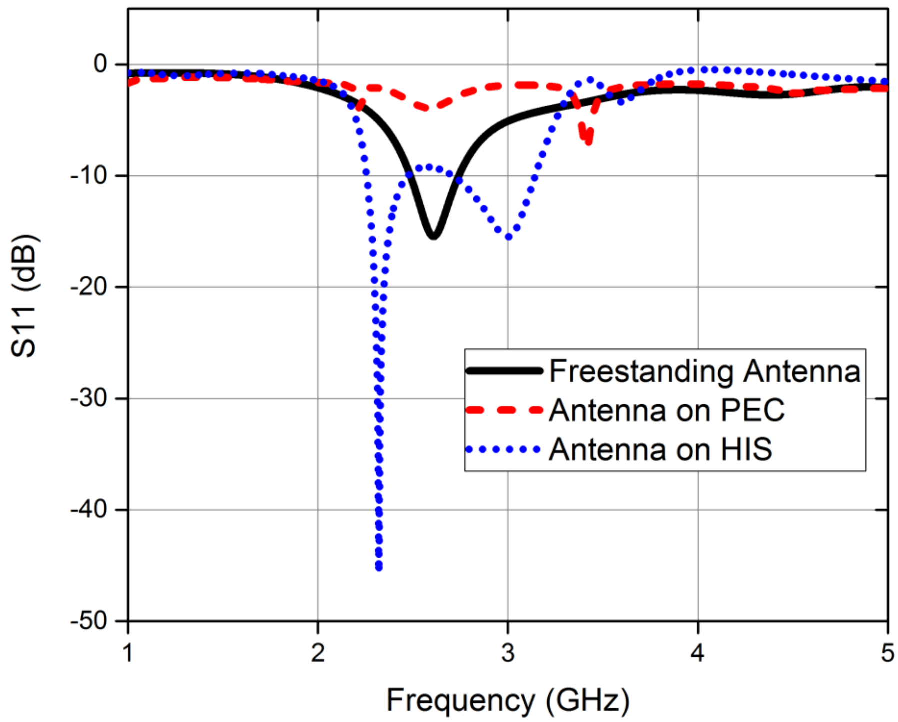

Figure 6.9 Simulated S11 of the antenna in a freestanding configuration, 5mm above a PEC, and 5mm above the designed HIS. The antenna over the PEC is shorted by the proximity to the PEC . The antenna over the HIS shows a shift and broadening of frequency, but maintains a good match at 2.6 GHz.

The gain of the antenna is pictured in figure 6.10. There is considerable improvement in gain when the antenna is backed by the HIS with a maximum of 7.5dB and no major side lobes.

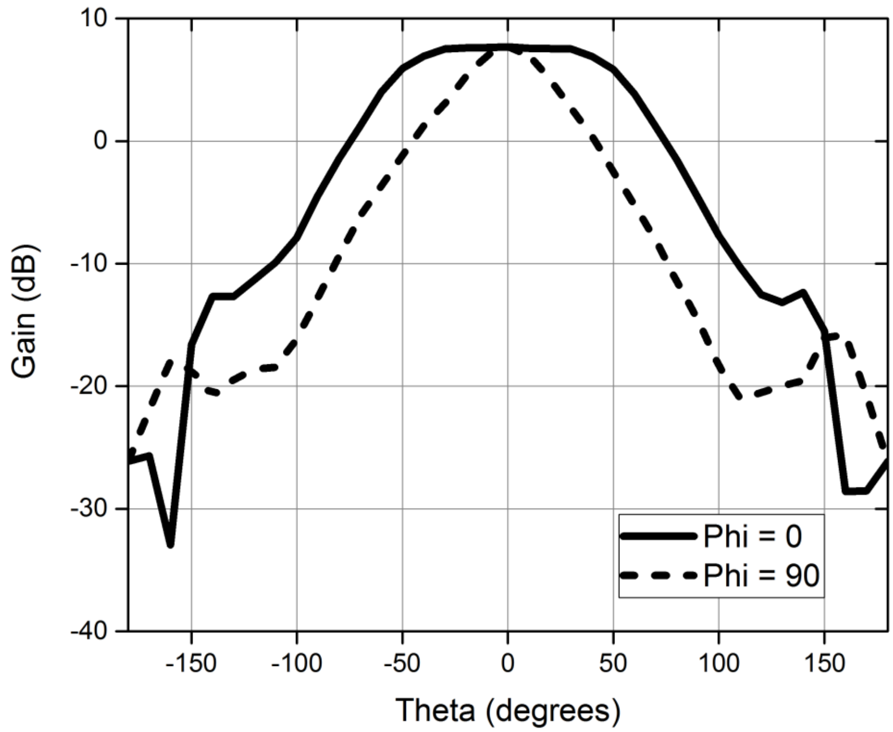

Figure 6.10 Simulated gain of antenna on HIS at 2.6 GHz

6.2 Material Characterization

As previously mentioned a FDM process was used to create all of the dielectric components in the design. A polycarbonate extrusion material was selected as a base material for its low loss tangent (tan δ = 0.0006) and relatively high dielectric constant (ε_r = 2.9). A clear non-pigmented plastic was used due to reported results of pigmentation having significant effect on the dielectric properties [42]. To achieve the other dielectric constants required by the design the volume fraction of polycarbonate to air was varied spatially. This allows us to realize any effective dielectric constant between air and the polycarbonate. The exact relationship between volume fraction and dielectric constant was determined experimentally. Here test plates of the material were printed at 15%, 30%, and 50% volume fill fraction and the dielectric constant was measured using a free-space focused beam measurement system.

The data was analyzed and found to fit a modified Maxwell-Garnett mixing formula:

$$\varepsilon_{eff} = \varepsilon_{air} \frac{2\delta_{PC}(\varepsilon_{PC} - \varepsilon_{air}) + \varepsilon_{PC} + 2\varepsilon_{air}}{2\varepsilon_{air} + \varepsilon_{PC} + \delta_{PC}(\varepsilon_{air} - \varepsilon_{PC})} \tag{6.1}$$

where ε_{eff} is the effective dielectric constant, ε_{air} and ε_{PC} are defined as the dielectric constant of air and polycarbonate respectively, and δ_{PC} is the volume fraction of the polycarbonate material. It should be noted that to achieve a smooth print surface of metallic elements we capped all dielectric volumes with a thin solid sheet of polycarbonate. This slightly modified the Maxwell-Garnett fit, as shown in Figure 6.11, where the solid blue curve refers to the adjusted properties when the capped surfaces are included. The adjusted Maxwell-Garnet provides a predictable rule governing the effective dielectric properties. Using this curve we found that volume fractions of 10%, 30%, and 100% were needed to match the desired dielectric properties of 1.5, 1.75, and 2.9 respectively. For printing of conductive elements we used the commercially available Methode 6130S silver ink. The conductivity of this ink after curing was measured to be 1.3 x 10^6 S/m within the frequency band of interest. It should be noted that this is approximately an order of magnitude less conductive than bulk copper and will result in a reduction in antenna efficiency.

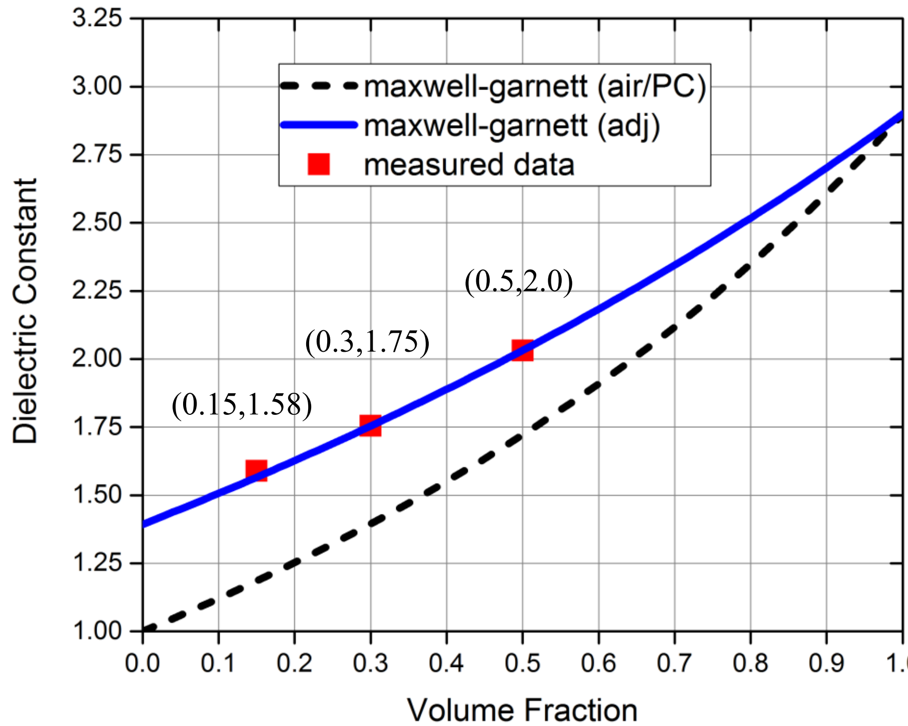

Figure 6.11 Comparison of the measured dielectric constants of the test slabs versus the Maxwell-Garnett curve. The printed caps on the test slabs increased the effective dielectric constant of the slabs. A modified Maxwell-Garnett curve was determined to predict the measured dielectric constants.

6.3 Measurement and Results

The final fabricated part is shown in Figure 6.12. Here a 3.5mm end launch SMA connector was attached to the antenna feed. Using an Agilent E8364B vector network analyzer the scattering parameter, S_{11}, was measured in a freestanding setup (no ground), above a baseline continuous conducting surface, and above the fabricated high impedance surface

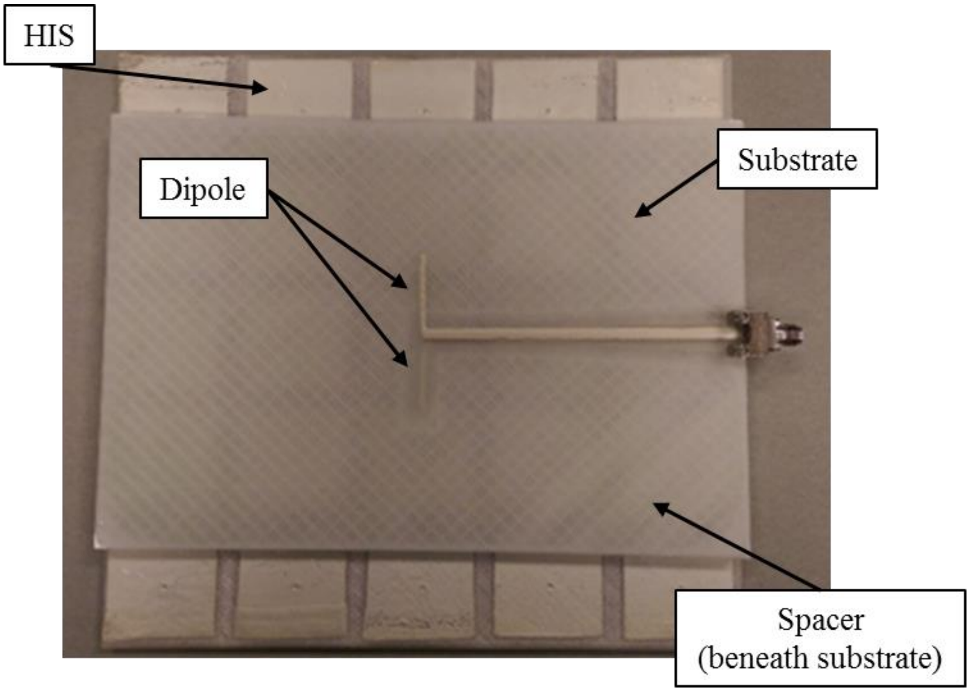

Figure 6.12 Fabricated antenna with embedded conductors between substrate and printed spacer on the HIS.

Inspection of the measured results, shown in Figure 6.13, show good freestanding antenna radiation at the designed frequency (2.6 GHz). The antenna also showed a standing wave at frequencies above 3 GHz. This is most likely due to a small warping of the printed ground arm of the antenna on the polycarbonate. The chemical solvent of the silver conductive ink reacted with the polycarbonate over time, causing the material to warp slightly. Faster sintering of the conductive ink minimized the warping on subsequent prints.

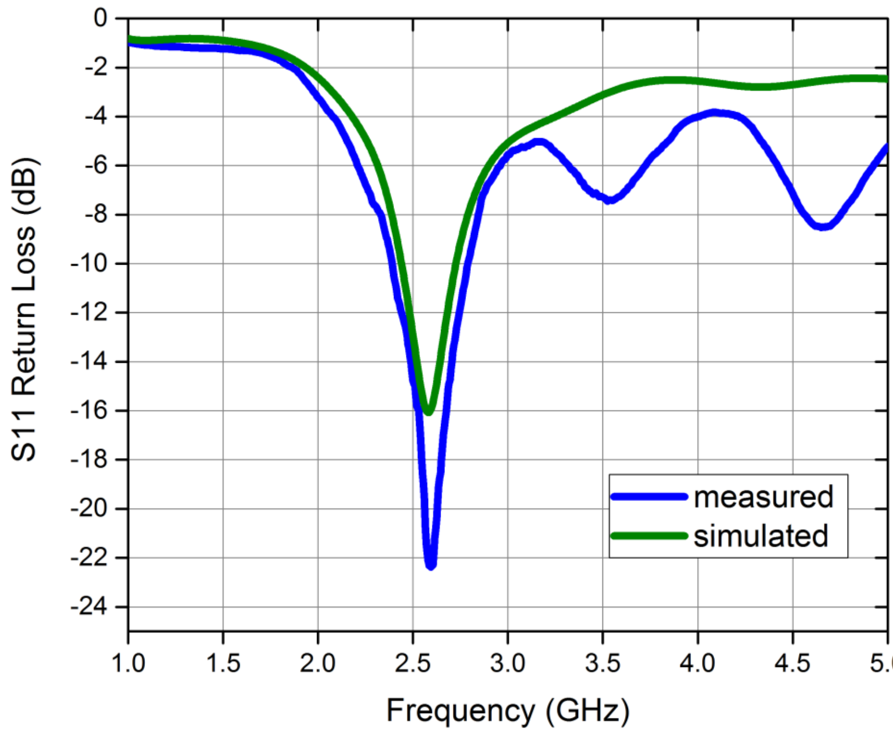

Figure 6.13 Comparison of the measured and simulated antenna S_{11} in a freestanding configuration

The S_{11} of the fabricated antenna on a copper ground plane and the HIS is compared in Figure 6.14. As predicted, antenna performance is significantly reduced when placed flush with a bulk conducting ground plane (i.e. S11= -6 dB). In contrast, the antenna remains relatively well matched (i.e. S11< -14 dB) when placed above the HIS. It should be noted that the optimal antenna placement above a continuous metallic ground plane is approximately 28.8mm (i.e. $\lambda/4$) at 2.6 GHz. The total thickness of the low profile antenna, including spacer layer, dipole layer and HIS layer, was 11mm. This equates to a stand-off distance of less than $\lambda/8$.

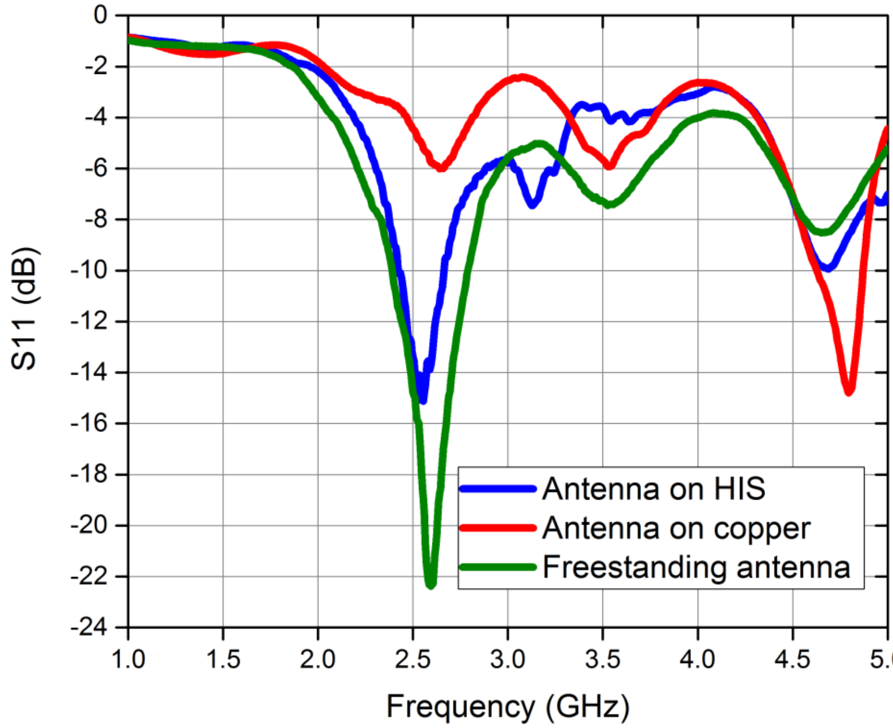

Figure 6.14 Comparison of the measured S_{11} of the antenna in a freestanding configuration (no ground), above a copper ground plane, and above the fabricated HIS

Radiation properties from the antenna above the HIS were confirmed by measuring the radiation pattern, pictured in Figure 6.15, using a near field scanning system (NSI, Inc, model NSI-700S-75). While a reasonably good match with predicted radiation patterns was observed, there was a distinct broadening of the measured 3 dB beam width – particularly, in the E-plane. This is likely due to increased material loss from the use of the silver conductive inks. In fact, HFSS simulations predict an overall antenna efficiency of 85% for the printed sample compared to 94% for an identical antenna fabricated using bulk copper.

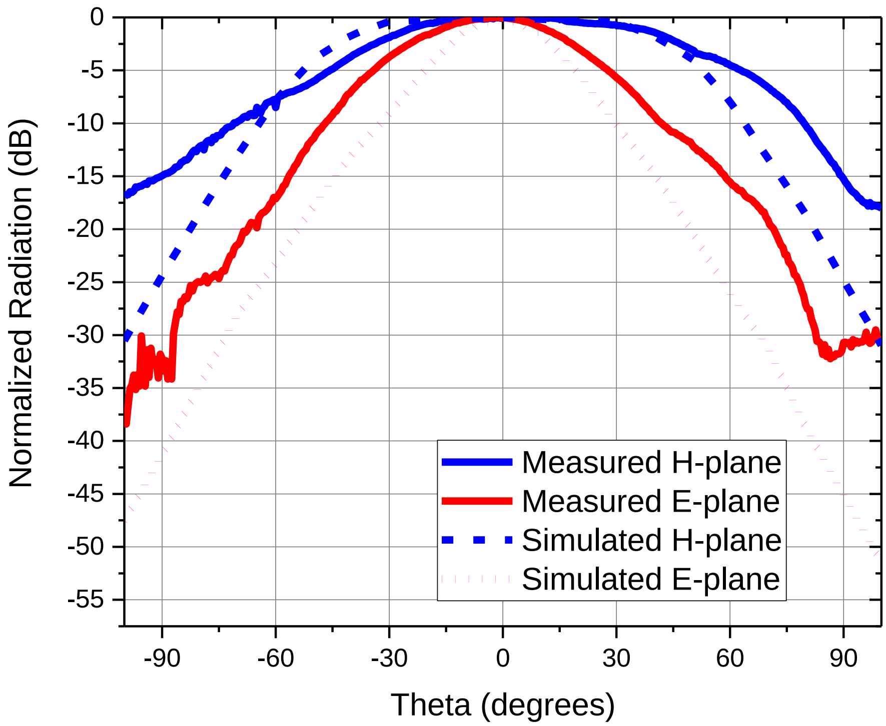

Figure 6.15 Comparison of the measured and simulated beam widths of the antenna above the HIS at 2.6 GHz.

6.4 Conclusions

In this chapter, I demonstrated the ability of multi-material AM to fabricate a mechanically rigid low profile antenna including all metallic and dielectric features. I also demonstrated how spatially varying dielectric properties can be achieved through controlled geometric deposition of materials at specific volume fractions. The final antenna was measured and showed good radiation properties with a reasonably close match to predicted performance. Multi-material AM is a powerful new tool for rapid prototyping of new concepts and exploring new antenna designs not realizable using standard fabrication processes.

Chapter 7

CONCLUSIONS

7.1 Summary

A new fabrication method for manufacture of electromagnetic multifunctional composites was explored. Multiple discrete electromagnetic devices were demonstrated functioning embedded within a structural composite by conductive screen printing and microdispensing. The increased attenuation of printed microstrip transmission lines was determined and an effective conductivity value was extracted relative to the number of repeated screen printing passes. In addition, conforming of the printed inks was determined to increase the electrical path length of printed electronics. Detailed metrology was performed on the printed conductors. Overlapping of conductive ink, variations in thickness, and voids were all found to ultimately affect the effective conductivity of the printed microstrip transmission lines.

A mechanical study of the embedded conductive inks within a structural was performed. It was found from a 3 point shear test that an approximate 30% reduction in mechanical shear strength occurred when a continuously printed ground plane was embedded about the midplane of a glass composite. There was also a 5% reduction in delamination resistance of a continuous printed ground plane when measured by a floating roller peel test.

The second device demonstrated was a conformal load bearing patch antenna. The antenna was modeled to operate at the GPS L1 (1.575 GHz) frequency band with an axial ratio below 3dB at 1.575 GHz. The antenna was printed with a higher conductivity, lower viscosity DuPont CB028 silver ink using a nScrypt 3Dn-300 microdispensing printer. The high repeatability of the microdispensing printer allows for quick design turnover and prototyping. Two subsequent antenna designs were fabricated. Both antennas were measured to have a shift downward in frequency from ink spreading and increased antenna patch geometry. Optimization was performed on the antenna model. It was determined that conductivity of ink when microdispensed on the woven glass fabric had a higher conductivity than previously measured with screen printing.

The third devices presented were an inductive and capacitive type frequency selective surface. A square type band stop and slot type band pass filter were demonstrated within a structural composite substrate at the Ka-Band. The performance of the printed frequency selective surfaces were compared to that of microdispensed frequency selective surfaces. It was determined that although the screen printed conductors are of a lower conductivity, the consistency of the screen printed samples over the entire surface area produced better filter responses and resonances over the microdispensed counterparts. Additionally, an anisotropy of the printed conductors was discovered when printed on woven fabrics. The filter response of the frequency selective surfaces improved when the electric field was aligned with the long bundles of the satin weave fabric, producing an anisotropy of the conductivity seen by incident radiation.

The fourth and final device shown in the dissertation was a low profile antenna with corresponding low profile ground completely fabricated by multi-material additive manufacturing. The antenna and high impedance surface ground plane were fabricated by a single nScrypt 3Dn-300. Multiple dielectric properties were fabricated by spatial controlling the geometric fill of polycarbonate. The antenna was measured and found to have improved radiation characteristics above the high impedance surface when compared to a continuous ground.

7.2 Future Work

In this dissertation, multiple discrete electromagnetic devices were designed, fabricated, and characterized within a structural composite. The area of multifunctional composites would benefit from the integration of multiple instances of the demonstrated devices within a single composite laminate. For example, communication arrays with multiple antennas or polarizing elements embedded above linearly polarized antenna elements. Additional studies can also be performed on the structural material used, such as varying glass weaves and resin. The structural impact determined in this dissertation should be thoroughly investigated. One solution to the structural degradation from interlaminar continuous printed surfaces can be replaced by sub-wavelength slotted ground planes. Finally, many composite structures must conform to some complex geometry. Therefore, a study on the draping of printed fabrics would greatly benefit the field of scaled multifunctional composite

REFERENCES

1. F.C. Campbell. *Structural Composite Materials*. ASM International. 2010

2. R.F. Gibson.'A review of recent research on mechanics of multifunctional composite materials and structures'. *Composite Structures*. Vol 92. 2010

3. A.J. Lockyer, K.H. Alt, J.N. Kudva, R.W. Kinslow. 'Conformal load-bearing antenna structures (CLAS): Initiative for multiple military and commercial applications'. *SPIE*, Vol. 3046. 1997

4. A.J. Lockyer, K.H. Alt, D.P. Coughlin, M.D. Durham, J.N. Kurva. 'Design and development of a conformal load-bearing smart-skin antenna: overview of the AFRL Smart Skin and Structures Technology Demonstration (S^3TD)'. *SPIE Conference on Industrial and Commercial of Smart Structures Technologies*. Vol 3674. 1999.

5. C.S. You, W. Hwang. 'Design of load-bearing antenna structures by embedding technology of microstrip antenna in composite sandwich structure'. *Composite Structure*. Vol. 71. pp 378-382. 2005

6. P.C. Kim, D.G. Lee, I. S. Seo, G.H. Kim. 'Low-observable radomes composed of composite sandwich constructions and frequency selective surfaces'. *Composites Science and Technology*. Vol 68. pp 2163-2170. 2008

7. C.K. Kim, L.M. Lee, H.C. Park, W. Hwang, W.S. Park. 'Impact damage and antenna performance of conformal load-bearing antenna structures'. *IOP Smart Materials and Structures*. Vol 12. 2003

8. L. Yao, Y. Qiu. 'Design and fabrication of microstrip antennas integrated in three dimensional orthogonal woven composites'. *Composites Science and Technology*. Vol 69. 2009.

9. L. Yao, M. Jiang, D. Zhou, F. Xu, W. Zhang, N. Zhou, Q. Jiang, Y. Qiu. 'Fabrication and characterization of microstrip array antennas integrated in three dimensional orthogonal woven composite'. *Composites: Part B*. Vol 42. 2011

10. S. Lee, K. Park, K. Oh, C. Kim. 'The use of carbon/dielectric fiber woven fabrics as filters for electromagnetic radiation'. *Carbon*. Vol 47. 2009

11. S. T. Wentworth, B. L. Dillaman, J. R. Chadwick, C. D. Ellis, R. W. Johnson. ‘Attenuation in Silver-Filled Conductive Epoxy Interconnects’. *IEEE Transactions on Components, Packaging, and Manufacturing Technology* – Part A, Vol. 20, No. 1, 1997

12. T. Bjorninen, S. Merilampi, L. Ukkonen, P. Ruuskanen, L. Sydanheimo. ‘Performance comparison of silver ink and copper conductors for microwave applications’. *IET Microwaves, Antennas & Propagation*. Vol. 4. Iss. 9, pp. 1224-1231. 2010

13. B. Karaguzel, C.R. Merritt, T. Kang, L.M. Wilson, H.T. Nagle, E.Grant, B. Pourdeyhimi. ‘Utility of nonwovens in the production of integrated electrical circuits via printing conductive inks’. *The Journal of the Textile Institute*. Vol 99. Issue 1. pp. 37-45. 2007

14. I. Locher, G. Troster. ‘Screen-printed Textile Transmission Lines’. *Textile Research Journal*. Vol. 77. pp. 837-842. 2007

15. I. Kazani, C. Hertleer, G.D. Mey, A. Schwarz, G. Guxho. L.V. Langenhove. ‘Electrical Conductive Textiles Obtained by Screen Printing’. *Fibres & Textiles in Eastern Europe*. Vol. 1. pp. 57-63. 2012

16. C. Li, D. Jiang, J. Zeng, S. Xing, S. Ju. ‘Electromagnetic transmission characteristics of composite frequency selective surfaces coated with polymer-silver paste’. *Composites Science and Technology*. Vol. 90. pp. 32-39. 2014

17. W.G. Whittow, Y. Li, R. Torah, K. Yang, S. Beeby, J. Tudor. ‘Printed frequency selective surfaces on textiles’. *Electronics Letters*. Vol. 50. No. 13. 2014

18. A. Tennant. W. Hurley. T. Dias. ‘Experimental knitted, textile frequency selective surfaces’. *Electronic Letters*. Vol. 48. No. 22. 2012

19. J.C. Bachelor, E.A. Parker, J.A. Miller, V. Sanchez-Romaguera, S.G. Yeates. ‘Inkjet printing of frequency selective surfaces’. *Electronic Letters*. Vol. 45. No. 1. 2009

20. S. Kim, B. Cook, T. Le, J. Cooper, H. Lee, V. Lakafosis, R. Vyas, R. Moro, M. Bozzi, A. Georgiadis, A. Collado, M. M. Tentzeris. ‘Inkjet-printed antennas, sensors, and circuits on paper substrate. *IET Microwave Antennas Propagation*. Vol. 7.Issue 10. 2013.

21. J. Virkki, T. Bjorninen, S. Merilampi, L. Sydanheimo, L. Ukkonen. 'Manufacturing and Applications of Screen-printed RFID Tags on Paper Substrate'. *PIERS Proceedings*. Stockholm, Sweden. 2013

22. M.L. Scarpello, I. Kazani, C.Hertleer, H. Rogier, D.V. Ginste. 'Stability and Efficiency of Screen Printed Wearable and Washable Antenna'. *IEEE Antennas and Propagation Letters*. Vol. 11. 2012.

23. S. Zhu, R. Langley. 'Dual-Band Wearable Textile Antenna on an EBG Substrate.' *IEEE Transactions on Antennas and Propagation*. Vol. 57. No. 4. 2009.

24. M. Klemm, G. Troster. 'Textile UWB Antennas for Wireless Boday Area Networks'. *IEEE Transactions on Antennas and Propagation*. Vol. 54. No. 11. 2006

25. D. Gay. *Composite Materials: Design and Applications Third Edition.* CRC Press. 2014

26. K. Bal and V.K. Kothari, "Permittivity of Woven Fabrics: A Comparison of Dielectric Formulas for Air-Fiber Mixture", *IEEE Trans on Dielectrics and Electrical Insulation*, Vol. 17, No. 3, June 2010, pp. 881-889.

27. R. Agarwal and A. Dasgupta, "Prediction of Electrical Properties of Plain-Weave Fabric Composites for Printed Wiring Board Design", *Journal of Electronic Packaging*, Vol. 115(2), June 1993, pp. 219-224

28. S. Rikte, M. Andersson and G. Kristensson, "Homogenization of woven materials", *International Journal of Electronics and Communications*, Vol. 53 (5), 1999, pp. 261-271.

29. W. Chin and D. Lee, "Binary mixture rule for predicting the dielectric properties of unidirectional E-glass/epoxy composite", *Composite Structures*, Vol. 74, 2006, pp. 153-162.

30. M.S. Mirotznik, S. Yarlagadda, R. McCauley, P. Pa. 'Broadband Electromagnetic Modeling of Woven Fabric Composites'. *IEEE Transaction on Microwave Theory and Techniques*. Vol. 60, No. 1. Jan 2012

31. Tencate Advanced Composites. Radomes & Antennas Low Dielectric Composites. www.tencate.com

32. K.K.B. Hon, L. Li, I.M. Hutchings. ‘Direct writing technology- Advances and developments’. *CIRP Annals – Manufacturing Technology*. Vol. 57. 2008

33. K.B. Perez, C.B. Williams. ‘Combining Additive Manufacturing and Direct Write for Integrated Electronics – A Review’. 2013. http://sffsymposium.engr.utexas.edu/Manuscripts/2013/2013-77-Perez.pdf

34. H.J. Lewis, A. Ryan. *New Trends in Technologies: Devices, Computer, Communication Systems*. Intech. http://cdn.intechopen.com/pdfs-wm/12292.pdf

35. D. Espalin, D.W. Muse, F. Medina, E. MacDonald, R.B. Wicker, "3D Printing Multi-Functionality: Structures with Electronics," International Journal of Advanced Manufacturing Technology, Volume 72, Issues 5-8, 2014, pages 963-978

36. C.A. Balanis. *Advanced Engineering Electromagnetics*. John Wiley and Sons. 1989.

37. B.A. Munk, *Frequency Selective Surfaces: Theory and Design*. Wiley Interscience. 2000

38. M.Lin, F.Chang. ‘The manufacture of composite structures with a built-in network of piezoceramics’. *Composites Science and Technology*. Vol. 62. pp 919-939. 2002

39. R. McCauley. ‘Material design methodology for structural and microwave multifunctional composite laminate systems’. *Master’s Thesis*. University of Delaware. Fall 2013

40. R. Garg, P. Bhartia, I. Bahl, A. Ittipiboon. *Microstrip Antenna Design Handbook*. Artech House. 2000

41. D. Sievenpiper.’High-Impedance Electromagnetic Surfaces’. *PhD Dissertation*. University of California Los Angeles. 1999

42. I.T. McMicheal, A.I. Zaghloul, M.S. Mirotznik. ‘A method for determining optimal EBG reflection phase for low profile dipole antennas’ *IEEE Transactions on Antennas and Propagation*. Vol. 61. No. 5. 2013

43. M.A. Hiranandani, A.B. Yakovlev, A.A. Kishk. ‘Artificial magnetic conductors realized by frequency-selective surfaces on a grounded dielectric slab for antenna applications’. *IEE Proc.-Microw. Antennas Propag*. Vol. 153. No.5. 2006

44. B. Sanz-Izquidero, E.A. Parker, J.C. Batchelor, J.A. Miller. ‘Body Armour with Integral High Impedance Surface’. *Proceedings of the 5th European Conference on Antennas and Propagation*.

45. J.R. Sohn, K.Y. Kim, H.-S. Tae, J.-H. Lee. ‘Comparative study on various artificial magnetic conductors for low profile antenna’. *Progress In Electromagnetics Research*. Vol. 61. 2006

46. S. Zhu, R. Langley. ‘Dual-Band Wearable Texilte Antenna on an EBG Substrate’. *IEEE Transactions on Antennas and Propagation*. Vol. 57. No. 4. 2009

47. P. I. Deffenbaugh R.C. Rumpf, K.H. Chruch, “Broadband Microwave Frequency Characterization of 3-D Printed Materials,” *IEEE Transactions on Components, Packaging, and Manufacturing Technology*, vol. 3, no. 12, pp. 2147-2155, 2013

Appendix

COPYRIGHT

Assignment of copyright and publication agreement

IOP Publishing Limited ("IOP") agrees to publish:

Manuscript Title: High Frequency Characterization of Conductive Inks Embedded within a Structural Composite (the "Article") written by

Names of all authors: Pa, Peter; McCauley, Raymond; Larimore, Zachary; Mills, Matthew; Yarlaggada, Shridhar; Mirotznik, Mark ("the Named Authors") in the following journal Smart Materials and Structures ("the Journal")

Name of copyright owner(s) (if not the Named Author(s) – see Important Information above):

Peter **("the Institution")**
Pa

IOP Ref: SMS-101748

Part 1 - Subscription Copyright Assignment

Assignment of copyright
1.1 In consideration for acceptance and publication of the Article, the Named Authors of the Article and/or the Institution hereby assign, where necessary by present assignment of future copyright, to IOP with full title guarantee the entire copyright in all original material published as part of the Article (which expression includes but is not limited to the text, abstract, tables, figures and graphs, related corrigenda or "comments" and multimedia content but excludes any other item referred to as supplementary material) throughout the world for the full term of copyright (including any extensions or renewals thereof) for all media and formats, whether known or unknown. Such assignment shall be effective only if the Article (or any resubmission of the Article) is accepted for publication. For the avoidance of doubt, copyright does not subsist in any fundamental data underlying the Article and nothing in this agreement is intended to limit access to or use of such data.

1.2 If the Article, or any part of it, is protected by Crown Copyright, in consideration for acceptance and publication of the Article, the relevant Named Authors and the relevant originating department or agency hereby grant IOP a royalty-free worldwide freely-transferrable licence for the full term of copyright (including any extensions or renewals thereof) for all media and formats, whether known or unknown, to do in relation to the Article all acts restricted by copyright worldwide including, but not limited to, the right of action under section 101A of the Copyright Designs and Patents Act 1988. Such licence shall be effective only if the Article is accepted for publication and shall be exclusive to IOP for a period of twelve calendar months following the date of online publication of the Article. Thereafter, the licence shall be non-exclusive.

1.3 In consideration for acceptance and publication of the Article, the Named Authors and/or the Institution hereby grant IOP a royalty-free non-exclusive worldwide freely transferrable licence for the full term of copyright (including any extensions or renewals thereof) to do in relation to any supplementary material not deemed to be part of the Article and/or any video abstract all acts restricted by copyright worldwide. This shall include, but not be limited to, making the material available under any licence that IOP deems appropriate for purposes including, but not limited to, the maximisation of visibility and the long term preservation of the content.

1.4 Each of the Named Authors consents to the publication and processing by IOP of their email addresses.

Representations and warranties

2.1 The Institution and/or the Submitting Author on behalf of the Named Authors (as appropriate) represent and warrant that:

2.1.1 the Article is the original work of the Named Authors;

2.1.2 the Article has not been published previously in any form, other than as part of the Named Authors' research theses or dissertations (which fact has been notified to IOP in writing) or as a preprint, for example on the arXiv.org service;

2.1.3 each of the Named Authors has made a material contribution to the conception and/or writing of the Article, has received the final version of the Article, has agreed to its submission on the terms contained herein and takes responsibility for it and submission has been approved as necessary by the authorities at the establishment where the research was carried out;

2.1.4 the Submitting Author completes and returns this agreement as authorised agent for and on behalf of all the Named Authors and has the full power to enter into this agreement and to make the grants and assignments it contains;

2.1.5 the Article has not been and shall not be submitted to another publisher prior to withdrawal or rejection by IOP;

2.1.6 the Article does not infringe any third party rights, it contains nothing libellous or unlawful, all factual statements are to the best of the Named Authors' knowledge true or based on valid research conducted according to accepted norms and all required permissions have been obtained in writing;

2.1.7 the Article expressly acknowledges any third party funding and/or potential conflicts of interest; and

2.1.8 any supplementary material or video abstract is the original work of the Named Authors, or is the property of the Institution, or permission has been obtained from its owner(s) for its publication by IOP and permission has been obtained for the inclusion of any third party content (including music).
2.2 The Named Authors and/or the Institution (as appropriate) indemnify and will keep indemnified IOP against all costs and expenses suffered or incurred by IOP as a result of and/or arising out of any breach of the representations and/or warranties in this section 2.

The Named Authors' rights

3.1 IOP grants the Named Authors the rights specified in paragraphs 3.2 and 3.3. All such rights must be exercised solely for non-commercial purposes. Where possible, any use should display citation information and IOP's copyright notice, and, for electronic use, best efforts must be made to include a link to the online abstract in the Journal.

Exercise of the rights in paragraph 3.2 may use the version of the Article published in the Journal ("Final Published Version").

Exercise of the rights referred to in paragraph 3.3 must not use the Final Published Version and extend only to the Named Authors' own format (which may include amendments made following peer review but not any editing, typesetting or other changes made by IOP) (the "Accepted Manuscript") and must be accompanied by the following statement of provenance:

'This is an author-created, un-copyedited version of an article accepted for publication in Smart Materials and Structures.
IOP Publishing Ltd is not responsible for any errors or omissions in this version of the manuscript or any version derived from it. The Version of Record is available online at [insert DOI].'

3.2 The rights are:

3.2.1 To make copies of the Article (all or part) for teaching purposes;

3.2.2 To include the Article (all or part) in a research thesis or dissertation;

3.2.3 To make oral presentation of the Article (all or part) and to include a summary and/or highlights of it in papers distributed at such presentations or in conference proceedings; and

3.2.4 To use figures and text from the Article falling within the quota outlined in the STM Permissions Guidelines (http://www.stm-assoc.org/permissions-guidelines/) at the relevant time in force.
For the avoidance of doubt, the Named Authors retain all proprietary rights in the Article other than copyright.

3.3 Additional rights of the Named Authors are to:

3.3.1 Use the Accepted Manuscript (all or part) without modification in personal compilations of the Named Authors' own works (provided not created by a third party publisher); and

3.3.2 Include the Accepted Manuscript (all or part) on the Named Authors' own personal website(s), institutional website(s) and third party websites in accordance with the Author Rights set out at the following url legal.ioppublishing.org/author-rights on the date of submission of this agreement.
Miscellaneous

4. To the extent that there are moral rights in the Article, all the Named Authors expressly reserve and assert their moral rights to be identified as the authors of the Article.

5. The Named Authors and/or the Institution shall execute such further documents, and take such actions and do such things, as may be requested by IOP at IOP's reasonable expense to give full effect to the terms of this agreement.

6. For the avoidance of doubt, the grants and assignment envisaged herein shall become effective only upon acceptance of the Article for publication. In the event that the Article is withdrawn prior to acceptance, or is rejected, this agreement shall have no effect and no party shall be bound by it.

7. This agreement shall be governed by English Law and subject to the non-exclusive jurisdiction of the English courts.

Confirmation

8. By typing the Submitting Author's name into the box at Part 3 below and clicking "Submit", the Named Authors agree to these terms. Authorised signatories of any third party copyright owner(s) agree, on behalf of such owner(s), to these terms by typing the owner's name into the "Institution" box at the top of the page.

Part 2 - Open Access Copyright Assignment
Assignment of copyright

1.1 In consideration for acceptance and publication of the Article, the Named Authors of the Article and/or the Institution hereby assign, where necessary by present assignment of future copyright, to IOP with full title guarantee the entire copyright in all original material published as part of the Article (which expression includes but is not limited to the text, abstract, tables, figures and graphs, related corrigenda or "comments" and multimedia content but excludes any other item referred to as supplementary material) throughout the world for the full term of copyright (including any extensions or renewals thereof) for all media and formats, whether known or unknown. Such assignment shall be

Journals Publication Agreement and Assignment of Copyright Form/Open Access Licence Agreement

The IET offers authors the option to publish their paper open access or in the traditional subscription access model. If you want your paper to be a subscription access paper you should complete Section A of this form. If you want your paper to be published open access you must complete Section B (**Please note that there is an article processing charge of $1450 USD for open access publishing**, contact the editorial office for further details journals@theiet.org.)

You cannot complete both Section A and B.

Section A: Subscription Access

Assignment date	The date on which the present eform is submitted
Consideration	Once the paper has been printed, we will send the corresponding author a PDF copy of their paper. Please note that this is subject to the terms and conditions of our Green Open Access policy..
Content	The paper submitted as part of the present submission process
The Contributor	The lead author whose name appears at the end of the present eform
The Publication	The journal to which the paper is being submitted as part of the present submission process
The Publisher	The Institution of Engineering and Technology, a charity registered in England and Wales (registered number 211014) whose registered office is at Savoy Place, 2 Savoy Place, London WC2R 0BL and whose office for notices relating to this Agreement is Michael Faraday House, Six Hills Way, Stevenage, Hertfordshire, SG1 2AY.
Permitted Uses	(i) in articles which the Contributor submits to learned or professional journals (ii) for publication in books, (iii) use in papers which the Contributor presents at professional conferences (iv) use in connection with training given by the Contributor (v) inclusion in any dissertation prepared by the Contributor (vi) as specified in the version of the Publisher's pre-print and post-print policy applicable at the date of this Agreement

1. This Agreement concerns the Content which the Contributor shall prepare alone or in conjunction with the Other Contributors and which the Publisher intends (but is not obliged) to first publish in the Publication.

2. By signing this Agreement and in recognition of the Consideration, the Contributor hereby assigns to the Publisher with full title guarantee, free of all third party rights of any kind, all right, title and interest in and to the Content including all copyright in the same, throughout the world, for the full term of such rights, including all extensions and renewals. If all or any part of the Content is not yet in existence, this assignment shall be effective immediately on the Content coming into existence. The Contributor will at the Publisher's reasonable expense, promptly do all acts and execute all documents which the Publisher considers are necessary or desirable to give full effect to the above assignment.

3. The Contributor irrevocably agrees that the Publisher shall have the right to use the Contributor's